2010

Computational Study of Direct Fuel Injection in the Rotax 914 Engine

Brad Pollock
Wright State University

COMPUTATIONAL STUDY OF DIRECT FUEL INJECTION

IN THE ROTAX 914 ENGINE

A thesis submitted in partial fulfillment
of the requirements for the degree of
Master of Science in Engineering

By

BRAD PAUL POLLOCK
B.S.M.E, University of Toledo, 2005

2010
Wright State University

WRIGHT STATE UNIVERSITY

SCHOOL OF GRADUATE STUDIES

December 14, 2010

I HEREBY RECOMMEND THAT THE THESIS PREPARED UNDER MY SUPERVISION BY Brad Pollock ENTITLED Computational Study of Direct Fuel Injection in the Rotax 914 Engine BE ACCEPTED IN PARTIAL FULFILLMENT OF THE REQUIREMENTS FOR THE DEGREE OF Master of Science in Engineering

Committee on
Final Examination

Haibo Dong, Ph.D.

John Hoke, Ph.D.

Hui Wan, Ph.D.

Andrew Hsu, Ph.D.
Dean, School of Graduate Studies

Haibo Dong, Ph.D.
Thesis Director

George P.G. Huang, P.E., Ph.D.
Chair, Department of Mechanical and Materials Engineering
College of Engineering and Computer Science

ABSTRACT

Pollock, Brad. M.S.Egr., Department of Mechanical and Materials Engineering, Wright State University, 2010. Computational Study of Direct Fuel Injection in the Rotax 914 Engine.

Direct injection spark ignition (DISI) is a fuel delivery method in which the fuel is introduced directly into the combustion chamber of an internal combustion engine. Although direct fuel injection was first pioneered in the early 1920's, it has only recently become a reliable option due to advances made in control systems and injection technology. Direct injection enables increased fuel efficiency and higher power output than a conventional Port Fuel Injection (PFI) system. By delivering pressurized fuel directly into the cylinder, the degree of fuel atomization and the fuel vaporization rate are increased. Hence, the air/fuel mixture can be more precisely maintained, benefiting both fuel economy and emissions. In addition, the cooling effect of fuel droplets changing to vapor inside the combustion chamber facilitates a higher compression ratio and lessens the likelihood of knock.

DISI has witnessed a resurrected interest in the automotive industry due to its promise of better fuel economy, additional power, reduced emissions and the ability to operate on multiple fuels. The aviation industry, on the other hand, has largely forgotten about the internal combustion engine subsequent to the invention of the jet engine. However, the introduction of unmanned aerial systems (UAS) has encouraged a renewed interest in small internal combustion engines such as the Rotax 914. Although, these

engines provide a cheap power plant, they lack the power and efficiency required for their application. Consequently, by employing DISI in UAS engines, it affords flexibility with regards to fuel choice while also providing longer flight times and more power with less weight.

As with any new application of technology, DISI in these smaller engines must first be tested and refined until it can seamlessly replace PFI. Experimental testing can be costly and time consuming, but computational fluid dynamics (CFD) can help speed the design process by performing parametric analysis to determine an optimum configuration to begin testing. For this thesis, a model of the Rotax 914 engine was developed to computationally model the effects of direct injection on the engine. Gambit was adopted for geometry generation and meshing, while Fluent was used for fluid motion and combustion simulation. A PFI version of the computational model was validated against experimental results of a Rotax 914 engine in order to add fidelity to the model. DISI was then applied to the model and a study was performed to determine operation capabilities under different operating conditions.

Contents

Nomenclature

PFI	Port Fuel Injection
DISI	direct injection spark ignition
SI	Spark ignition
Φ	Equivalence ratio
GDI	Gasoline Direct Injection
CFD	Computational fluid dynamics
HCSI	Homogeneous Charge Spark Ignition
SCSI	Stratified Charge Spark Ignition
C8H18	Carbon-di-oxide
CO2	Iso-Octane
MDM	Moving Dynamic mesh
bTDC	Before Top Dead Center
aTDC	After Top Dead Center
TDC	Top Dead Center
BDC	Bottom Dead Center
CA	Crank Angle Degree
MAP	Manifold Absolute Pressure
AvGas	Aviation Gasoline
100LL	100 Octane Low Lead Aviation Fuel

List of Figures

List of Tables

ACKNOWLEDGMENTS

I would like to thank my advisor Dr Haibo Dong for all the time and effort he has put into my time spent at Wright State University as a Graduate Student. I have learned so much from his classes and so much more outside of the classroom. Additionally, I would like to thank Dr Hui Wan for his help through this project.

I would like to thank the members of my committee, Dr. Frederick Schauer and Dr. John Hoke, for their patience, time and flexibility. Working with them has given me a true understanding of what it is to be a research scientist. I would also like to thank Adam Brown and Eric Anderson and the rest of the Small Engines Research Labs for allowing me to participate in the data acquisition process.

I would like to thank the members of the Flow Simulation Research Group for all the support that they have provided, especially Sunil Moda and Asela Benthara for helping me learn how to properly use Fluent and everything else they have done to help me.

Finally, I would like to thank my loving and supportive wife Erin and our three children Emma, Jamison and Jaxon for putting up with me through this process and for all the love and support you have given me.

Chapter 1: Introduction

1.1 Statement of Problem

Recently, in the automotive world, there has been a resurrected interest in the use of direct injection spark ignition (DISI) technology in new engines. The theory behind this technology is not new. In the 1920's Swedish engineer Jonas Husselman began injecting fuel in his engines near the end of the compression stroke and igniting it with a spark plug taking advantage of the ultra lean burn principle. His direct injection engines were started with gasoline, but designed to run on heavy fuel oils and, as a result of the technology available at his time, nowhere near as advanced or efficient as their present day counterparts [35]. Use of the technology was expanded to production aircraft during WWII by the German's (Junkers Jumo 210, Daimler-Benz DB 601, both 1937), Soviet (Shvetsov ASh-82, 1943, Chemical Automatics Design Bureau - KB Khimavtomatika) and US (Wright R-3350, 1944) [35]; however, as the jet engine matured, it quickly left the piston engine in its wake. Although, the automotive industry dabble with DISI from the 1950's on through the 1970's, the technology was not present to fully appreciate all the benefits that direct injection has to offer [35].

It was not until recent years, amid higher emission standards, higher gas prices and a desire to get more power from smaller form factors, in which direct injection technology finally began to take off again. With advances ranging from improved electronic control units (processor power, memory, size) to determine the fuel necessary

for given load; to the injectors that delivers the fuel at precisely the right time and conditions without prematurely failing; to the emissions system to deal with the increased emissions, it is now possible to more fully realize the potential of direct injection.

Direct injection is alluring to auto engineers for a couple of reasons: the potential savings from fuel efficiency and the potential performance boost, especially if used in conjunction with a turbocharger or supercharger. Bosch, a German based auto component supplier, estimates that its gasoline direct injection system cuts fuel consumption by 15 percent and can provide up to 50 percent more low-end torque than a comparable indirect injection system [45]. A second efficiency plus for direct injection engines is that they can burn their fuel more completely. In a direct injected spark ignited gasoline engine the fuel can be injected near the spark plug where the combustion chamber is hottest, whereas in a traditional port injected gasoline engine the fuel air mixture disperses widely within the chamber, leaving a substantial amount unburned and therefore ineffective. Additionally, injecting directly into the cylinder allows for a more optimal spray pattern and better droplet break-up which translates to a more complete combustion and more power with less pollution from each drop of gasoline.

In addition to increased fuel efficiency, direct injection allows more accurate control over fuel metering and injection timing. This means that more power can be obtained without injection lag and wasted excess fuel associated with port injection. As an example, Cadillac sells their CTS with the option of direct or indirect injection versions of their 3.6 liter V6 engine. The conventional indirect injection engine produces 263 horsepower and 253 lb-ft of torque. However, the direct injection version delivers an

additional 40 more horsepower (304hp) and more than 20 extra lb-ft of torque (274lb-ft), all while providing one additional city MPG (18 MPG vs 17 MPG) and the same highway MPG.

Furthermore, DISI allows engines to operate on a wider variety of fuels then are possible with current PFI methods [15]. The Cadillac direct injected CTS runs on regular 87 octane gasoline compared to competing luxury cars with similar 300hp V6 engines that require premium fuel. There is even the possibility to run on bio-fuels in addition to the lower octane gasoline. As is usually the case with technologies new to the marketplace, direct injection engines have a higher upfront cost compared to their indirect injected counterparts; however, they make up for it in the long run with better fuel efficiency, more power and flexibility with regard to the types of fuel they can use. Additionally as the technology further matures and demand for DISI engines increase, the upfront cost will begin to decrease closer to that of its indirect injection counterpart.

The possibilities with direct injection are so fruitful that even smaller two stroke outdoor recreation and power sport equipment manufacturers are getting into the direct injection game. Not only does DISI provide them with better fuel efficiency and more power, but it also dramatically decreases the emissions that are notoriously high for two stroke engines [46]. Direct fuel injection is a fuel-delivery technology that allows engines to burn fuel more efficiently, resulting in more power, cleaner emissions, and increased fuel economy.

It seems as though DISI has been resurrected in all areas, save for aviation. Excluding small personal and recreational planes, the aviation industry is dominated by

the use of jet engines. For a majority of the tasks, this is the optimal solution; however, for the military as well as search and rescue applications a jet engine may not be the most advantageous approach. For example, the US Air Force, in order to adapt to changes in the modern battlefield, has begun to employ smaller unmanned air vehicles (UAVs) for many of its missions. Many of these new UAVs utilize small commercial gasoline powered engines that are not necessarily optimized to run as efficiently as they could in their new application. In addition, most are not intended to operate on low octane fuels, such as JP8, that is widely used throughout the Air Force inventory. Operating UAVs on high octane gasoline presents several operational and logistical problems for the Air Force. JP8 is prevalent on most every Air Force base and advanced location, while high octane gasoline may be more difficult to acquire especially in remote locations. Additionally, storing and transporting high octane gasoline can cause the octane levels to deteriorate over time. Therefore by employing DISI in UAV engines, such as the Rotax 914, it affords the Air Force the flexibility it needs in regards to fuel choices while also providing longer flight times and more power with less weight [2].

1.2 BACKGROUND AND RELEVANCE TO PREVIOUS WORK

This project was motivated by research performed by the Flow Simulation Research Group (FSRG) regarding modeling direct injection technology in different engine applications including rotary engines and reciprocating engines such as the Pontiac Solstice. In this work, Gambit 2.4 has been used for modeling and meshing of the complex fluid volumes. To make the high-quality meshes needed to maximally

represent the engine geometry, dynamic layering and local remeshing techniques have been utilized. Motion of the fluid volume is set based on the engine specification. Fluent has been utilized for application of boundary conditions and continuum types as well as for carrying out simulations.

1.3 GENERAL METHODOLOGY AND PROCEDURE TO BE FOLLOWED

Experimental investigations of direct injection engines are limited in their ability to quickly and easily provide data for a parametric study. Computational fluid dynamics (CFD) on the other hand allows one to quickly and easily change parameters including injection location, speed, size, angle and fuel type as well as engine physical properties such as piston pocket size and design without waiting for test specimen modification, assembly, instrumentation and testing. CFD is the method employed in the current study; however, it still needs experimental results to provide kinematical and flow condition data for increased fidelity. Any serious CFD study has to be preceded by a comprehensive validation effort which requires well established experimental data. Thus in the project described here, CFD and experimental results work in close coordination to address the key fluid-dynamical issues. The primary objectives of the CFD effort are to (a) develop a computational model of a PFI Rotax engine (b) validate the model against experiments done over various engine operating conditions, and (c) apply DISI to the

Rotax engine and perform parametric study to understand their different effects on performance.

1.4 Literature Review

A brief literature review was conducted in order to gain a better understand of the current trends in direct injection and computational fluid dynamic modeling of internal combustion engines.

Colucci and associates [1] discussed many of the models available in Fluent for in-cylinder modeling including: the use of moving mesh strategies, spray modeling and combustion modeling. They presented three mesh motion strategies used by Fluent to tackle the task of volume deformation related to in cylinder motion: spring smoothing, local re-meshing, and dynamic layering. Additionally, Colucci described the primary and secondary model for spray atomization. The primary models portray the initial particle conditions to mimic spray from the nozzle (spray angle, nozzle diameter, etc.) while the secondary models represent the effects of spray breakup, collision/coalescence and dynamic drag downstream of the nozzle. Finally, they briefly discuss the partially premixed combustion model as well as the auto-ignition model.

Fritz Bedford et al. [2] analyzed in-cylinder combustion modeling for DISI diesel engine with a previous version of Fluent. They used the results of their simulations to validate the model against experimental data for a Caterpillar 3400 series heavy duty DI diesel engine in order to improve the accuracy of the thermal stress analysis of the engine components. Their work provided a foundation for the selection of the models used in

the simulations presented in this paper. Bedford's discussion on the spark model and autoignition model for knocking provided background used in the implementation of both models. While the correlation reached with experimental results provided confidence in the Ansys Fluent software package used in this project.

Zhao et al. [3] presents an in depth analysis of the gasoline direct injection (GDI) engine in terms of fuel system, combustion chamber, combustion process, fuel economy and emissions. The theoretical advantages of GDI versus PFI provided include improved fuel economy (up to 25% improvement), improved transient response, more precise air-fuel ratio control, extended EGR tolerance limit, emissions advantages and enhanced potential for system optimization. Fuel economy improvements are cited to be a result of: less pumping loss and less heat losses due to unthrottled stratified operation; higher compression ratio, lower octane requirement and increased volumetric efficiency due to charge cooling with injection during induction; and fuel cutoff during vehicle deceleration resulting from elimination of manifold film presence. For PFI engines during cranking and cold starts, fuel is injected that significantly exceeds the ideal stoichiometric ratio. As combustion does not immediately begin on the first crank with PFI, a transient film forms in the intake valve area of the port. This puddling may cause the engine to misfire or experience burn on the first 4-10 cycles resulting in a significant increase in UHC emissions, both of which can be avoided by injecting the charge directly into the combustion chamber. In addition to the vast amount of background offered, Zhao provides an exhaustive study of the recent direct injection technology from most major engine manufacturers (Mitsubishi, Toyota, Ford, etc.).

Yang and Anderson [4] explored the fuel-air mixing in a DISI engine in order to improve the full-load torque output. They discussed the differences between the fuel-evaporation heat source in DISI versus PFI engines. At full-load, for PFI engines, most of the fuel injected contacts the valve and port relying mainly on heat transfer from the hot surfaces for evaporation as backflow of burned gases is minimum. While in contrast, DISI engines use the fine droplets of the injected fuel to absorb thermal energy from the air and cool the charge. Additionally, the fuel injection timing affects the heat transfer rate from the combustion chamber surface to the charge. As fuel is injected early in a DISI engine it more closely mimics the PFI engine by cooling the gas at an earlier time thus increasing the heat transfer from the wall to the gases and reducing the cooling effect of the fuel. While for late injection, the gas temperature is higher so the heat transfer rate from the wall is lower and then the fuel is injected cooling the charge. As a result the gas temperature at ignition will be lower along with the engine's tendency to knock. They compared experimentally two different injection timings for the same DISI engine and saw a decrease in knocking tendency with retarded injection timing and an increase in volumetric efficiency when the fuel was injected and vaporized before the intake valve was closed. While a low mixture temperature for high compression ratio required the fuel be injected as late as possible. Since the two strategies are contradictory, Yang and Anderson investigated the use of a split injection in which a portion of the fuel was injected during the intake stroke to realize high volumetric efficiency and the remaining fuel was injected as late as possible to increase the knock limited spark advance.

Yunlong, Zhi and Jianxin of Tsinghua University further explored the use of a two-stage injection strategy in order to reduce knock by employing a stratified

stoichiometric mixture (SSM) in a DISI engine using both numerical and experimental methods [5]. They explained how the rich mixture near the spark plug increased the speed of the flame propagation, while the lean mixture in the end gas suppressed the auto-ignition tendency of the fuel. Furthermore, by keeping the overall mixture stoichiometric a three way catalyst (TWC) could be used to solve the emissions problem. They found the two-stage injection SSM suppressed the knocking tendency significantly while gradually decreasing the knocking intensity with an increase in the second fuel mass or retarding of the second injection. Additionally, the combustion rate increases and the phase advances when the rich zone becomes homogeneous while the combustion rate decreases, the phase retards and peak pressure and pressure rise rate decrease when the rich zone is not homogeneous. Finally, SSM results in a smaller decrease of power output when compared to the method of retarding the spark timing for knock suppression as well as better fuel economy and total emissions than burning an over-rich air-fuel mixture.

The Orbital Engine Company has done extensive research in the field of DISI engine starting more than ten years before the release of their 2-stroke marine and automotive applications in 1996 [6]. Cathcart [7] presents three main types of direct injection: wall guided in which the piston bowl reflects/guides the injected fuel to the spark plug; charge motion/air guided where the swirl and tumble motion of the charge inside the cylinder directs the fuel towards the spark plug; and spray/jet guided in which fuel is sprayed directly to the spark plug location (see Figure 1.4.1). The former two methods are mainly used for single fluid (fuel only) injection and result in longer

preparation time for the fuel. However, air-assisted fuel systems make use of two fluid (air and fuel) injection and as a result do not require increased preparation time.

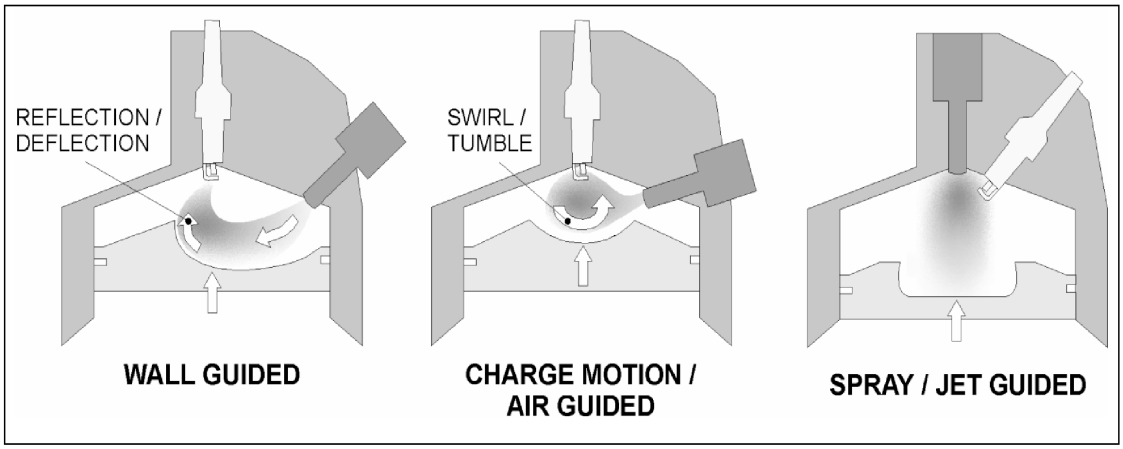

Figure 1.4.1 Direct Injection Combustion Systems [7]

The Orbital combustion process (OCP) is based on the combination of a low pressure air-assisted fuel injection system with a spray guided combustion system. This air-assisted injection system is characterized by very small droplet sized, low penetration rates and diffuse sprays, which is ideally suited for spray guided combustion. This type of combustion does not rely on bulk air motion to assist the ignitability of the injected fuel or burn quality, but rather the reduction in tumble flow has an improvement in the stratification process resulting in improved fuel economy at part load stratified operation [7]. The fuel system consists of a solenoid actuated outwardly opening direct injector that delivers the fuel-air charge directly into the combustion chamber. Fuel is metered separately into the top of the injector by a conventional multi-port fuel injector. The rate of fuel delivery can be altered by adjusting the delay between the end of the fuel metering and the start of the fuel-air injecting event dramatically reducing the air/fuel ratio gradients near injection timing resulting in improved robustness [Houston & Zavier].

The resultant spray is highly atomized with Sauter Mean Diameter (SMD) of less than 8 microns in the main spray versus 27 microns or more with high pressure single fluid injection. This highly atomized spray leads to very fast evaporation of the fuel, lessening the need for further preparation time in the cylinder. In addition, this air-assisted system operates at relatively low pressures (~6.5 bar gauge) when compared to single fluid systems (~60-200 bar).

Cathcart and Tubb [8] build upon the success realized with naturally aspirated operation and explore the OCP's ability to operate under boosted conditions. Specifically, they discuss low part load operation, high part load operation and mid to high part load operation. For low part load operation the inlet manifold pressure becomes less then atmospheric and as a result the compression pressures are very similar to the naturally aspirated engine. For high to full load operation, the inlet manifold is boosted above atmospheric and the cylinder pressure is increased throughout the cycle as compared to naturally aspirated. In these conditions, the engine is operated in homogeneous combustion mode with early injection timing during the intake stroke. However, for mid to high part load operation there may be the option of boosting the engine in order to increase the lean operating region. In this situation, the cylinder pressure is above that of naturally aspirated and poses a potential challenge for low pressure air-assisted injection. However, through testing, it was found that the increased dilution level from boosting the inlet manifold resulted in an additional reduction in fuel consumption when compared to stoichiometric operation while maintaining acceptable emission levels.

Payri et al. [9] investigated the three-dimensional flow calculations of the intake and compression stroke of a four-valve direct-injection engine with different combustion chambers. Validation calculations were performed to explore the limits of the CFD representation of the in-cylinder flow and compared with laser Doppler velocimetry measurements. It was shown that the piston geometry had little influence on the in-cylinder flow during the intake stroke and the first part of the compression stroke. Although, it was revealed that near TDC and early in the expansion stroke the piston shape played a large role in both the ensemble-averaged mean and the turbulence velocity fields.

Cao et al. examined the effects of injection timing and piston bowl geometry on PCCI combustion and emissions [10]. They observed that the earlier the ignition timing, the more homogeneous the mixture as a result of the longer residence time for the air-fuel mixing. For the most advanced injection, the fuel rich mixture was formed at the upper edge of the piston bowl with relatively low temperature as a result of charge cooling. Additionally, lean mixtures with higher temperatures were found near the center and bottom of the piston bowl. Cao explored three different combustion chamber geometries: open bowl, vertical side wall bowl and re-entry bowl. The volume and depth of each bowl was kept constant to maintain the compression ratio. Less fuel was observed to be distributed in the center of the re-entry bowl due to the evaporation of the fuel before the transition point. More of the charge fell in the lean range for the re-entry bowl compared to the other two. The open bowl produced the most stratified mixture with only a small percentage of the charge in the 0.8 to 1.2 equivalence ratio range which resulted in the highest CO emissions. Whereas the re-entry bowl produced the highest UHC and lowest

NO emissions. The vertical side wall bowl produced the lowest combined CO and UHC emissions.

Papageorgakis and Assanis [11] discussed direct injection technology of gaseous mixtures, with the goal of optimizing performance with respect to fuel economy and emissions. They used KIVA-3 with the renormalization group theory (RNG) k-ε model to perform a parametric study to explore the effects of crown shape, injector targeting, glow plug presence, injection velocity, injection timing, number of injector holes, and initial swirl ratio on combustion and emissions. Three different crown shapes including flat piston, bowl-in piston and Mexican-hat piston shapes were investigated. Four different angles for injector holes with respect to horizontal (5°, 15°, 30°, 45°) were evaluated for mixture stratification. The presence of a glow plug was discussed only to see its effects on global mixing with optimized placement or operation outside of the scope of the paper. Three different injection velocities (300, 500 and 700 m/s) were analyzed to determine how the associated turbulence affected mixing. Three injection timings were evaluated: 25° bTDC (baseline), 40° bTDC and 10° bTDC to determine timing effects on combustion. Three hole configurations: four, eight and sixteen holes, were examined to determine how the number of holes affected injection. Finally, the ratio of angular velocity of air over engine crankshaft angular velocity, initial swirl ratio (ISR), was examined with four ISR values selected (0, 1, 2, 3). It was determined that the Mexican-hat piston performed the best with 45° injection with respect to horizontal. Additionally, higher injection velocities increased the turbulence resulting in better mixture preparation. Furthermore, fuel injected earlier during the compression stroke

aided the mixture preparation. Eight holes in the injector proved most effective for constant total amount of fuel injected per cycle. Finally, higher initial swirl ratios resulted in more angular momentum of the ambient air and a decrease in mixing effectiveness.

In 1997, David Falkowski et al. published a paper [13] discussing the use of kerosene based aviation fuel in a SI stratified-charge two stroke engine. Experimentally they were able to operate the engine on multiple fuels due to the stratified-charge combustion behavior. Knock was detected and limited the engine operation to one-half fuel delivery. An investigation was done to decrease or eliminate the knock at the lowest cost to engine performance utilizing spark timing, air injection timing, exhaust port timing and decreasing the fuel spray angle. Retarding the spark timing caused the knocking condition to disappear; however, it cost 6% in break torque. Increasing the exhaust valve position decreased the knock by lowering the effective compression ratio, decreasing the amount of piston work done on the charge during compression. It also more effectively clears out the exhaust gasses in the cylinder, cooling the cylinder and scavenges more hot active radicals out of the exhaust, yet it costs 10% in break torque. Knock intensity was decreased by retarding the air injection into the cylinder; however, this method decreased the brake torque by 13%. Reducing the cone angle of the fuel spray from 80° To 20° reduced the knock intensity while only lowering the brake torque by 2.5%. Retarding the spark timing was the only method that completely eliminated the knocking condition, although at a considerable cost of performance.

Singh and McChesney investigated the performance of a rope start two-stroke outboard engine, capable of running on multiple fuels with a primary focus on JP-5/8 [14]. Additional fuels were studied as well including gasoline, diesel, kerosene, etc. while concentrating, among other things, on power, torque, effects of compression pressures on combustion characteristics, detonation characteristics and behavior in stratified and/or homogeneous combustion. The study showed little performance difference between JP-5 or JP-8. Kerosene and diesel showed some resistance to idling, while JP -5/8 showed no problems starting or idling. The spark plug fouling time increased as the compression pressure decreased in the engine as well as with the addition of a wasted spark at BDC. There was little change in torque and power between grades of fuels once the engines were calibrated for that specific fuel. JP-5/8 had the same combustion speed as gasoline, but the same characteristics for combustion as diesel. Kerosene had the most frequent heavy knocking and while JP-5/8 did exhibit knocking, it was infrequent and non-destructive.

1.5 Thesis Outline

This project consists of two main sections. The first section discusses how the computational model is developed and validated, while the second section explores the use of DISI technology within the Rotax 914 engine for different operating conditions.

In the second and third chapters, a computational model of a DISI engine based on the Rotax engine is developed. The process for going from the physical engine to the computational engine is explained in detail. Additionally, the computational models that

are used to represent the complex intake, injection, combustion and exhaust processes are discussed. To computationally model the combustion process of the Rotax engine, Gambit was employed for geometry generation and meshing, while Fluent was used for fluid flow and combustion simulation. Next, experimental results are presented along with analogous computational simulations. Finally, the computational simulations are compared with the experimental results in order to confirm the validity of the computational model.

In the second phase, the computational model will be extended to study the effects of DISI while performing a parametric study in order to understand the different effects on performance of the Rotax engine in this mode. Chapter 4 looks at the current, flat piston, configuration of the Rotax 914 engine, while Chapter 5 replaces the flat piston with a bowl type piston to study the advantages of advanced piston design.

Chapter 2: Computational Modeling

2.1 Modeling and Meshing

2.1.1 Modeling

In order to investigate the complex physics and fluid interactions that occur in a spark ignition engine, a model was created that would computationally simulate the Rotax 914 engine over varied engine conditions. The software package used to carry out the computational simulations, Ansys Fluent, required a starting volume mesh and description of the motion of moving zones within the model, thus necessitating extra steps to prepare the model before simulation could be begin. The process of creating the Fluent model began by creating a SolidWorks mock-up of the Rotax engine from a 3D scan of the actual engine, provided by Innovative Scientific Solutions Inc (ISSI). From this model, an ".igs" file was produced and imported into Gambit 2.4 to be used for modeling and mesh creation of the complex fluid volumes of the engine. This allowed for an accurate recreation of the physical engine in the computational domain. Figures 2.1.1(a-d) shows pictorially the different steps involved in this process. Figure 2.1.1 (a) shows the cylinder head and piston from an actual engine similar to the one used for creating the computational model. While there is a cut through the center of the cylinder head pictured, this was done for analysis by ISSI and not present in the part used for creating the computational model. Figure 2.1.1 (b) shows the SolidWorks assembly for the engine made from the 3D scans of the engine. Each part was modeled in SolidWorks individually and then assembled for this picture. Figure 2.1.1 (c) shows the complete

mesh created from the imported SolidWorks model. Figure 2.1.1 (d) shows the final Fluent model of the engine ready for simulation.

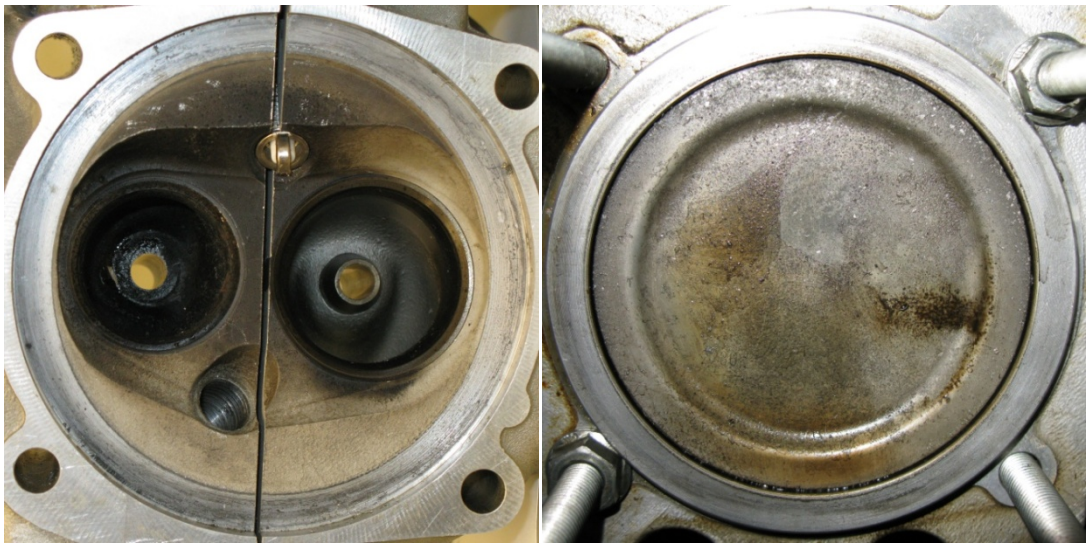

Figure 2.1.1 (a) Rotax 914 Engine Cylinder Head (left) and Piston (right)

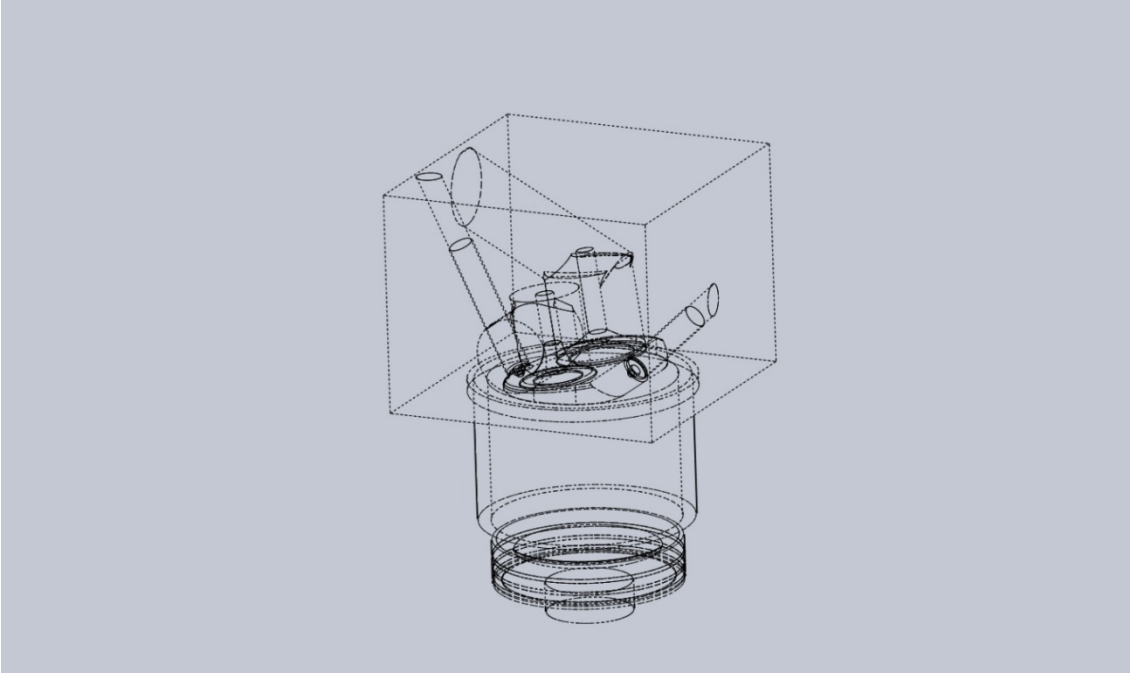

Figure 2.1.1 (b) SolidWorks Assembly of Rotax Engine

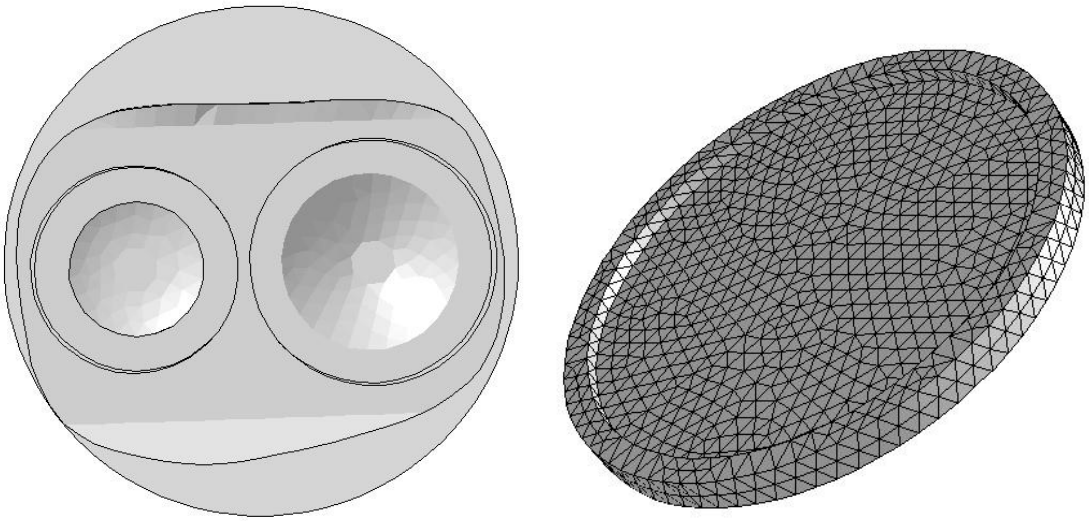

Figure 2.1.1 (c) Complete Gambit Mesh of Rotax 914 Cylinder Head (left) and Piston (right)

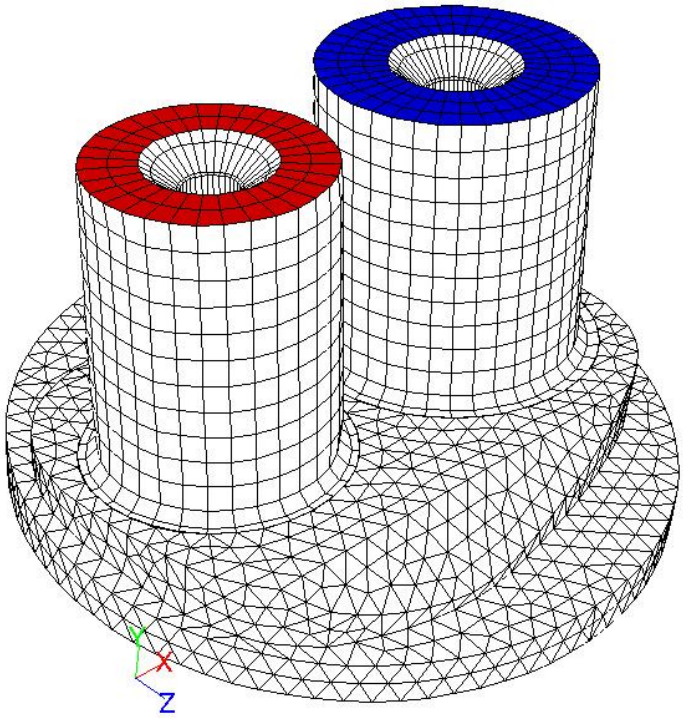

Figure 2.1.1 (D) Final Fluent Model of Rotax 914 Engine

In order to facilitate meshing, the geometry first had to be refined. The model that was imported into Gambit had several small faces and gaps that needed to be simplified and smoothed in order to avoid problems during mesh creation and ultimately during simulations. Figure 2.1.2 shows the SolidWorks model as it is first imported into Gambit. Each of the dots represents the junction of two lines that need to be simplified for the mesh to operate more efficiently.

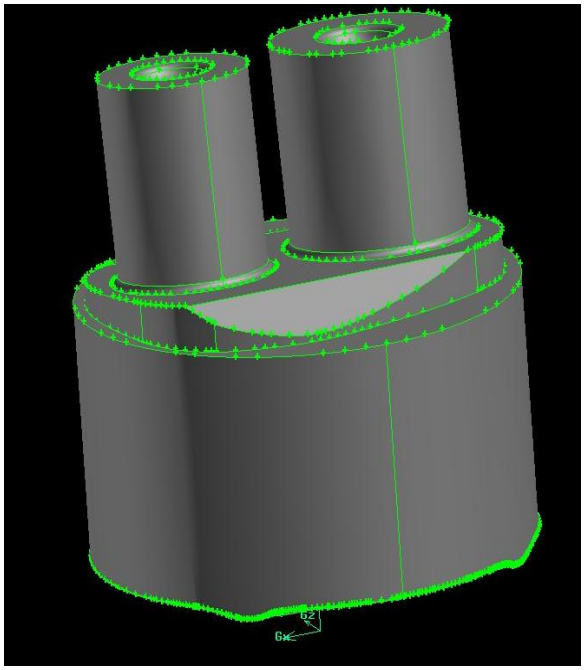

Figure 2.1.2 SolidWorks Model in Gambit Before Clean-up

Several new faces and volumes were created, meshed and finally refined until the max cell skewness was within acceptable limits. When applying the mesh it is essential to always check for highly skewed elements. The closer the skewness is to zero the better, but a value of 0.9 or lower can be considered a good mesh; however, the skew should not exceed 1. Depending on the location, it may be necessary to eliminate highly skewed elements. This is especially critical if the element is in a dynamic mesh zone as

this region needs to be meshed with as little skew as possible to ensure a fast and accurate simulation. The dynamic mesh model will move boundaries or objects and then adjust the mesh accordingly. This is well suited for boundaries that move rigidly with respect to each other, such as the motion of the piston with respect to the engine cylinder.

2.1.2 Meshing

After the model is satisfactorily refined, it is still not yet ready for meshing. The model contains several distinct regions with different boundary conditions and fluid interactions. Each of these areas must be meshed separately to allow for an accurate model of each region and application of boundary conditions later in Fluent. In doing so, the complete geometry must be divided into smaller volumes. The quality of the mesh in each sub volume must be maintained as to not affect the overall quality of the entire mesh when they are joined together. Figure 2.1.3 shows how the intake and exhaust valve areas are separated from the rest of the cylinder.

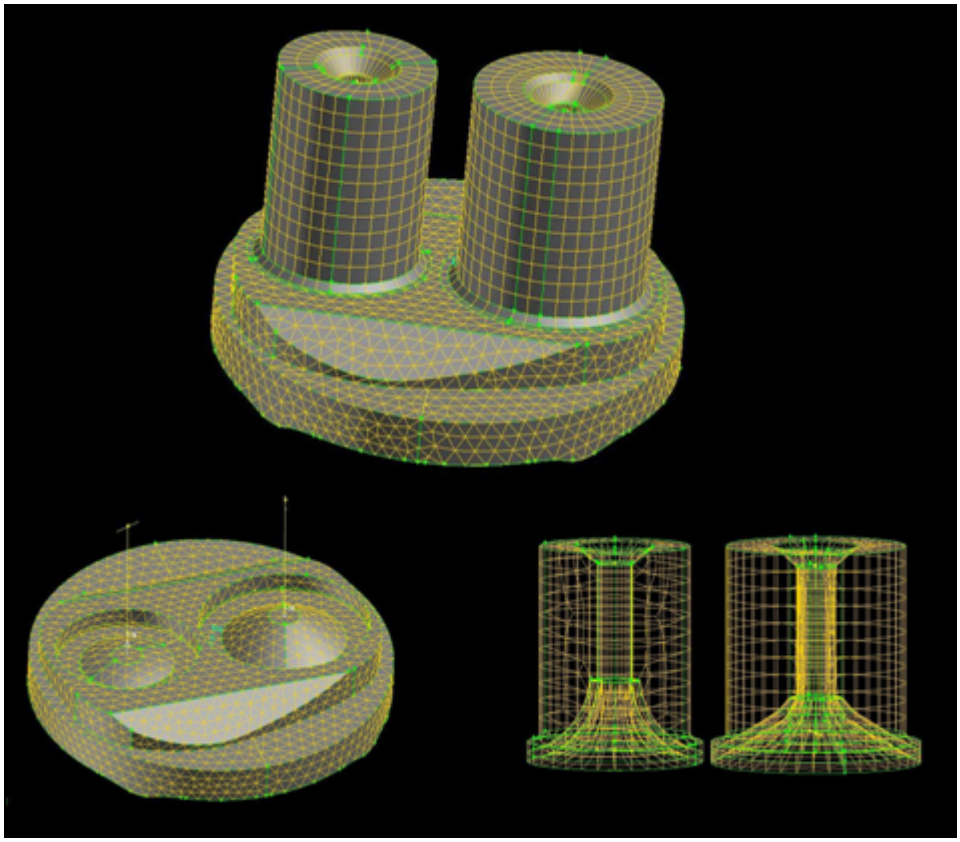

Figure 2.1.3 Shows the Valve Area Separated from the Cylinder

The first step was to set up the mesh for the moving parts of the model. To begin the intake and exhaust valves were separated from the main geometry. A new volume was created at the bottom part of each valve near their junction with the cylinder. These new volumes were converted into a dynamic mesh zone while the top of the valve remained a rigid mesh zone. When the valve moves only the mesh inside the dynamic mesh zone is regenerated with respect to the motion of the valve. This allows for the accurate modeling of the interaction that occurs between the fluid moving in or out of the engine and the valve itself. The top volume remains rigid, as there is minimal dynamic interaction between the boundaries and the fluid region. The use of both dynamic and

rigid mesh zones allows the simulation to run faster with less mesh errors and better accuracy.

The exhaust valve is shown in figure 2.1.4, as an example of this process. The valve is divided into four volumes in which volumes A1 and A2 are sub volumes of the top rigid volume (A), while volumes B1 and B2 are sub volumes of the bottom moving volume (B). The volumes are meshed individually and then joined together to form the complex mesh of the exhaust valve. This process is then repeated for the intake valve.

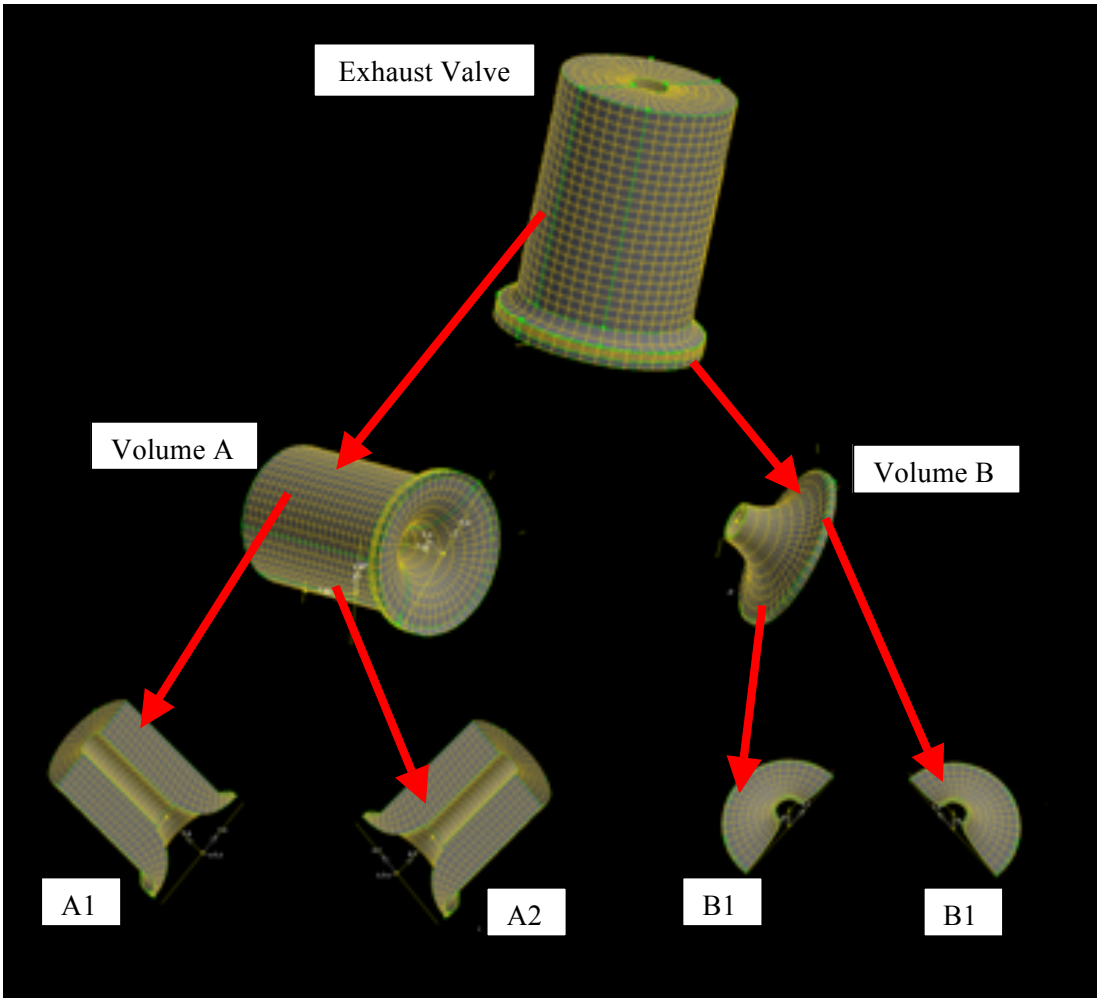

Figure 2.1.4 Exhaust Valve Meshing Process

Figure 2.1.5 (a) shows the completed computational mesh for the original condition Rotax 914 engine before it is imported into Fluent to set up boundary conditions, continuum types and mesh motion. Figure 2.1.5 (b) shows the computational mesh for the Rotax 914 engine with a modified "bowl" type piston that will be discussed further in Chapter 5.

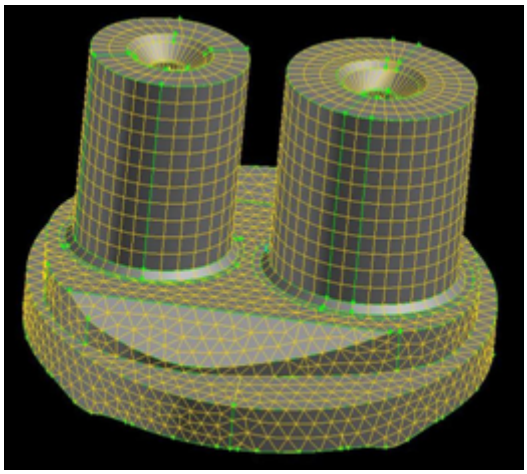

Figure 2.1.5 (a) Completed Computational Mesh of Flat Piston Rotax 914

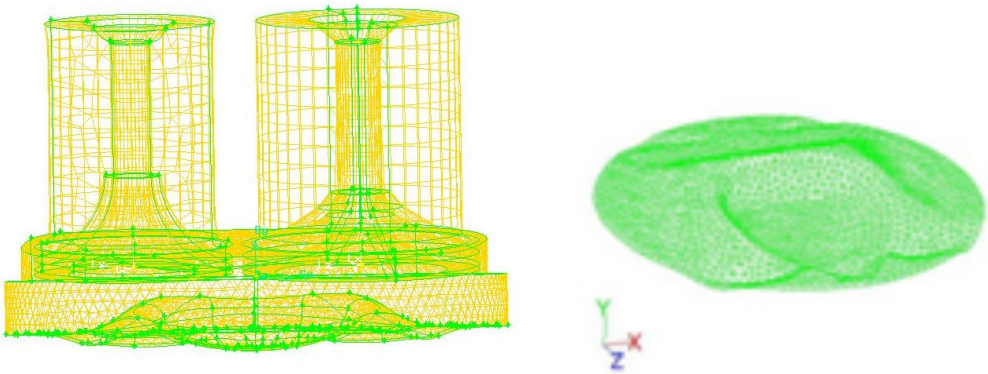

Figure 2.1.5 (b) Completed Computational Mesh of Bowl Piston Rotax 914 & Piston

2.1.3 Boundary Conditions

The dynamic mesh motion is defined by the behavior of each volume and sub volume mesh. In Gambit, each mesh is assigned a name based on its location and function that will be used by Fluent to activate specific motion, such as opening or closing a valve. In addition to its name, the properties of each mesh are also assigned. For example, the cylinder wall is named cylinder and assigned a stationary mesh. The area between the valve and cylinder is designated as a pressure outlet and assigned a deforming mesh. The piston is considered a surface with a deforming mesh. Each zone is defined by a continuum type, boundary condition and type of motion. These are essential to creating a well defined mesh motion that will be readily used in the Fluent simulation. Figure 2.1.6 shows the different boundary conditions and continuum types used for the intake valve area. The same conditions are used for the exhaust with "exhaust" replacing "intake" in the naming convention. While figure 2.1.7 shows the different boundary conditions and continuum types used for the cylinder.

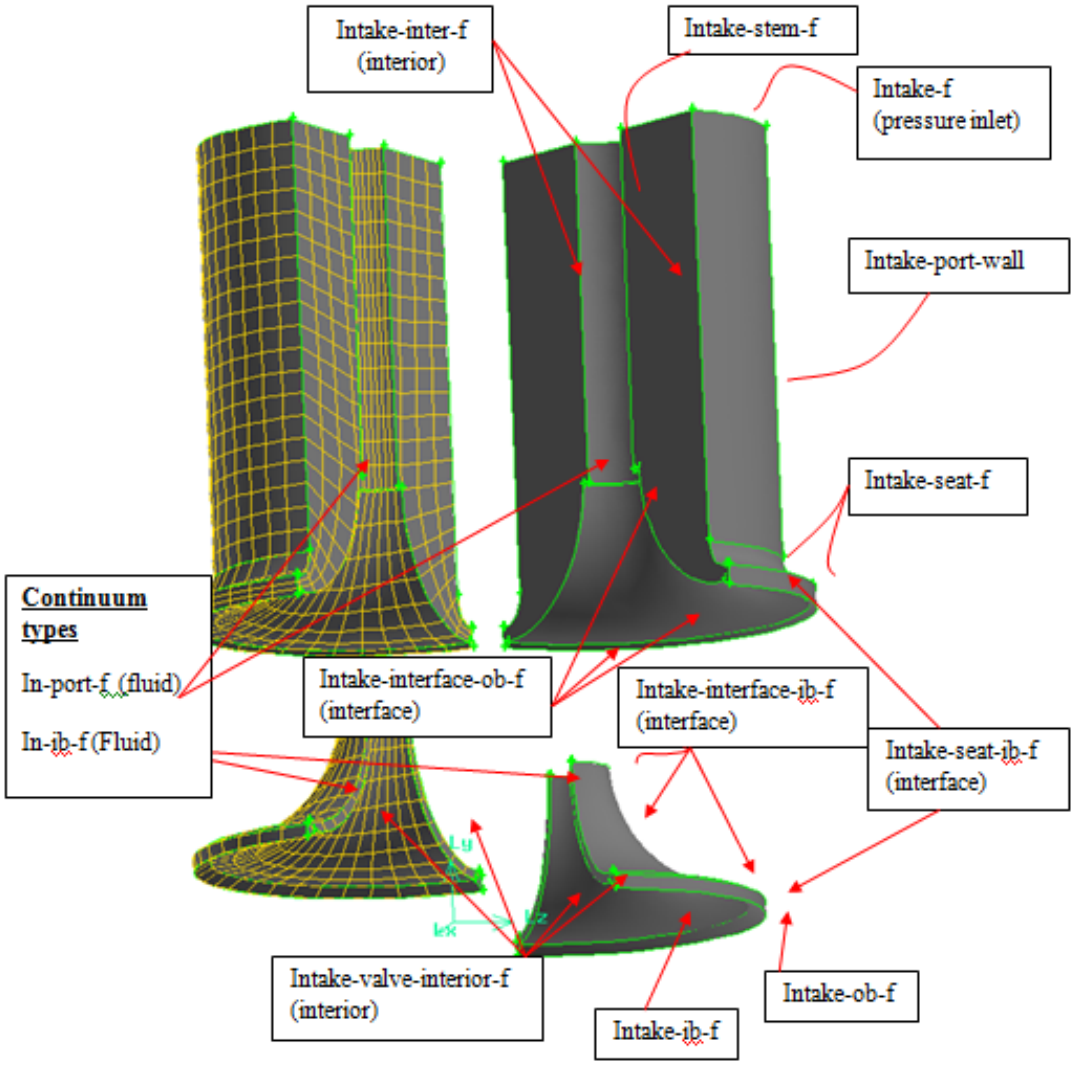

Figure 2.1.6 Intake Valve Area Boundary Conditions and Continuum Types

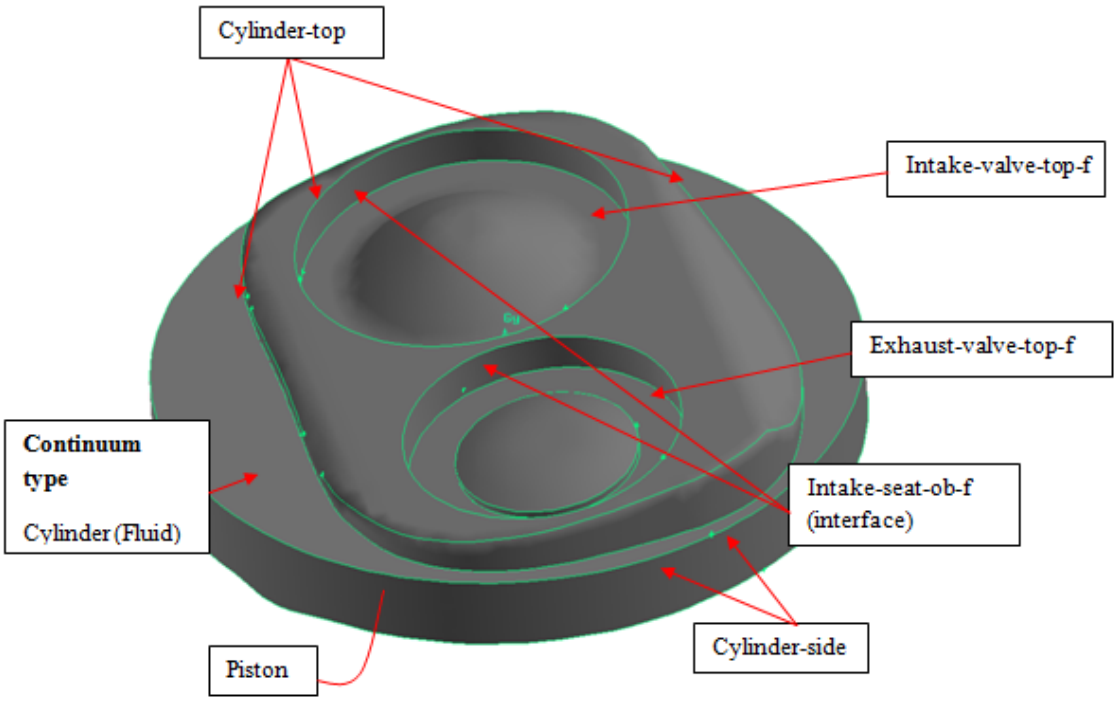

Figure 2.1.7 Rotax 914 Cylinder Head

Three mesh motion strategies are employed to tackle the task of volume deformation related to in cylinder motion: spring smoothing, local re-meshing, and dynamic layering. When a boundary displacement within a mesh volume is large, individual cell quality can deteriorate which can lead to accuracy and convergence issues. As a result Fluent can be made to locally re-mesh these problem areas as well as faces on deforming boundary layers to maintain compatibility with changing internal volume mesh. This technique along with spring smoothing was used in the upper portion of the combustion chamber, while layered elements reside between this tetrahedral mesh zone and the piston. In addition, dynamic layering allows for Fluent to handle the opening and closing of the valves. Cell layers are removed as the valve approaches the closed

position; however, the final layer is not allowed to collapse to zero volume. Rather, the valve motion stops at a given tolerance and the port and chamber are disconnected by deactivating the intake/exhaust area.

Tables 2.1.1 shows the boundary conditions used to define the model within Gambit. These will be used in fluent to set the different boundary conditions, for example the intake pressure inlet allows for the application of different manifold pressures upstream of the cylinder. Table 2.1.2 lists the continuum types assigned in Gambit and used in Fluent for defining fluid regions and interaction areas.

Table 2.1.1 Boundary Conditions

Name	Boundary Condition
Intake-seat-ib	interface
Exhaust-seat-ib	interface
Intake-valve-interior	interior
Exhaust-valve-interior	interior
Intake-interface-ib	Interface
Exhaust-interface-ib	Interface
Intake-interface-ob	Interface
Exhaust-interface-ob	Interface
Exhaust-ob	wall
Exhaust-ib	wall
Intake-ob	wall
Intake-ib	wall
Intake-seat	wall
Exhaust-seat	wall
Intake-port-wall	wall
Exhaust-port-wall	wall
Intake-inter	interior
Exhaust-inter	interior
Intake-stem	wall
Exhaust-stem	wall
Intake	pressure inlet
Exhaust	pressure outlet
Intake-seat-ob	interface
Exhaust-seat-ob	interface
Cylinder-top	wall
cylinder-side	wall
Intake-valve-top	wall
Exhaust-valve-top	wall
Piston	wall

Table 2.1.2 Continuum Type

Name	Continuum Type
In-port-f	fluid
In-port-b	fluid
Ex-port-f	fluid
Ex-port-b	fluid
In-ib-f	fluid
In-ib-b	fluid
Ex-ib-f	fluid
Ex-ib-b	fluid
cylinder	fluid

Once the boundary condition and continuum types are set, the model is exported to Fluent where the final mesh motion is defined based on the real engine motion. The constant motion of the piston throughout the cycle necessitated the use of moving dynamic mesh (MDM). This technique constantly rebuilds the grid as the piston moves into a new position at each time step in the simulation. Figure 2.1.8 (a-e) shows the motion of the model through two crank rotations.

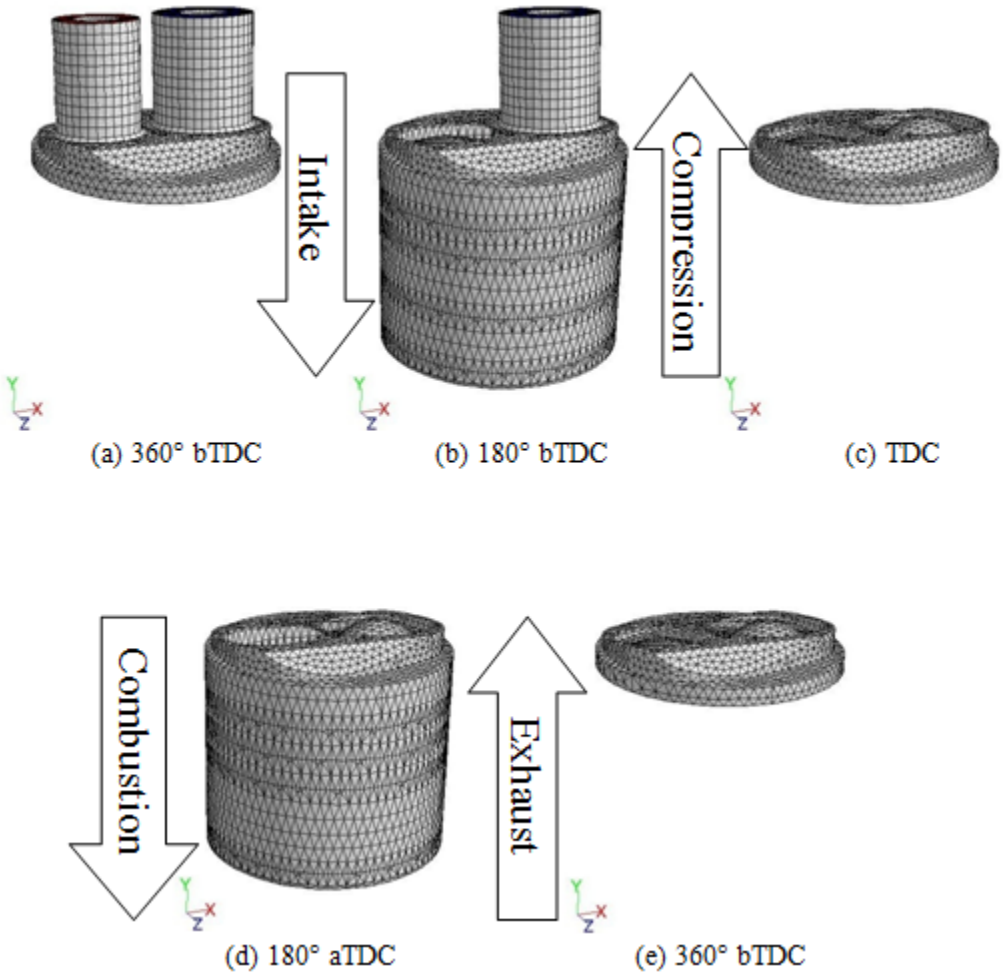

Figure 2.1.8 Mesh Motion of Model

2.2 Computational Models

The computational models presented in this section are all built into the Ansys Fluent software package; however, it is prudent to expound on their attributes before continuing on to the simulations.

2.2.1 Turbulence Models

Fluent provides many different options for turbulence modeling; however, for this situation, the k-ε models provide a good basis for analysis. These models are fairly inexpensive in terms of computation; however, they provide a more accurate turbulence computation then the less expensive single equation Spalart-Allmaras model [21].

By employing two equations, the k-ε models represent a simple "complete model" of turbulence by solving two separate transport equations allowing velocity and length scales to be determined independently. The standard k-ε model falls within a class of models that have been the workhorse of practical engineering flow calculations since it was proposed by Launder and Spalding [16]. It is a semi-empirical model that is based on model transport equations for the turbulent kinetic energy (k) and its dissipation rate (ε). The model equation for k was derived from the exact equation whereas the model equation for ε was obtained using physical reasoning. It is well-known for its robustness, economy and reasonable accuracy for a wide range of turbulent flows. Assumptions for this model include: flow is fully turbulent as well as effects of molecular viscosity being negligible. As strengths and weaknesses of the standard k-ε model have become

identified, advances have been made to the model in order to improve its performance. Two variants of the standard k-εmodel are available in Fluent: the RNG k-εmodel [17] and the realizable k-εmodel [18].

The RNG k-ε model uses renormalization group theory to analytically derive a more accurate and reliable equation for a wider class of flows than the standard k-ε model. RNG has an additional term in its equation for ε that significantly improves the accuracy for rapidly strained flows. The effect of swirl on turbulence is included in RNG model enhancing accuracy for swirling flows. The RNG theory provides an analytical formula for turbulent Prandtl numbers, while the standard model uses user-specified, constant values. While the standard model is a high Reynolds number model, the RNG theory provides an analytically derived differential formula for effective viscosity that accounts for low Re-effects [17]. However, due to the extra terms and functions in the governing equations and a greater degree of non-linearity, computations with the RNG k-ε model tend to take more CPU time than the ones with the standard k-ε model. In contrast the realizable k-ε model requires only slightly more computational effort than the standard k-εmodel while providing additional benefits. Therefore, the realizable k-ε model was used for these simulations.

The realizable k-ε model includes new formulation for the turbulent viscosity and the dissipation rate. The term *realizable* means that the model satisfies certain mathematical constraints on the Reynolds stresses, consistent with the physics of turbulent flows. Realizable k-ε model gives a more accurate prediction of the spreading

rate of both planar and round jets than the standard k-ε model. Also it is likely to provide superior performance for flows involving rotation, boundary layers under strong adverse pressure gradients, separation, and recirculation. This model differs from the standard model in two important ways. The realizable model contains new formulation for the turbulent viscosity. A new transport equation for the dissipation rate, ε, has been derived from an exact equation for the transport of the mean-square vorticity fluctuation [18].

2.2.2 Combustion Models

Fluent utilizes five different methods for modeling species transport and combustion including: species transport; non-premixed combustion; premixed combustion; partially premixed combustion; and composition PDF transport. Species transport, as the name suggests, models the mixing and transport of chemical species by solving conservation equations describing convection, diffusion, and reaction sources for each component species [33]. The spark model is not available in species transport and thus not a good choice for this specific application.

For the case of non-premixed combustion, fuel and oxidizer enter the combustion chamber in distinct streams. The solution of transport equations for one or two conserved scalars (the mixture fractions) is computed, while equations for individual species are not solved. Instead, species concentrations are derived from the predicted mixture fraction fields. The thermochemistry calculations are preprocessed and tabulated for look-up with an assumed-shape Probability Density Function (PDF) [33]. Spark ignition is an option for non-premixed combustion; however, one must balance energy input and diffusivity to

produce a high enough temperature to initiate combustion, which is a nontrivial undertaking.

In contrast, for premixed combustion modeling the reactants are mixed at the molecular level prior to ignition. Combustion then occurs when the flame front propagates into the unburnt reactants. Premixed combustion is much more difficult to model than non-premixed combustion due to the fact that premixed combustion usually occurs as a thin, propagating flame that is stretched and contorted by turbulence. For subsonic flows, the overall rate of propagation of the flame is determined by both the laminar flame speed and the turbulent eddies. The laminar flame speed is determined by the rate that species and heat diffuse upstream into the reactants and burn. To capture the laminar flame speed, the internal flame structure would need to be resolved, as well as the detailed chemical kinetics and molecular diffusion processes. However, practical laminar flame thicknesses are of the order of millimeters or smaller and therefore resolution requirements are usually much too costly computationally. While premixed combustion may be adequate for a normally aspirated engine, direct injection requires the fuel be added separate from the air charge and as a result, premixed combustion in not a sufficient model.

The partially premixed model is a simple combination of the non-premixed model and the premixed model. It entails the use of premixed flames with non-uniform fuel-oxidizer mixtures (equivalence ratios). The premixed reaction-progress variable determines the position of the flame front. Ahead of the flame front, the species mass fractions, temperature, and density are calculated from the mixed yet unburnt mixture

fraction. Behind the flame front, the mixture is burnt and the laminar flamelet mixture fraction solution is utilized. While within the flame, a linear combination of the unburnt and burnt mixtures is applied. The partially premixed model incorporates the same underlying theory, assumptions, and limitations of both the non-premixed and premixed models. In particular, the single-mixture-fraction approach is limited to two inlet streams, which may be pure fuel, pure oxidizer, or a mixture of fuel and oxidizer. This is good for both direct injection, the focus of this study, as well as port injection, used for validating the computational model. Furthermore, the premixed models require the laminar flame speed that depends strongly on the composition, temperature, and pressure of the unburnt mixture. For adiabatic perfectly premixed systems, the reactant stream has one composition, and the laminar flame speed is constant throughout the domain. However, in partially premixed systems, the laminar flame speed will change as the equivalence ratio changes [33]. Additionally, partially premixed combustion makes available a spark model that is utilized to simulate the spark plug in the Rotax engine. The spark model will be further discussed in the next section.

2.2.3 Spark Ignition

Generally, a spark begins the combustion at a desired time and location in the combustion chamber of a spark ignited (SI) internal combustion engine. The spark is usually created by sending a high voltage across two narrowly separated wires in a spark plug. When compared to the main combustion, the spark event typically happens very quickly with energy levels several orders of magnitude less than the chemical energy released from the fuel. Yet, the physical description of this simple event is very involved

and complex, making it difficult to accurately model in the context of a multidimensional engine simulation. Despite the amount of research devoted to spark ignition physics and ignition devices, the ignition of a mixture at a point in the domain is more dependent on the local composition than on the spark energy [15]. Thus, the spark event does not need to be modeled in great detail, but simply as the initiation of combustion over a given duration at a specified location. The Spark Model used by Fluent is based on a one-dimensional analysis by Lipatnikov [19].

The model is sensitive to perturbations and can be subject to instabilities when used in multi-dimensional simulations. The instabilities are inherent to the model and can be dependent on the mesh, especially near the beginning of the spark event when the model reduces diffusion to simulate the initial laminar spark kernel growth. The instability is susceptible to numerical errors which are increased when the mesh is not aligned with the flame propagation. As the spark kernel grows and the model allows turbulent mixing to occur, the effect of the instability decreases.

2.2.4 Autoignition

Autoignition phenomena in engines are due to the effects of chemical kinetics of the reacting flow inside the cylinder. Fluent considers the following two types of autoignition models: knock model in SI engines and ignition delay model in diesel engines.

The concept of knock defines a limit in terms of efficiency and power production of premixed engines and as a result has been studied extensively [23]. The efficiency of the engine, as a function of the work extracted from the fuel, increases as the compression ratio increases. However, as the compression ratio increases, the temperature and pressure of the air/fuel mixture in the cylinder also increase for the duration of the compression cycle. If the temperature and pressure increase is large enough, the mixture will spontaneously ignite and release its heat before the spark plug fires or before the flame front propagates through that portion of the cylinder. The premature release of all of the energy in the air/fuel charge is almost never desirable, and as a result the spark event no longer controls the combustion. As a result of the premature release of the energy, catastrophic damage to the engine components can occur. The sudden, sharp rise in pressure inside the engine can be heard clearly through the engine block as a pinging or knocking sound, hence the term "knock" [15]. For commonly available pump gasoline, knock usually limits the highest practical compression ratio to less than 11:1 for premium fuels and around 9:1 for lower octane fuels.

By comparison, ignition delay in diesel engines has not been as extensively studied as SI engines, mainly because it does not have such a sharply defining impact on engine efficiency. Ignition delay in diesel engines refers to the time between when the fuel is injected into the combustion chamber and when the pressure starts to increase as the fuel releases its energy. The fuel is injected into a gas which is usually composed entirely of air; however, it can have a considerable amount of exhaust gas (EGR) mixed in to reduce nitrogen oxide emissions (NOx). Ignition delay depends on the composition

of the gas in the cylinder, the temperature of the gas, the turbulence level, and other factors. Since ignition delay changes the combustion phasing, which in turn impacts efficiency and emissions; it is important to account for it in a diesel engine simulation [23].

The main difference between the knock model and the ignition delay model is the manner in which the model is coupled with the chemistry. The knock model always releases energy from the fuel while the ignition delay model prevents energy from being released prematurely. The knock model in Fluent is compatible with the premixed and partially premixed combustion models. The autoignition model is compatible with any volumetric combustion model, with the exception of the purely premixed models. These models are inherently transient and as such are not available with steady simulations. In general, they require adjustment of parameters to reproduce engine data and require tuning to improve accuracy. Once the model is calibrated to a particular engine configuration, then different engine speeds and loads can be reasonably well represented. Detailed chemical kinetics may be more applicable over a wider range of conditions, though are more expensive to solve.

2.2.5 Injections

Fluent provides several types of injectors including: single, group, solid-cone, surface, etc. For these simulations solid-cone was selected as it effectively mimicked that of a typical fuel injector. Based on the injector type, several more parameters must be

fully define in order to proceed with injection. The particle type used in this simulation is droplet particle which is a liquid droplet in a continuous-phase gas flow that obeys the force balance and that experience heating/cooling followed by vaporization and boiling. The droplet type is available when heat transfer is being modeled and at least two chemical species are active or partially premixed combustion model is active. The ideal gas law is used to define the gas-phase density when droplet type is selected. Distribution for particles in the injection is defined by the Rosin-Rammler distribution model. This provides for more variation when compared to the uniform distribution model. The minimum, maximum and mean diameters of particle sizes are defined as well as the spread parameter and number of diameters in addition to the initial velocity, temperature, and total flow rate for the injector. The wave breakup model [20] is used to model spray atomization for these simulations. It is chosen, as opposed to the Taylor Analogy Breakup (TAB) model, because it more accurately predicts spray droplet sizes [21]. Essentially, the wave model assumes that the drop parcels are the same sized as the nozzle exit diameter and breakup occurs once the waves on the drop surface become unstable. The breakup time is governed by local conditions, physical properties of the liquid and gas and injector characteristics.

2.2.6 Solver Settings

Pressure-velocity coupling is utilized in order to derive an additional condition for pressure by reformatting the continuity equation. The pressure-based solver allows for the problem to be solved in either a segregated or coupled manner. Fluent offers five

methods for pressure-velocity coupling: SIMPLE, SIPMLEC, PISO and Fractional Step Method (FSM) make use of the segregated algorithm; while the Coupled scheme is based on the coupled solver. All of these methods, except the Coupled scheme, are based on the predictor-corrector approach.

The SIMPLE (semi-implicit method for pressure linked equations) algorithm uses a relationship between velocity and pressure corrections to enforce mass conservation and to obtain the pressure field [28]. This algorithm substitutes the flux correction equations into the discrete continuity equation to obtain a discrete equation for the pressure correction in the cell. The pressure-correction equation may be solved using the algebraic multigrid (AMG) method. Once a solution is obtained, the cell pressure and the face flux are corrected. There are a number of variants to the basic SIMPLE algorithm; Fluent offers the SIMPLEC (SIMPLE-Consistent) algorithm. The SIMPLEC is similar to the SIMPLE method with a different expression used for the face flux correction [25, 28]. However, both SIMPLE methods are generally used for steady-state calculations and not applicable in this situation.

In the FSM, the momentum equations are decoupled from the continuity equation using approximate factorization [28, 29]. This allows the user to control the order of splitting error. As a result, the FSM employed by Fluent is a velocity-coupling scheme in a non-iterative time-advancement algorithm. As a result the Fractional Step Method cannot be utilized in this project.

While SIMPLE and SIMPLEC are generally used for steady-state calculations, PISO (Pressure-Implicit with Splitting of Operators) is commonly employed for

calculations that are transient. For this study PISO unsteady pressure-based solver is used for calculations on highly skewed meshes enabling full pressure-velocity coupling. One of the limitations of the SIMPLE and SIMPLEC algorithms is that new velocities and corresponding fluxes do not satisfy the momentum balance after the pressure-correction equation is solved. As a result, the calculation must be repeated until the balance is satisfied [26, 28]. To improve the efficiency of this calculation, the PISO algorithm performs two additional corrections: neighbor correction and skewness correction [26, 27].

The main idea of the PISO algorithm is to move the repeated calculations required by SIMPLE and SIMPLEC inside the solution stage of the pressure-correction equation [26]. This process (momentum or "neighbor" correction) allows the corrected velocities to satisfy the continuity and momentum equations more accurately. While the PISO algorithm takes a little more CPU time per solver iteration, it dramatically decrease the number of iterations required for convergence, especially for transient problems. Additionally, it allows for the use of larger time steps while maintaining stable calculations and under-relaxation factors for both pressure and momentum.

Meshes that are highly distorted pose convergence difficulties. Fluent uses the process of skewness correction to solve a highly skewed mesh in roughly the same number of iterations as an orthogonal mesh. For skewed meshes, the relationship between the correction of mass flux at the cell face and the difference of the pressure corrections at the adjacent cells in not ideal. The unknown components of the pressure-correction gradient along the cell faces are solved and used to update the mass flux

corrections [27]. It should be noted that, for meshes with a high level of skewness, the simultaneous coupling of the neighbor and skewness corrections may lead to divergence. This can be solved by utilizing additional iterations of skewness correction for each neighbor correction. While this comes at a computational expense, it allows a more accurate adjustment of the face mass flux correction [26].

Gradients are used throughout calculations from determining values of scalars at the cell faces, to discretizing the convection and diffusion terms to computing velocity derivatives. Fluent offers three methods by which gradients can be calculated: Green-Gauss cell-based, Green-Gauss node-based, least squares cell-based. The Green-Gauss cell-based method uses an arithmetic average of the values at the neighboring cell centers to calculate the value at a given cell center. However, the node-based method uses an arithmetic average of the nodal values on the face of neighboring cells utilizing a weighted average similar to that proposed by Holmes and Connel [30] and Rauch et al. [31]. While the node-based method is more accurate then the cell-based method, it is prohibitively more expensive computationally. The least squares method assumes that the solution varies linearly from cell center to cell center. This method uses the Gram-Schmidt process [32] to solve the minimization problem for a linear system of non-square coefficient matrix in a least squares sense. For skewed or distorted unstructured meshes, the least-squares accuracy is comparable to the node-based method. Additionally, it is less expensive to compute then the node based method; however, it is still substantially more costly to compute then the cell-based method. As a result Green-Gauss cell-based method was used for determining gradients.

Standard scheme is employed for discritization of pressure while first-order upwind scheme is used for all other equations (density, momentum, energy, etc.). While a second-order scheme generally yields more accurate results than a first-order scheme, they are more costly computationally and can lead to convergence problems. Convergence problems met by using a second-order scheme are generally solved by instead utilizing a first-order scheme. Implicit relaxation, or under-relaxation, can help stabilize convergence issues in the pressure-based solver. While this comes at the expense of computational time, it can help to combat oscillatory convergence as a result of overshooting the apparent solution. Tannehill et al. even suggests that in non-linear problems it is often necessary for convergence [28].

Chapter 3: Experimental Setup, Results and Model Validations

In order to provide confidence in the model of the Rotax engine used in this paper, a validation study was conducted to benchmark computational simulations against experimental results. The benchmarking work was a collaboration and validation effort using both an experimental facility and Wright State University computational capabilities. It is therefore worthwhile discussing briefly the experimental engine test stand setup and how tests were conducted as well as results from those tests. The author was not responsible for construction or implementation for the engine test cell, save for assistance in data taking in addition to a few tertiary additions to the test stand. Equipment selection, ranging from dyno/controller to sensors (both type and functionality), was done by the experimental facility and as a result only the more pertinent facts will be briefly discussed and not necessarily the reason for their selection/use.

3.1 Experimental Setup

The experimental facility consists of an isolated engine test cell and a control center for operating the engine and dynamometer. The Rotax 914 engine is attached to a bedplate in the test cell by way of a vibrationally isolated test stand. The engine itself utilizes all the parts normally associated with an aircraft application with the addition of a larger external cooling radiator. The larger radiator is used to dissipate heat from testing

that is normally removed by a smaller radiator and free stream air coming through the engine cowl. The engine power is absorbed by a Taylor DE150 eddy current dynamometer. The dynamometer is controlled by a DynLock IV controller. The output speed of the engine is maintained by providing variable braking torque by way of the Taylor dynamometer. Data was acquired using a high-speed data acquisition system consisting of a high speed computer, I/O module, dynamic pressure transducer, in-line charge converter, sensor signal conditioner, spark plug adaptor and engine knock sensor.

The data presented here was taken as a baseline of the original engine performance to be used for comparison with further research and development. The experimental facility is examining the knock limited performance of the Rotax engine with hopes of ultimately running on heavy fuels such as diesel or jet fuel as well as introducing direct injection technology to the engine. The engine was designed to run on 100 octane low lead (100LL) aviation gasoline (Av-Gas). It was determined that the baseline data would encompass the operational range of the engine both in speed (engine RPM) and intake air pressure.

In order to determine the knock limit, the test facility had to be capable of detecting knock in the engine remotely. Because the engine is not available with a knock detection circuit, one had to developed and calibrated for this application. Two automotive knock sensors (piezoelectric accelerometers) mounted to opposite sides of the engine block would function as the primary method for knock detection throughout the testing; however, as they were not designed specifically for this application, they had to be calibrated for use on this engine. In order to do so, two opposing cylinders were fitted

with pressure sensors to map the pressure in the cylinder over the cycle. A determination could be made as to whether or not knock had occurred as well as the intensity of the knock by analyzing the pressure plots for the cylinders. This could then be referenced against the knock sensor signal to calibrate its knock detection capabilities. As the engine was designed to run on 100LL and not likely to knock, other tests were performed with lower octane fuels in order to achieve knocking conditions and facilitate the calibration.

The data taking process began by starting the engine and bringing it to an idle speed. It was observed that as the cylinder head temperature varied during testing, so did the frequency and intensity of knock. As a result each data set was recorded with the cylinder head within a predetermined temperature range to insure accuracy and consistency. After the engine reached the desired temperature range, the intake manifold pressure was adjusted to a given starting point and data was taken. The manifold pressure was kept constant while the speed was increased incrementally up to the engines maximum rated operating condition. The data acquired at each operating condition included cylinder pressure and knock signal from the block mounted knock sensor. The engine was tested under load conditions (manifold pressures) chosen to simulate operation in an aircraft.

3.2 Experimental Results

As discussed in the previous section, several data points were taken throughout the operational range of the engine. It is not practical to validate the model for each and

every situation, but rather for key conditions within the aircraft operation envelope. The following data sets represent the more significant performance regions. All data was taken within the conditions presented above and with a stoichiometric air/fuel ratio ($\Phi = 1$).

Figure 3.2.1 shows the output obtained for 21 cycles recorded with the high speed data acquisition system for 5500 rpm and 35" Hg (17.2 psi) inlet pressure. It is easy to see that there is a substantial variation between cycles of more than 300 psi . Figure 3.2.2 shows the pressure traces for the highest, lowest and average cylinder pressure conditions. Figure 3.2.3 shows the cylinder pressure trace of 21 cycles for 5000 rpm and 30" Hg (14.7 psi) inlet pressure. Again, it can be seen in figure 3.2.4 that there exists a large, nearly 300 psi, pressure difference between the highest and lowest pressure traces. Figure 3.2.5 shows the output obtained for 4000 rpm and 35" Hg (17.2 psi) inlet pressure for 17 cycles. The data acquisition system records data for a specific time interval. As the rpm of the engine is decreased, fewer peaks are available within the recording window. This can be seen by the fact that there are fewer pressure peaks for this case then for the 5500 rpm case. However, as shown in figure 3.2.6, it is easy to see that there is still a distinct variation between cycles. The variation has dropped to just under 200 psi, but the overall pressure in the cylinder has also significantly decreased.

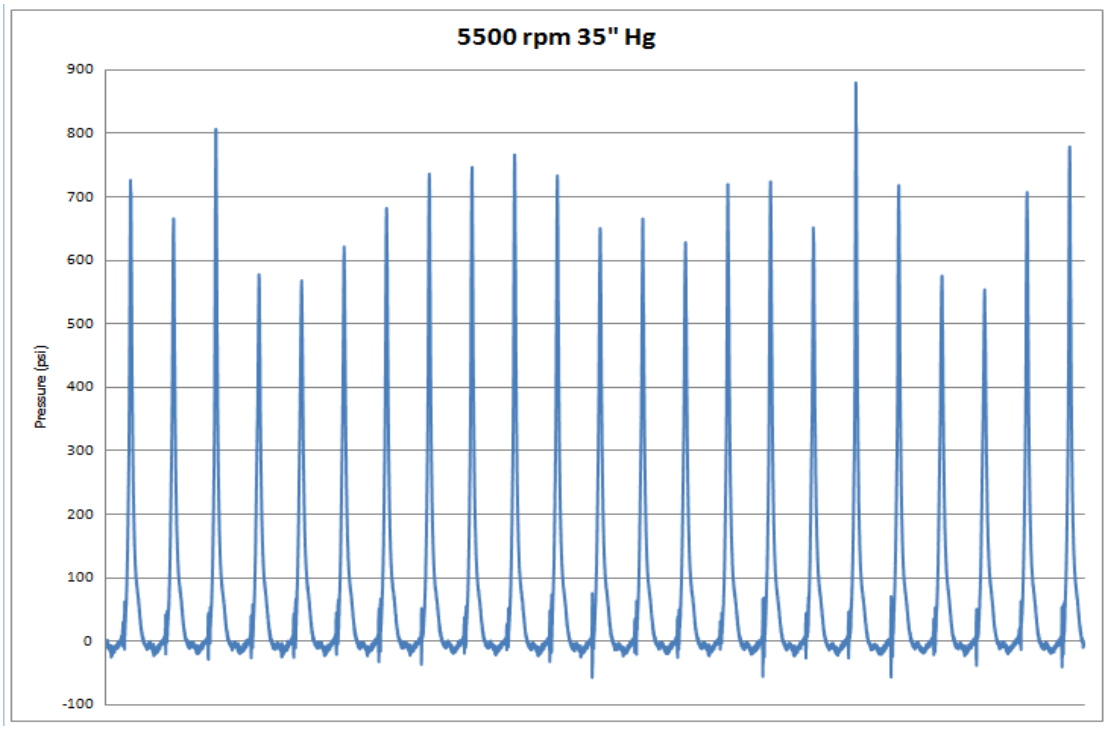

Figure 3.2.1 Pressure for several cycles at 5500rpm 35” Hg

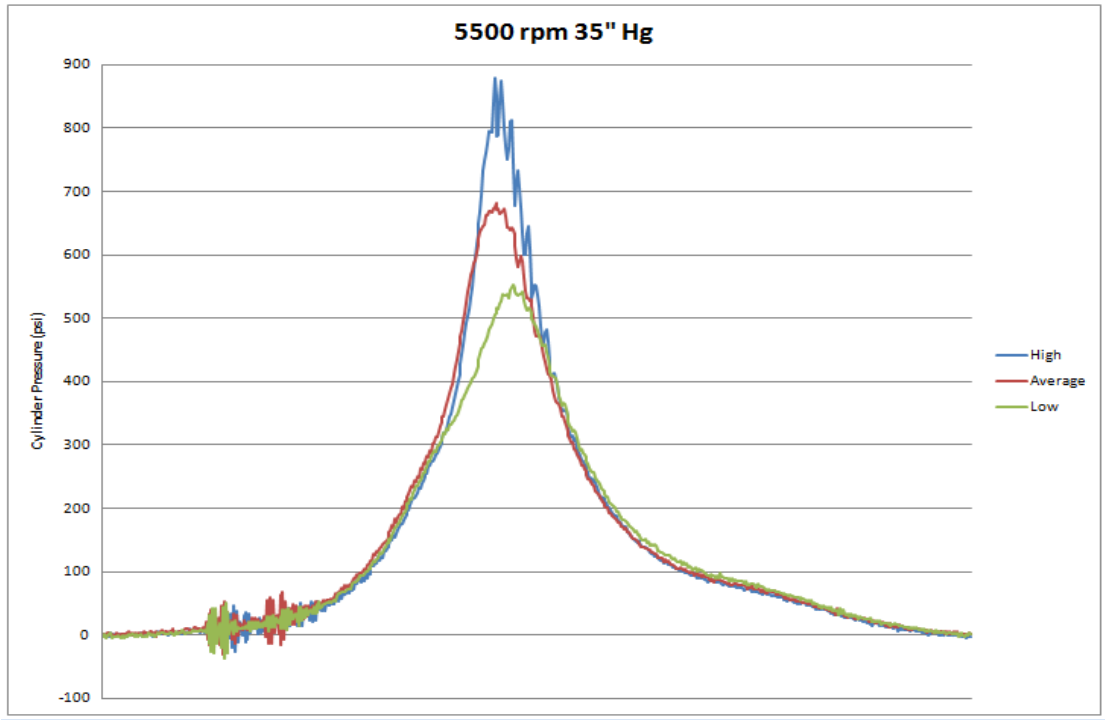

Figure 3.2.2 Pressure variation of 5500 rpm 35” Hg

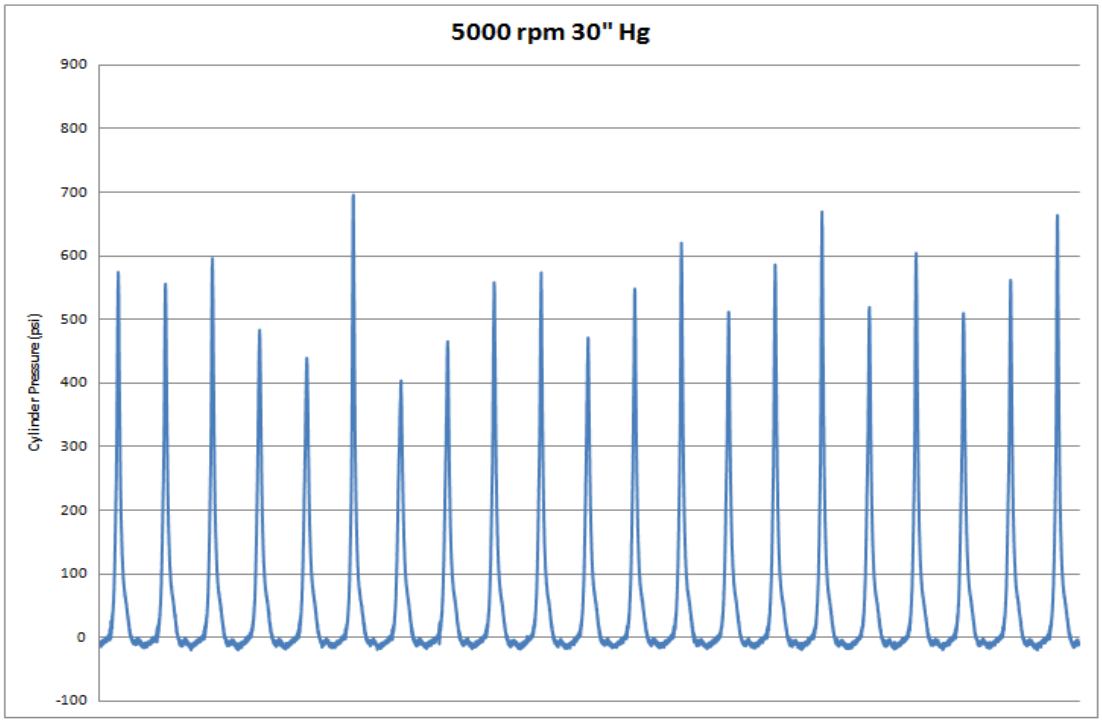

Figure 3.2.3 Pressure for several cycles at 5000rpm 30” Hg

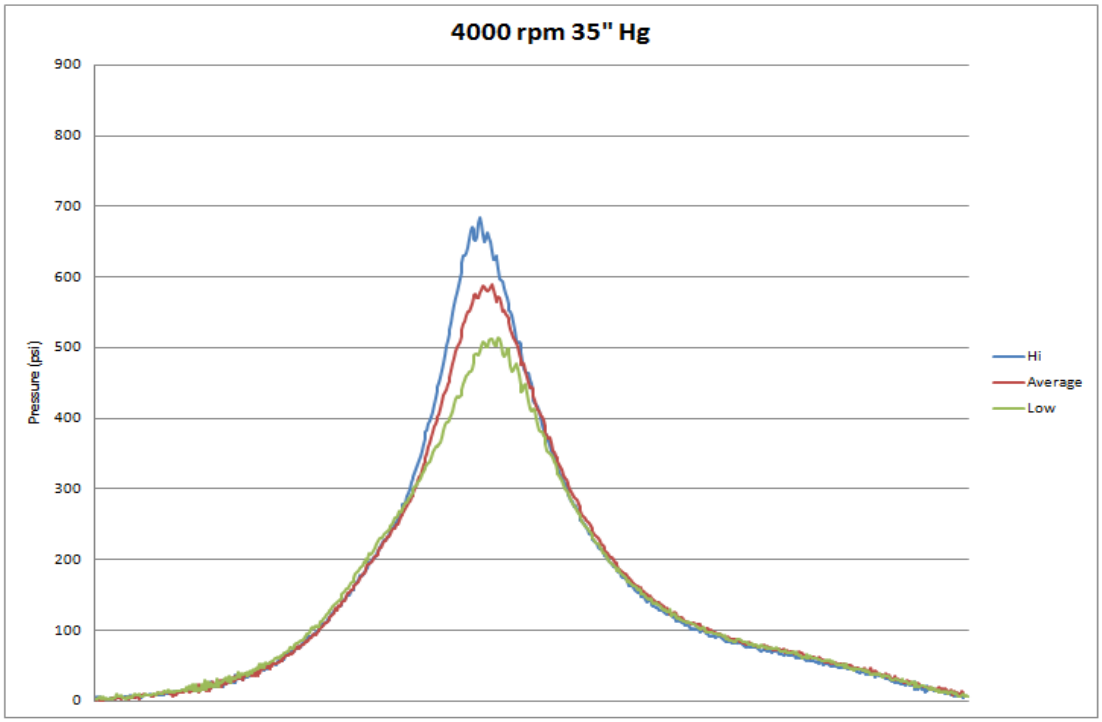

Figure 3.2.4 Pressure variation of 5000 rpm 30” Hg

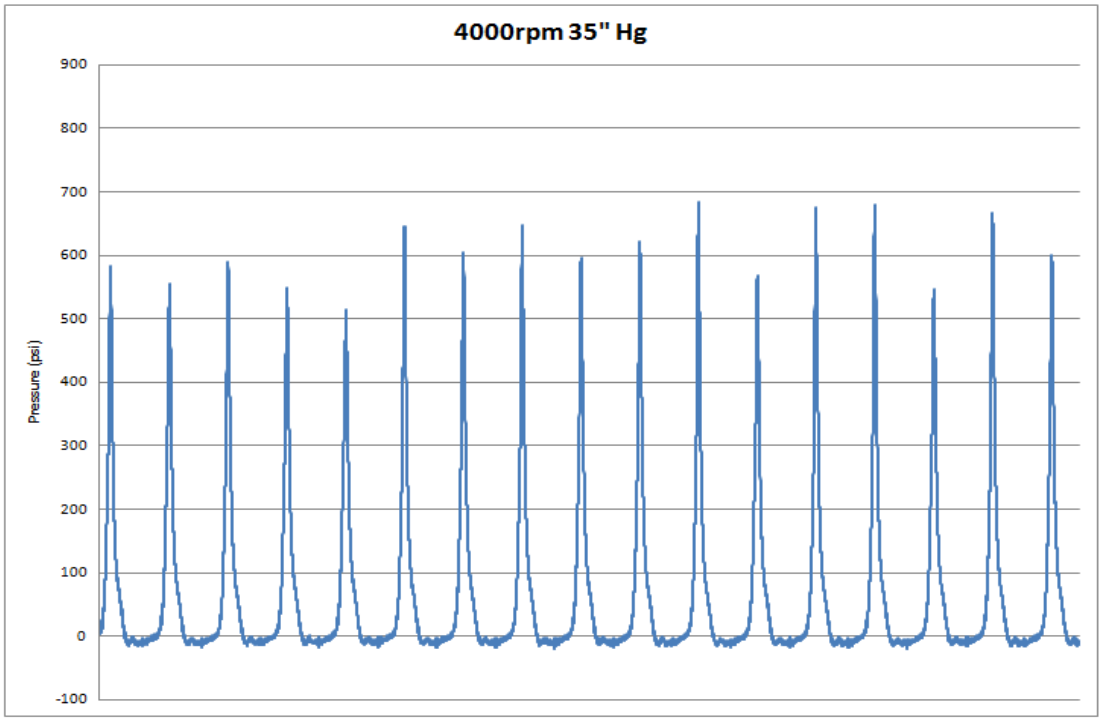

Figure 3.2.5 Pressure for several cycles at 4000rpm 35” Hg

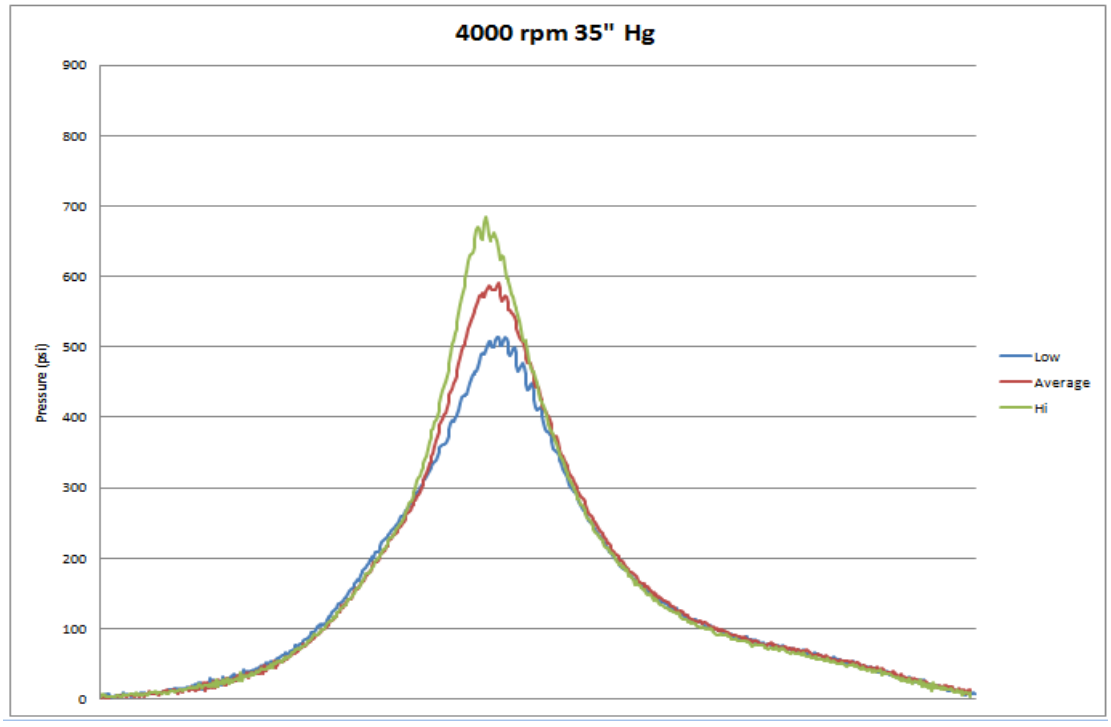

Figure 3.2.6 Pressure variation of 4000 rpm 35” Hg

3.3 Computational Results

The same model developed in Chapter 2 was used for both model validation as well as the direct injection study to be discussed in Chapter 4. Additionally, it is the model used in Chapter 5 with the exception of the modified bowl piston. The only difference between the cases (save for the piston in CH 5) was how the fuel was injected into the cylinder. The methods of fuel injection for the direct injection cases will be discussed later; however, for the validation case, fuel was injected via 4 injectors near the intake valve pressure inlet (top of intake area). Although in the real engine the fuel is injected into the intake manifold upstream of the cylinder intake by means of a single fuel injector, for simulation purposes it can be assumed that the fuel is roughly a homogeneous mixture before it travels through the virtual intake boundary of the model and the 4 separate injectors help to simulate this.

3.3.1 Computational Cycle

Before the computational results of the validation study are presented, it is prudent to first discuss the engine cycle within the computational domain. Figure 3.3.1(a)-(d) shows the distribution of fuel inside the chamber before combustion during the first stroke of the engine cycle. Fuel is injected into the intake area simulating port fuel injection. The fuel begins mixing with the air as it travels down the intake and through the intake valve, entering the combustion chamber in figure 3.3.1(a). The downward motion of the piston, in figure 3.3.1(b) & (c), draws the air-fuel mixture past

the intake valve and into the cylinder where it continues to mix. As the piston reaches bottom dead center and begins the compression stroke, the contours of fuel begin to stabilize as the mixture becomes ready for ignition as seen in figure 3.3.1 (d). For the most part, the mixture is now mostly homogeneous.

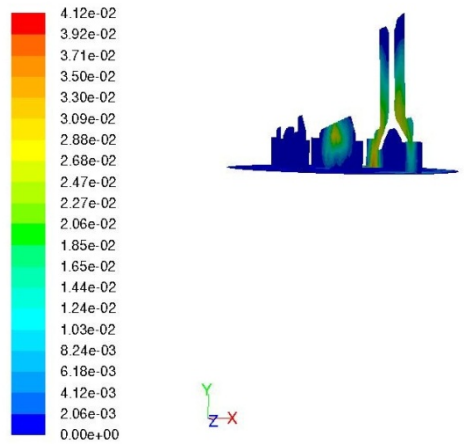

(a) 30° aTDC – Intake Stroke

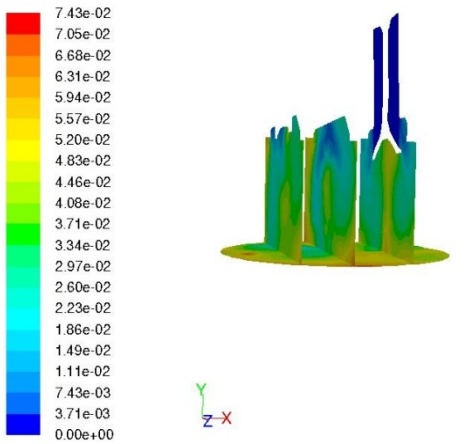

(b) 90° aTDC – Intake Stroke

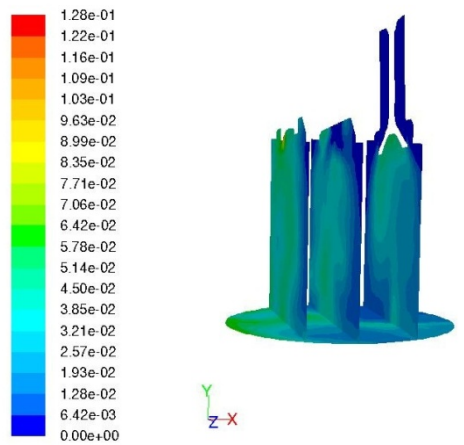

(c) 30° bBDC

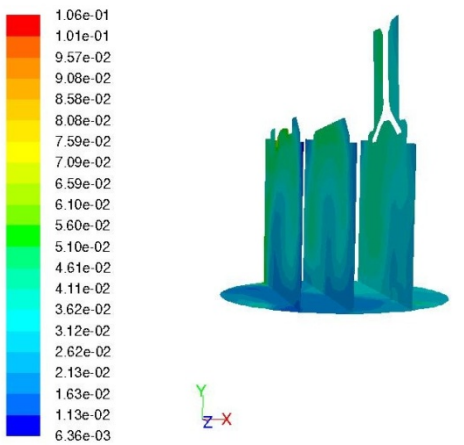

(c) 30° aBDC

Figure 3.3.1 Fuel distribution inside the chamber before combustion

Figure 3.3.2(a)-(d) shows the fuel distribution inside the chamber before spark through the combustion and expansion processes. Figure 3.3.2(a) shows the fuel mixture in the cylinder at 30° bTDC, which corresponds to 4° CA before spark. The charge is mostly homogeneous with a slightly rich concentration near the spark area. Figure 3.3.2(b) shows the fuel beginning to burn at TDC, shortly after the spark is ignited, while (c) shows the flame front propagating through the combustion chamber as the fuel is consumed. Figure 3.3.2(d) shows the power stroke which results from the rapid expansion of the burning gas in the cylinder. It is observed that there is some unburned fuel left in the cell. This is due to pockets of lean air-fuel mixture resting on the piston near the cylinder walls resulting in incomplete burn and wasted fuel.

Figure 3.3.3(a)-(b) shows the production of CO_2 during combustion process. Because CO_2 is one of the main products of combustion and not present in the incoming charge it can be used as a measure of combustion. While H_2O is also one of the main products of combustion, CO_2 exists only in the vapor phase throughout entire engine cycle making it superior to H_2O for determining combustion. Figure 3.3.3(a) shows the initiation of combustion where the CO_2 production is just beginning; whereas figure 3.3.3(b) shows the completion of combustion and also CO_2 production. Figure 3.3.3(b) shows the exhaust manifold now activated before the exhaust valve is opened. The dark blue color inside the manifold signifies that the CO_2 in the cylinder has not had a chance to exit. Additionally, small pockets of blue exist around the area where the piston meets the cylinder wall. This illustrates a lack of combustion in those areas.

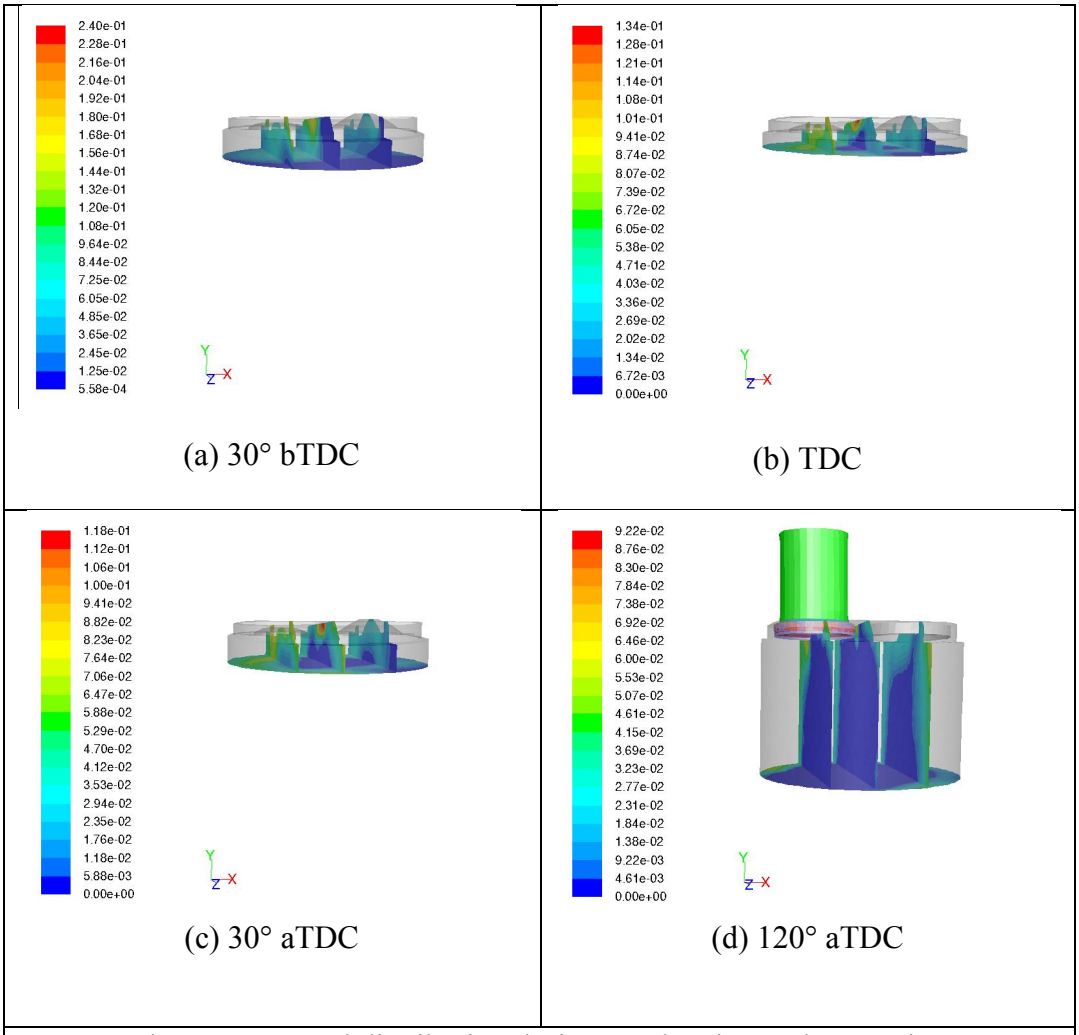

Figure 3.3.2 Fuel distribution during combustion and expansion

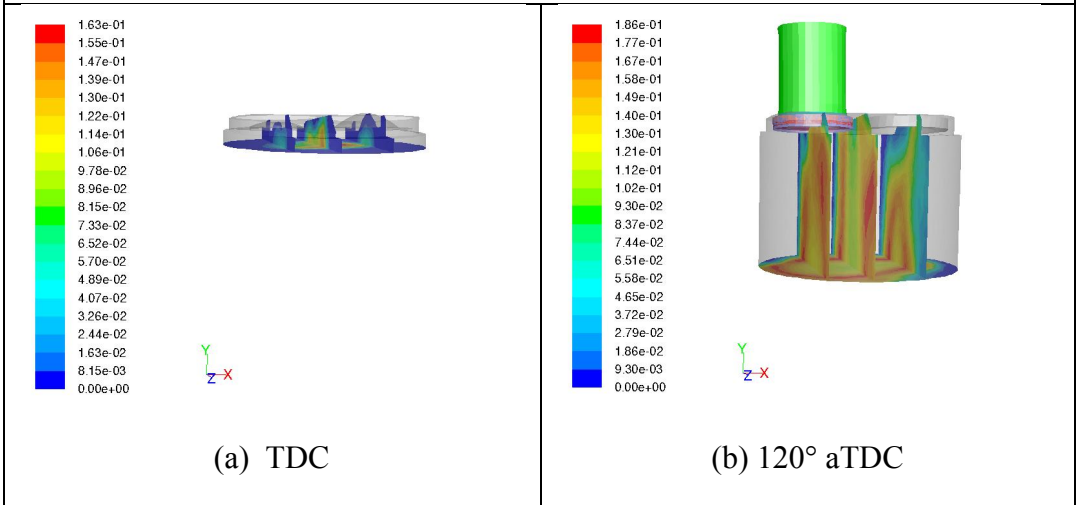

Figure 3.3.3 Production of CO_2 during combustion cycle

Figure 3.3.4 shows the changes in temperature in the chamber right before combustion through the power stroke. Figure 3.3.4(a) shows the temperature increase due to compression of the air-fuel mixture in the cylinder immediately before the spark plug ignites it. Figure 3.3.4(b) shows the drastic temperature increase due to combustion 26° after spark at TDC. This is near the beginning of the combustion process where the flame front is just starting to expand. The flame front quickly expands to cover most of the chamber as seen in figure 3.3.4(c). The flame continues to consume the remaining burnable fuel in the chamber through the power stroke as seen in figure 3.3.4(d). With little ignitable fuel left the charge in the cylinder begins to cool as it reaches the end of the power stroke and prepares to exit the chamber through the exhaust valve.

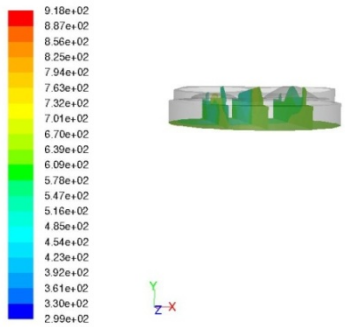

(a) 30° bTDC

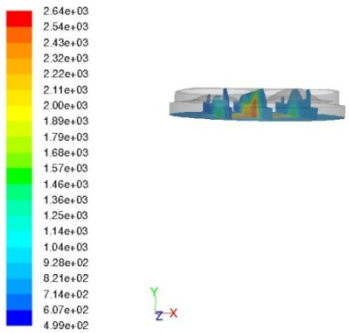

(b) TDC

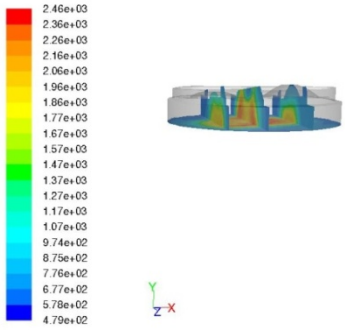

(c) 30° aTDC

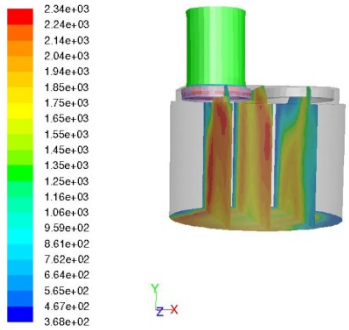

(d) 120° aTDC

Figure 3.3.4 Temperature changes through the cycle

3.3.2 Cold Flow

Before combustion cases were completed, a cold flow analysis was performed to determine, among other things, the pressure rise due to compression and to observe the charge motion in the cylinder and see how the air-fuel mixture interacted with the engine geometry. Figure 3.3.5 shows the pressure rise due to compression plotted against experimental data. It can be seen that combustion in the experimental engine adds 200-500 psi of additional pressure to the compression pressure rise. In this case the variation in pressure peaks due to combustion is equal to the pressure rise from compression.

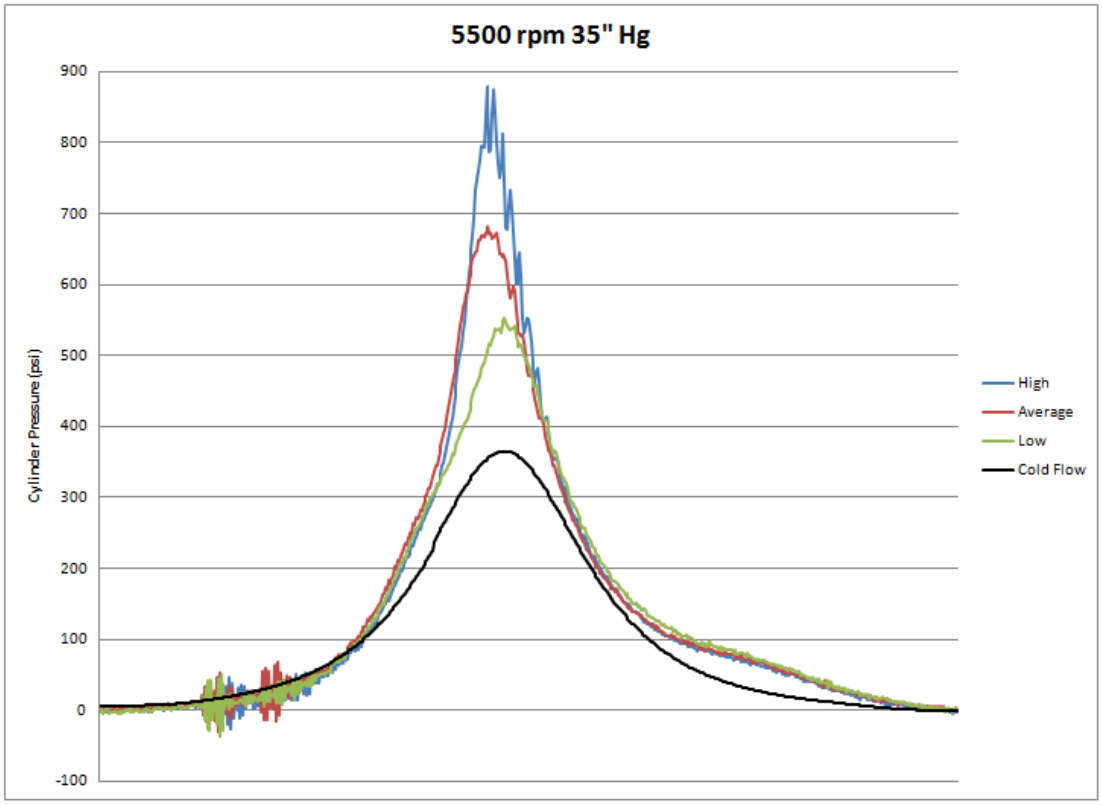

Figure 3.3.5 Pressure rise due to compression shown with experimental data

For the case where no fuel is injected, the air taken into the cylinder is subjected to turbulence resulting in to two different and distinct forms of motion: swirl and tumble [47, 49, 50]. Swirl is air motion around the cylinder with the rotational axis around parallel to the central axis of the cylinder or about the y-axis as seen in figure 3.3.6(b). Tumble is motion of the fluid around the axial plane between the cylinder head and piston face as seen in figure 3.3.6(a). Both motions aid in the air fuel interaction to help create a homogeneous mixture. Swirl helps to bring the mixture around the cylinder, while tumble aids in bring the mixture up to the spark area [50, 52]. Figure 3.3.6 shows adequate swirl and tumble motion in the computational model which will lead to a homogeneous air-fuel mixture and good combustion.

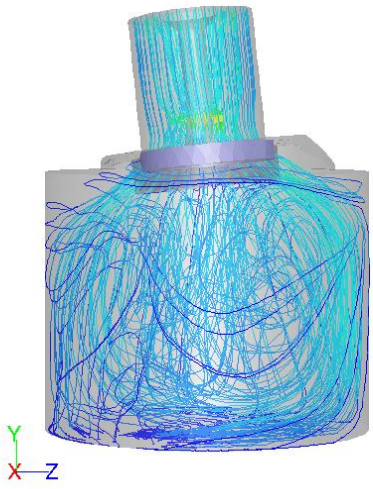

(a) Tumble

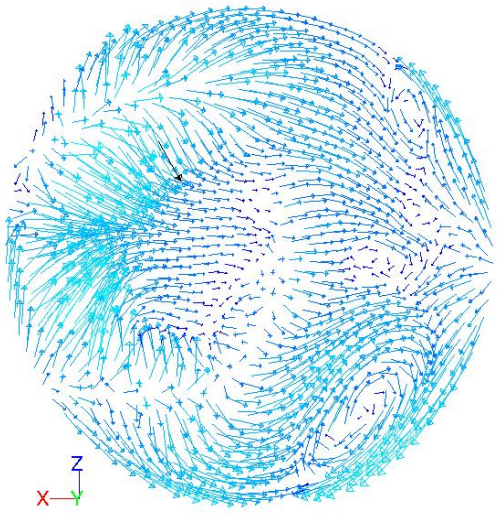

(b) Swirl

Figure 3.3.6 Tumble and swirl motion of air in cylinder

When fuel is injected into the intake manifold, the air and fuel enter into the combustion chamber and interacts in the tumble and swirl motion described above. Through this mechanism fuel (liquid) begins to vaporize and mix with the air in order to become ready for combustion. The motion of the fuel in the chamber is studied using particle tracks shown in figure 3.3.7 below. This provides information about fuel vaporization [51] by observing how the fuel is influenced by the tumble in fuel-air mixture formation. In addition, the turbulence helps to increase fuel atomization in the cylinder. At high pressure, the air motion offer resistance to the particles in the cylinder and the turbulence aids in the shearing of fuel thus increasing vaporization.

Although care is taken to atomize fuel during the injection process, some large droplets compared to the mean diameter still exist. These droplets that are not vaporized can cause wall wetting and remain in the cylinder even after combustion. It is not possible to completely vaporize and combust all fuel in the chamber every time [51]. This is evident in the low combustion cases in the experimental data presented in figures 3.2.1, 3 and 5 above. Figure 3.3.8 shows the vaporization process through the intake and compression strokes.

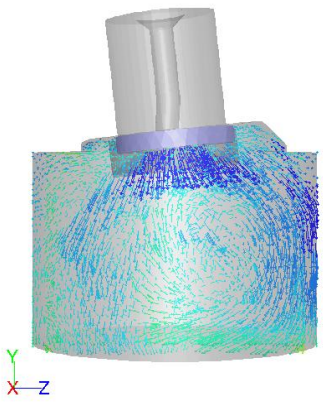

(a) 240° aTDC

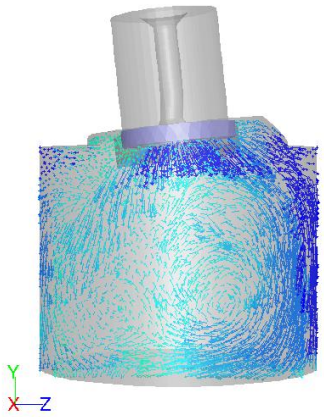

(b) 180° aTDC

Figure 3.3.7 Vectors of air-fuel mixing

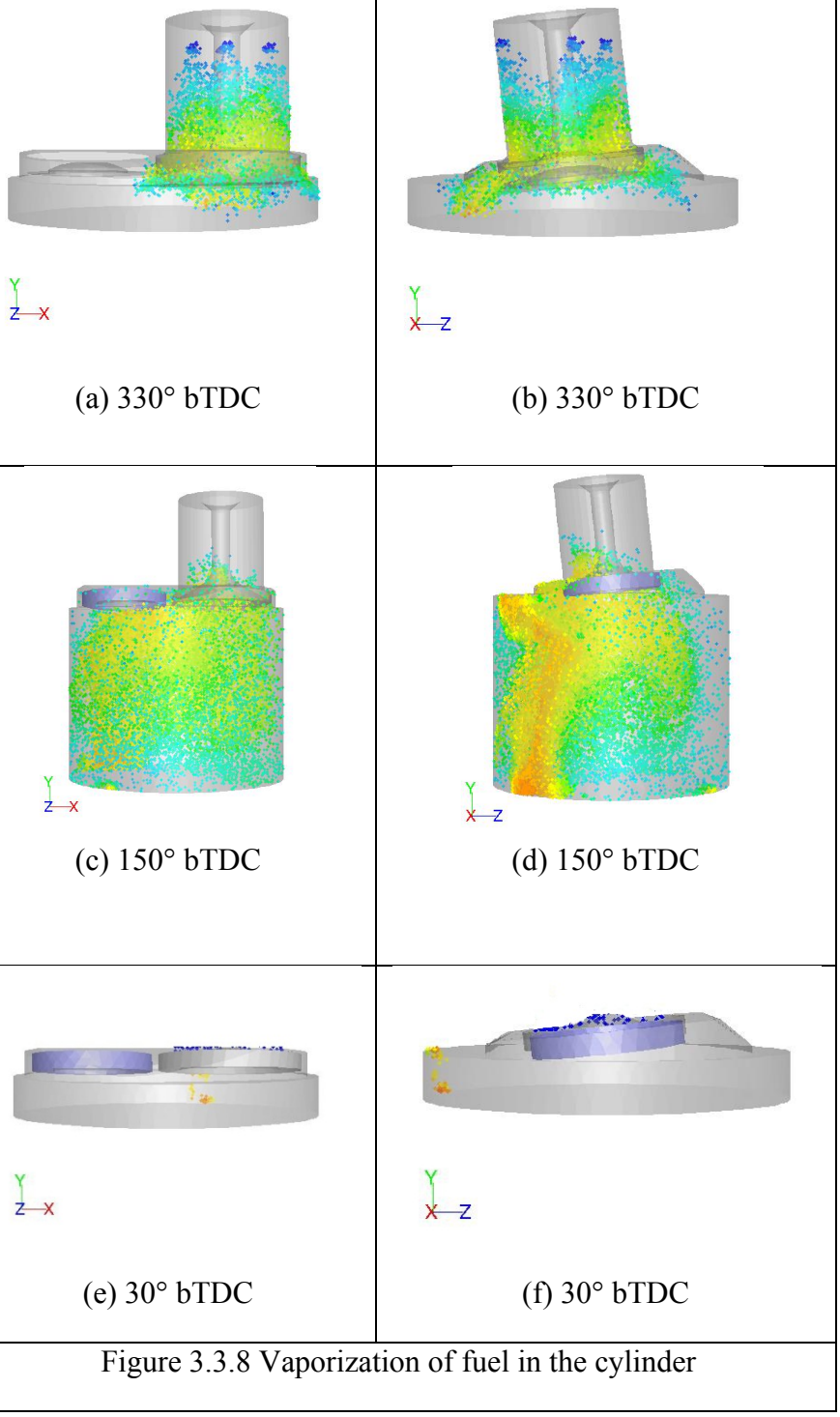

(a) 330° bTDC

(b) 330° bTDC

(c) 150° bTDC

(d) 150° bTDC

(e) 30° bTDC

(f) 30° bTDC

Figure 3.3.8 Vaporization of fuel in the cylinder

3.3.3 Computational Results

The following cases correspond to the experimental results presented in the beginning of this chapter. Pressure results in this section are presented in pounds per square inch (psi) to correspond to experimental data. Figure 3.3.1 shows the pressure plot for 5500rpm and 35" Hg inlet pressure. Figure 3.3.2 shows the results for 5000rpm and 30" Hg inlet pressure and figure 3.3.3 shows the pressure plot of 4000rpm and 35" Hg.

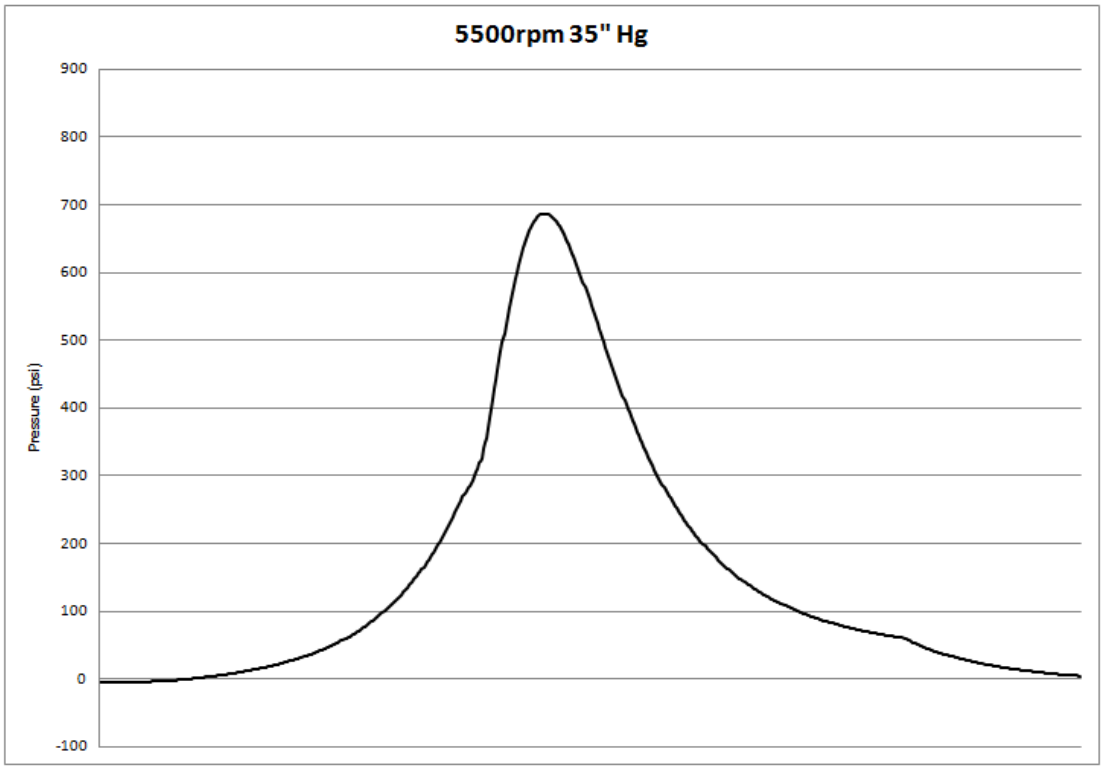

Figure 3.3.6 Pressure plot for 5500rpm and 35" Hg

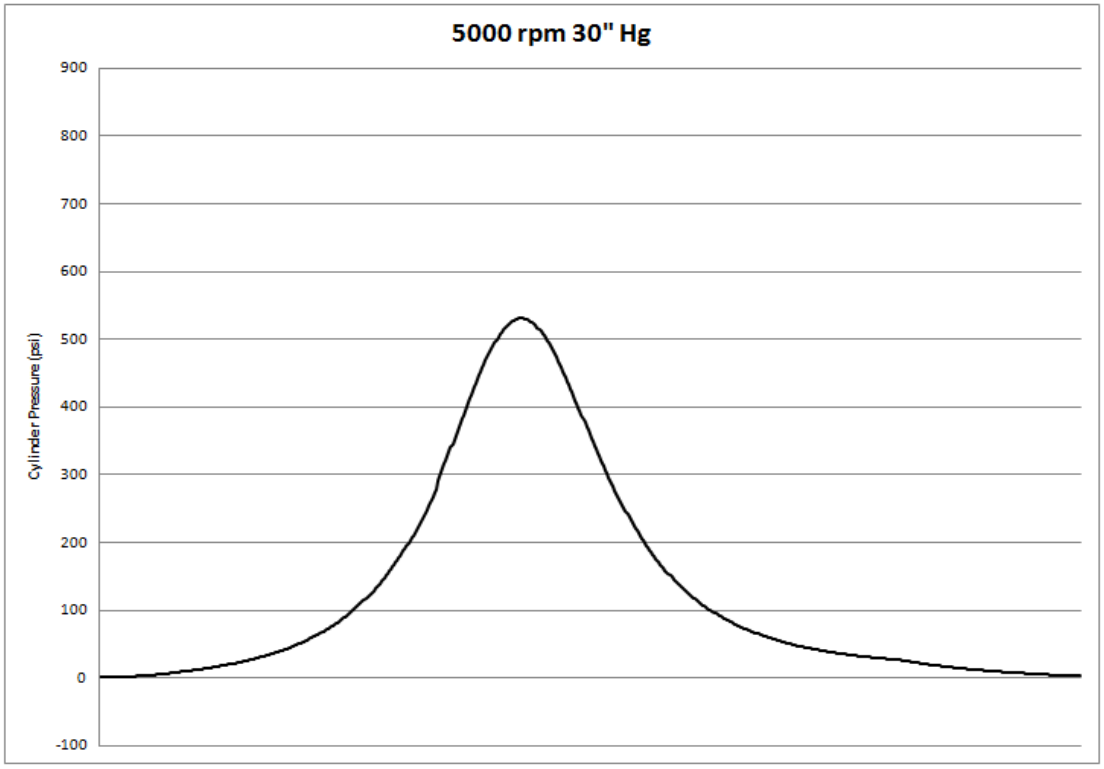

Figure 3.3.7 Pressure plot for 5000rpm and 30” Hg

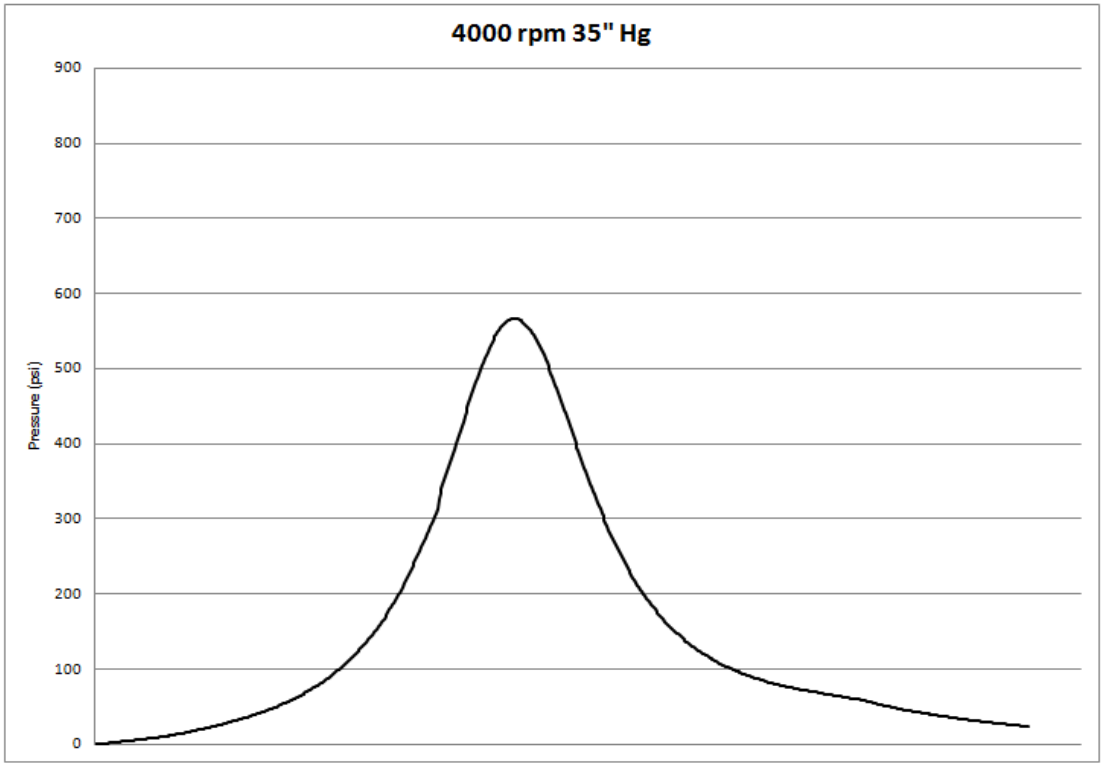

Figure 3.3.8 Pressure plot for 4000rpm and 35” Hg

3.4 Validation Study

Results for both the experimental and computational cases have been presented in the previous two sections. In order to build confidence in the computational model for the next section of this study, a comparison will now be made between the physical engine and the computational model of the engine. The engines will be compared based on the tangible attributes to ensure the model matches the physical characteristics of the engine. Subsequently the boundary conditions defined in the model will be evaluated against those of the existing engine. Finally the output of the model and the experimental engine will be placed together to evaluate how well the model mimics the real engine.

3.4.1 Physical Comparison

As discussed in Chapter 2, an actual Rotax 914 engine was scanned using a 3d scanner in order to get the foundation for the computational model. It can readily be seen that the model engine looks exactly like the real engine. Figure 3.4.1.1 shows a direct comparison of the piston and cylinder head for both the model and the real engine. Additionally, the model in the computational domain is scaled to match the exact dimensions of the physical engine. Figure 3.4.1.2 shows some of the specifications of the physical engine used to create the computational model.

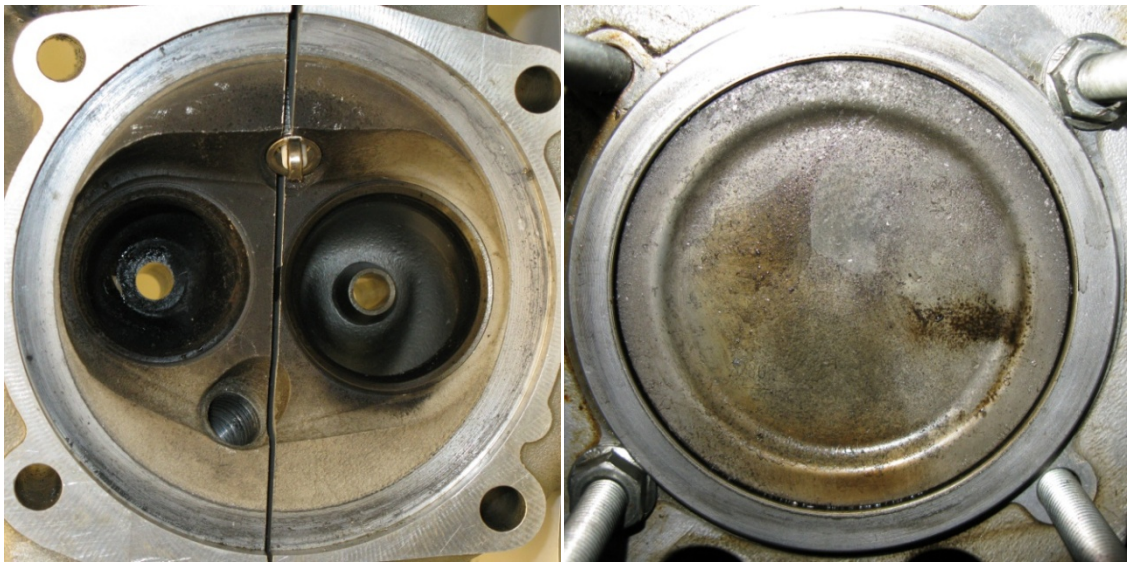

(a) (b)

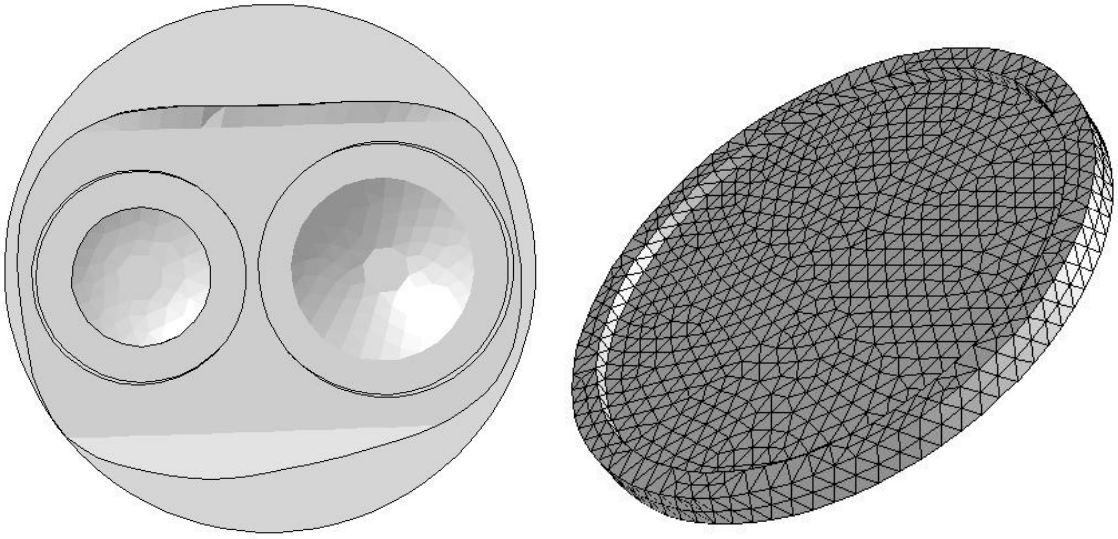

(c) (d)

Figure 3.4.1.1 Rotax 914 Engine and Computational Model Comparison

Parameter	Data
Bore	79.5 mm (3.1 in.)
Stoke	61 mm (2.4 in.)
Displacement Volume	1211.2 **cm^3** (73.9in^3)
Clearance Volume	151.4 **cm^3** (9.24in^3) total 37.85 **cm^3** (2.31in^3) / cylinder
Compression ratio	9.0:1
Valve Lift (Intake)	9.78 mm (.385 in)
Valve Lift (Exhaust)	9.78 mm (.385 in)

Figure 3.4.1.2 Rotax 914 Engine Specifications

3.4.2 Boundary Conditions & Initial Conditions

After verifying that the model and actual engine have the same physical characteristics, the next step was to verify that the same conditions were used for each comparison case. The initial conditions represent the initial guess the solver will use for calculations. Boundary conditions are the values defining the limits of the model in the computational domain and were obtained from the experimental data whenever possible, such as temperatures for intake and exhaust gas and injected fuel. Tables 3.4.2.1-4 shows some of the boundary and initial conditions and how they relate to the experimental data. Many of these parameters will vary from case to case such as fuel flow rate, engine speed, pressure etc.

Injection		CFD	Experimental
	Fuel used	Iso-Octane	Iso-Octane
	Composition of fuel	100% Octane	100% Octane
	fuel flow rate:	0.021265Kg/s	0.021265Kg/s
	Velocity of injection	120 m/s	120 m/s
	Radius of injector	1 mm	
	Initial Fuel temperature	314 K	314 k
	Density of the fuel	702 kg/m^3	698 kg/ m^3

Figure 3.4.2.1 Injection parameters

Spark		CFD	Experimental
	radius:	0.0026m	0.0026m
	energy:	0.1J	0.1J
	start angle:	705	705
	Spark duration/spark dissipation	0.001s/0.001s	0.001s/0.001s

Figure 3.4.2.2 Spark parameters

Dynamic mesh		CFD	Experimental
	Engine Speed:	5000 rpm	4997 rpm
	Start Crank Angle:	360	n/a
	Crank Period:	720	720
	Crank Step Size:	0.5°	n/a
	Compression Ratio:	9.2:1	9.2:1
	Connecting Rod:	0.144145m	0.144145m
	Bore ×Stroke	86.86mm× 86.86mm	86.86mm× 86.86mm

Figure 3.4.2.3 Engine/Mesh parameters

Boundary Conditions		CFD	Experimental
	Equilibrium Operating Pressure	101325 Pascal	101325 Pascal
	Fuel Temperature (used as initial fuel temperature)	314 K	314 K
	Super charge Pressure (used as pressure at intake)	101580 Pascal	101580 Pascal
	Super charge temperature (used as temperature at intake)	323 K	323 K

Figure 3.4.2.4 Pressure/Temperature parameters

3.4.3 Output Comparison

Figure 3.4.3.1 shows the pressure traces for both the experimental and computational results for the case of 5500 rpm and 35” Hg MAP. The computational results match the pressure for the average cycle experimental case fairly well. The computational results slightly over predict the pressure peak and are a bit wide from TDC through the expansion stroke.

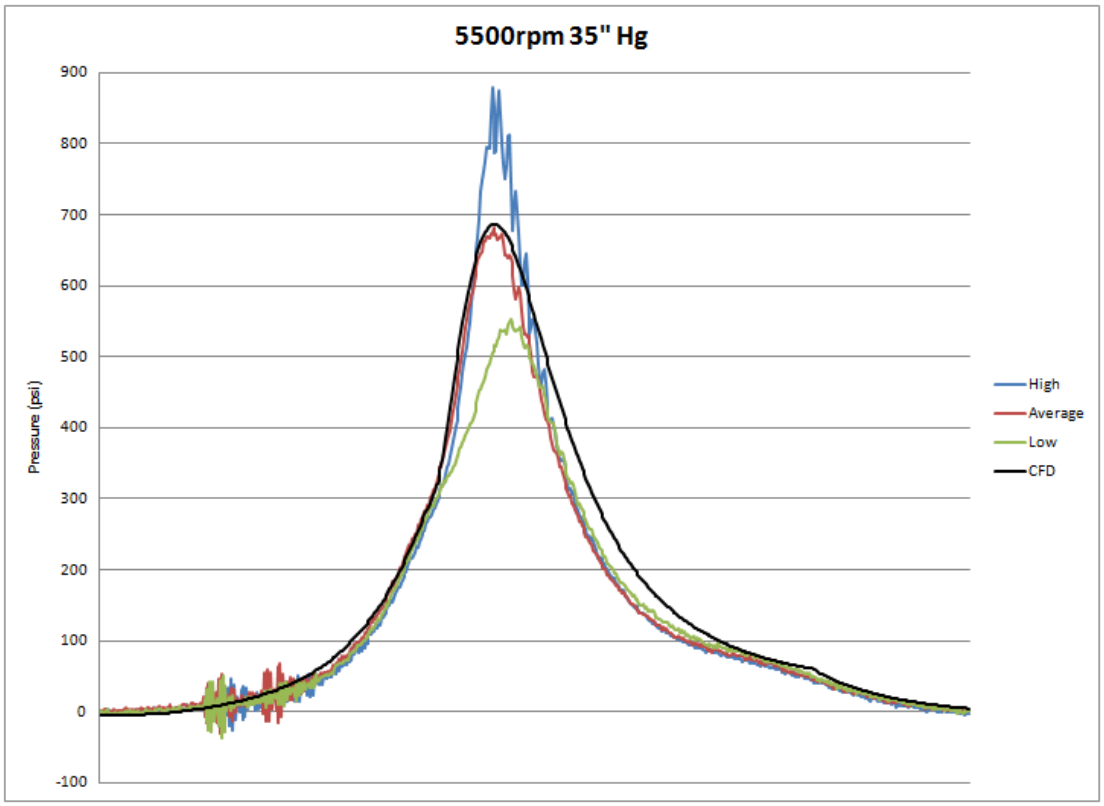

Figure 3.4.3.1Computational results compared to experimental for 5500 rpm 35” Hg

Figure 3.4.3.2 depicts the pressure traces for both the experimental and computational results for the case of 5000 rpm and 30” Hg MAP. Once again, the end of the combustion and expansion stroke are slightly wide of the experimental results; however, the compression stroke matches well with a slightly under predicted pressure peak as compared to the cycle average for this speed and load condition.

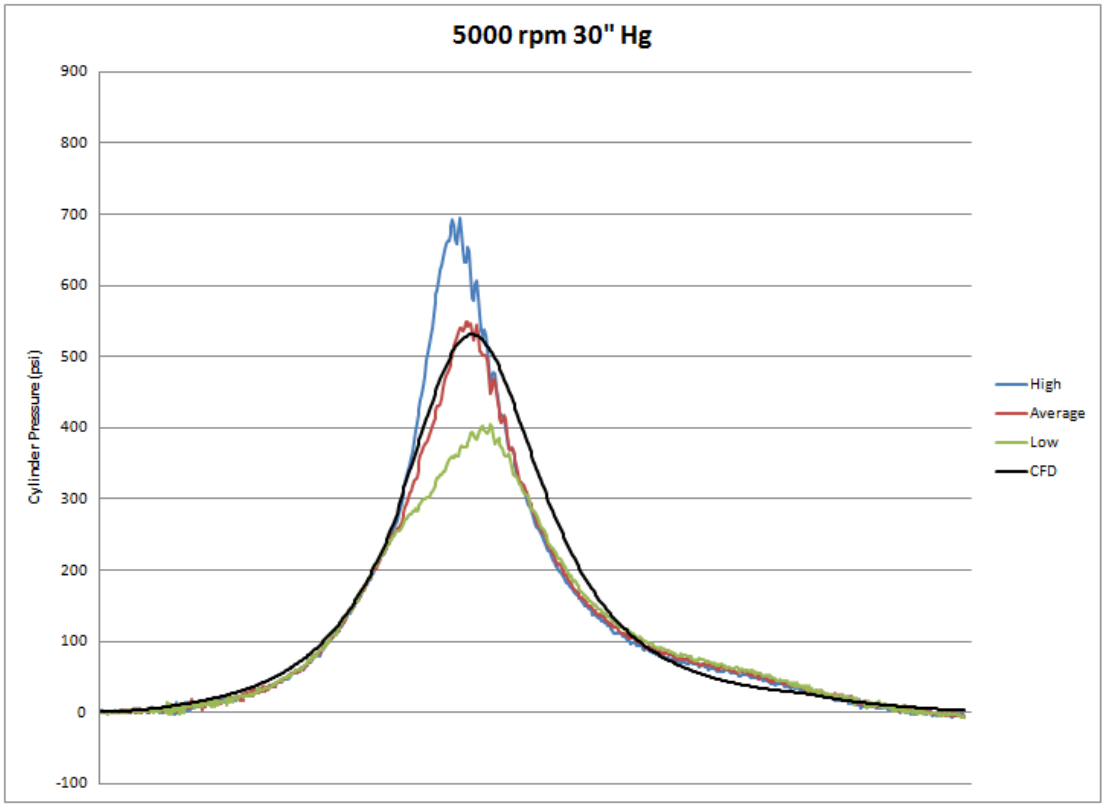

Figure 3.4.3.2Computational results compared to experimental for 5000 rpm 30” Hg

Figure 3.4.3.3 shows the comparison of pressure for the case of 4000rpm and 35" Hg MAP. Once again the pressure peak is slightly under predicted, although the compression, combustion and expansion show good correlation to experimental values.

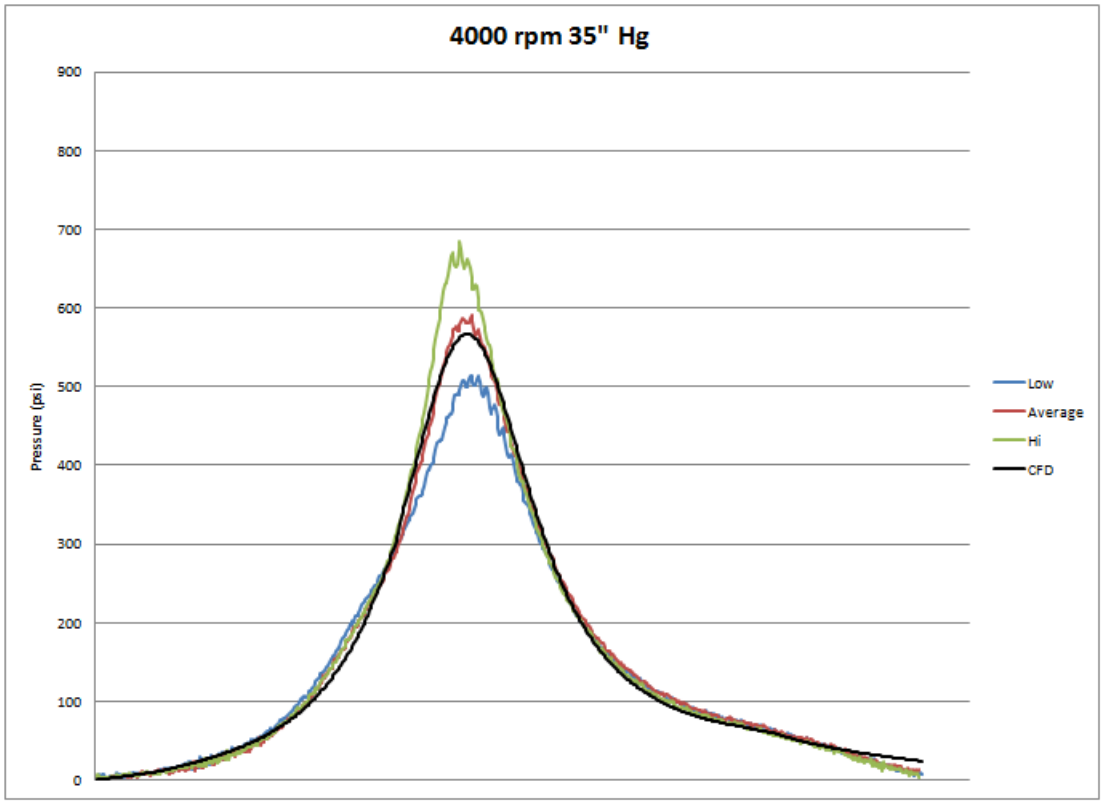

Figure 3.4.3.3Computational results compared to experimental for 4000 rpm 35" Hg

Chapter 4: Direction Injection Study

The flat piston computational model of the Rotax 914 engine developed in the second chapter and validated in the previous chapter will be used to explore the effects different engine parameters have on direct injection spark ignition operation. For the following parametric study, only one parameter was changed at a time. This allowed the effects of that specific parameter to be paramount in the results.

4.1 PFI Settings

To begin this study on the effects of direct fuel injection, the stock configuration of the engine was simulated for 5500rpm 35" Hg. Injection was carried out during the intake stroke and aligned with inflowing air from the intake valve with injection similar to port fuel injection operation. Spark timing was set based on the actual Rotax engine. Figure 4.1.1 shows the pressure plot for this case. Figure 4.2.1 shows a comparison between the port fuel injected simulation discussed in the previous chapter and the direct injection case with similar parameters. One can see that the pressure peak is slightly higher for the direct injection case then for the port fuel injection case. This is likely due to the efficient and consistent manner in which direct injection transports fuel to the combustion chamber.

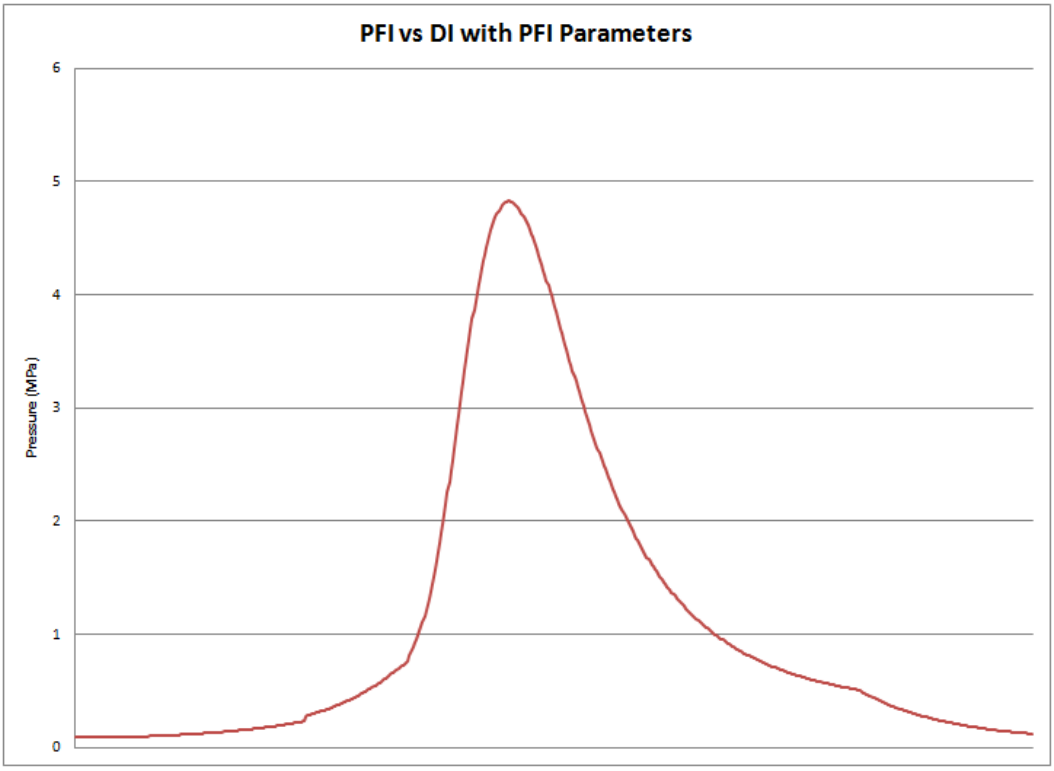

Figure 4.1.1 Pressure plot for 5500rpm and 35” Hg

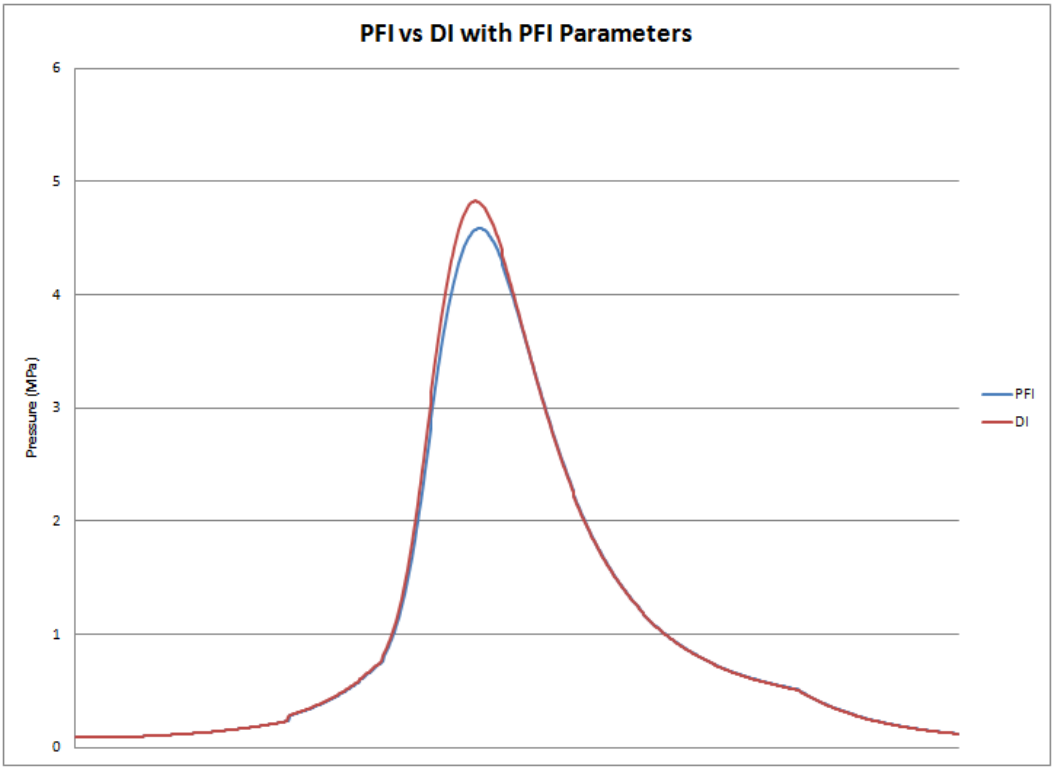

Figure 4.1.2 Pressure plots for PFI and DI simulations under same operating conditions

One interesting observation made when switching from port fuel injection to direct fuel injection was an increase in the mass fraction of fuel in the chamber before ignition. Figure 4.1.3 shows one of the more extreme comparisons of mass fraction of fuel inside the combustion chamber for port fuel injection and direct fuel injection occurring late in the compression stroke. It was observed that for port fuel injection, the fuel initially increases dramatically as the inlet valve is first opened. This was then preceded by a dwell in mass fraction of fuel in the cell which was then followed by another drastic increase in fuel. This is likely due to turbulence at intake. It was also noted that the final mass fraction of fuel in the combustion chamber before ignition was less than that of the direct injection case for the same amount of fuel injected. This can be attributed to the interaction of the fuel with the intake valve resulting in fuel collecting on the valve as well as fuel bouncing back into the inlet port as the valve closes. However, as seen in figure 4.1.3 for direct injection there was no dwell noted in any of the cases. Since fuel was injected directly into the chamber, no fuel was lost to inlet wetting or intake turbulence. Though there were differences observed in the fuel delivery, it should be noted that as the model is allowed to achieve steady state after several cycles the gap would disappear. This indicates that the transient response of the direct injection engine to changing operation demands is nearly immediate, while the response of the PFI engine depends on the fuel flow and injection within the intake manifold.

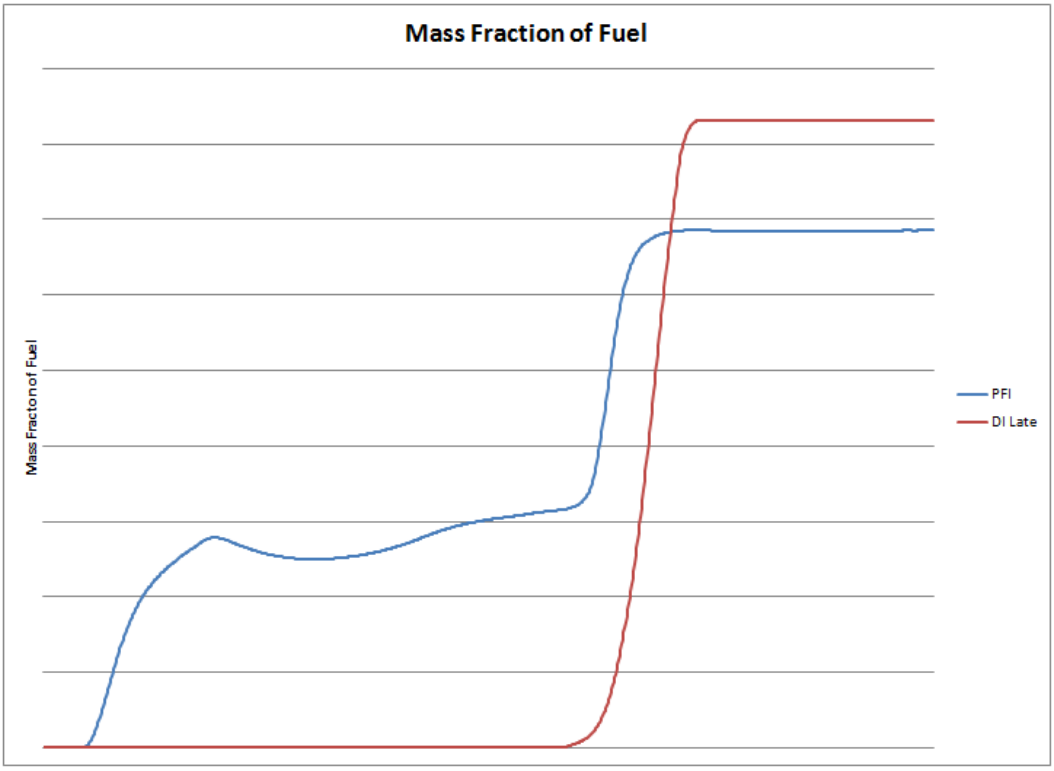

Figure 4.1.3 Mass fraction of fuel

4.2 Spark Timing Study

The first characteristic of the engine to be explored in this study was spark timing. With the exception of spark timing the configuration described in previous section was used for all cases. Spark timing was varied according to table 4.2.1 for each of the cases discussed below.

Case	Spark Timing	CA° bTDC
1	685	35
2	690	30
3	695	25
4	700	20
5	710	10
6	720	0

Table 4.2.1 Spark Timing

Figure 4.2.1 shows the pressure plots for each of the different spark timing cases. Some of the cases tend to overlap, so in order to get a better understanding of the effects spark timing the peak pressure for each spark time is plotted against one another in figure 4.2.2. This graph shows a comparison of the pressure peak for each of the analyzed spark timings. It can be seen that as spark timing is retarded from TDC the maximum pressure peaks increase up to 25° bTDC, after which further delay provides no additional benefit to peak pressure. However, retarding the spark beyond maximum peak pressure can serve to diminish the engine tendency to knock and may be a required compromise. For this study the spark timing corresponding to maximum pressure peak occurs near the PFI stock spark timing. This spark timing will be used for subsequent analysis.

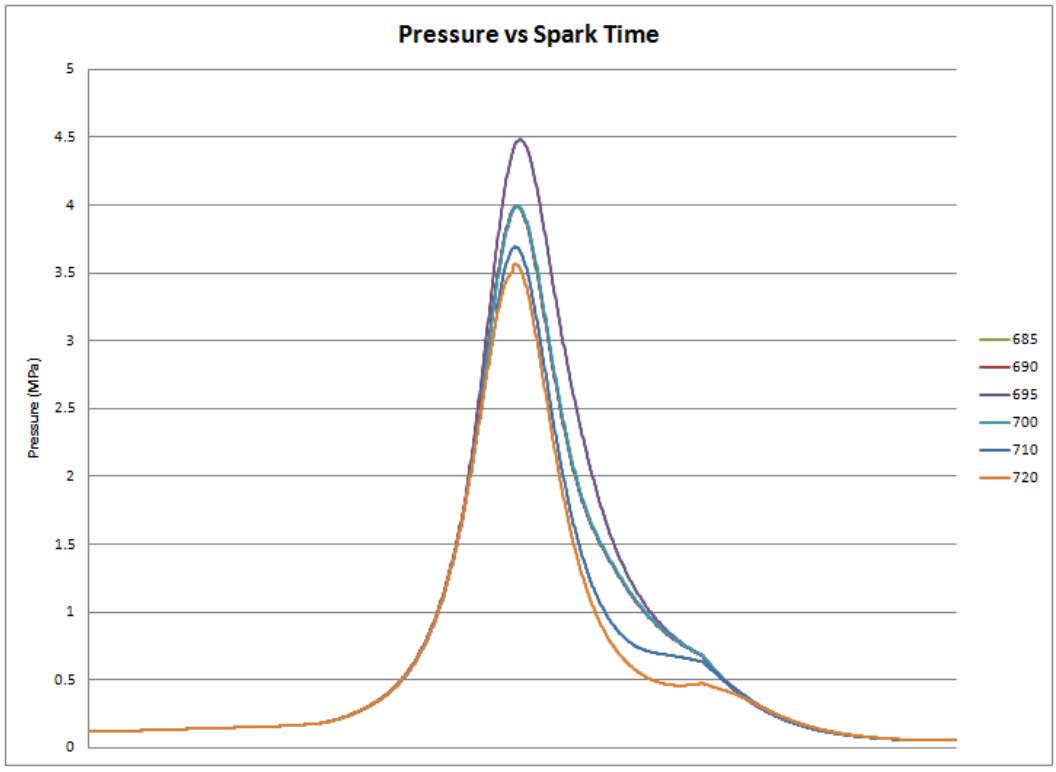

Figure 4.2.1 Pressure as a Function of Spark Timing

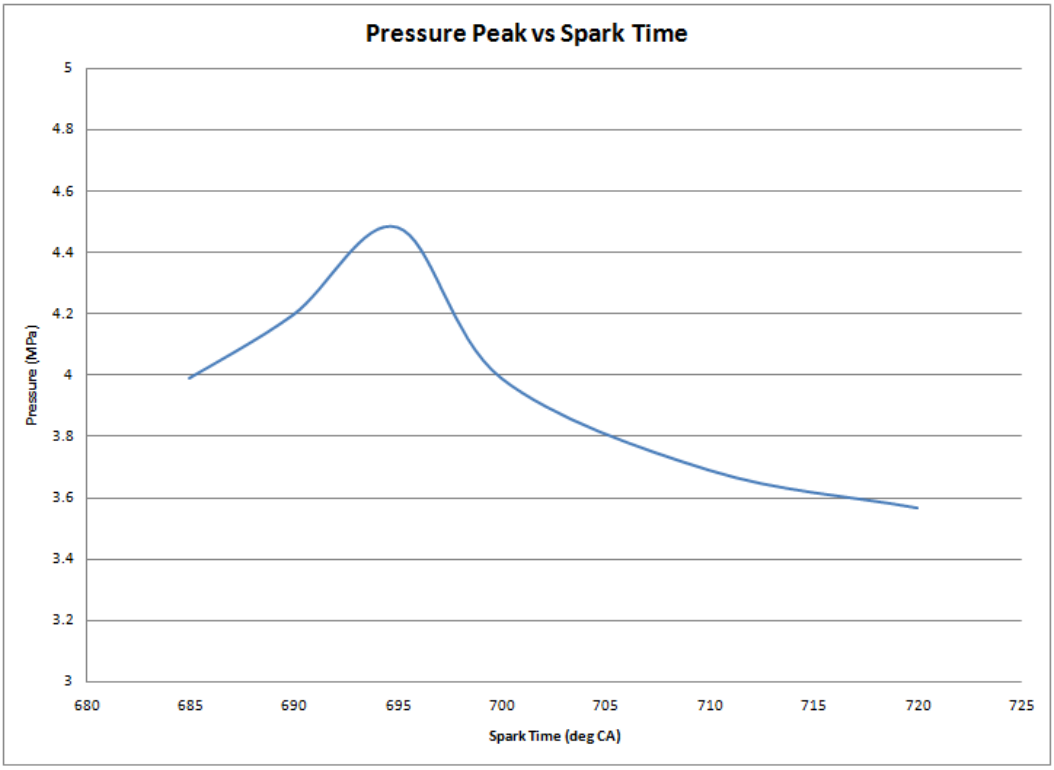

Figure 4.2.2 Pressure Peak as a Function of Spark Timing

4.3 Injection Angle

All injections were performed from the approximate location of one of the spark plug holes in the actual engine. Injections were executed in the Y-Z plane in the direction of the piston. Table 4.3.1 shows the three different injection angles that were evaluated for both early and late injection timing. Figure 4.3.1 shows a visual representation of the injection within the combustion chamber for each injection angle.

Case	Angle
1	30°
2	45°
3	60°

Table 4.3.1 Fuel injection angle

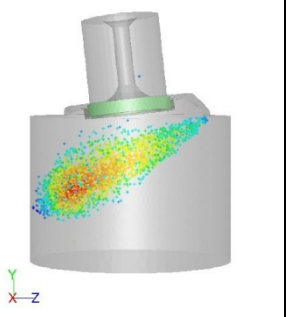

(a) 30°

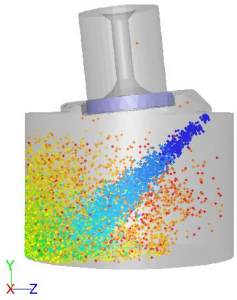

(b) 45°

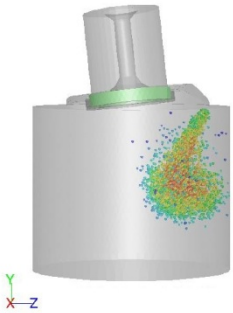

(c) 60°

Figure 4.3.1 Injection angle in the combustion chamber

Figure 4.3.2 shows a comparison of the pressure peaks for each of the injection angles under early injection timing. The difference between each case is so minimal that a small area near the peak must be examined to see any significant variation. Figure 4.3.3 shows that, for early injection, 45° and 60° are superior to 30° injection angle. However, as all three pressure peaks are within 0.1MPa of each other, it can be said that for the flat piston early injection is not effected by variation in injection angle.

Figure 4.3.4 shows the same comparison of pressure peaks for each of the injection angles under early late timing. Once again the difference between each case is so minimal that a small area near the peak must be examined. However, even in figure 4.3.5, which shows pressure near the peak, there is little discernable difference between pressure peaks. In this case, all three pressure peaks are within 0.01MPa of each other. Therefore, in the case of the flat piston, pressure peak is insensitive to injection angle in both early and late fuel injection strategies.

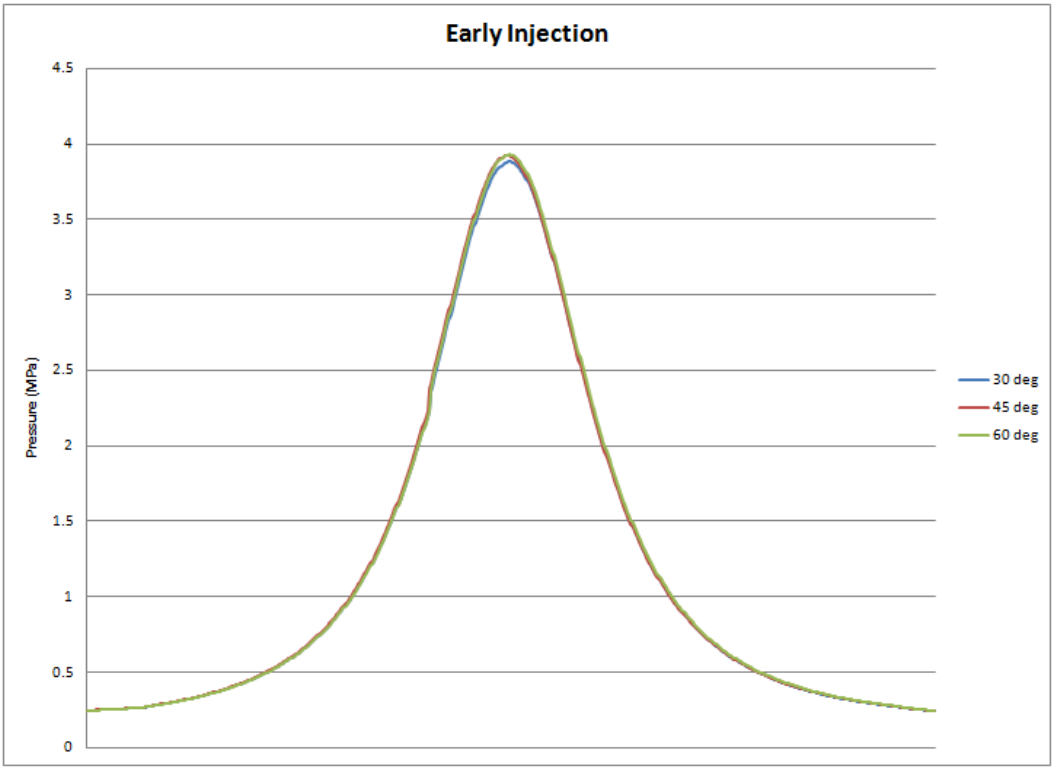

Figure 4.3.2 Early injection pressure peaks for different injection angles

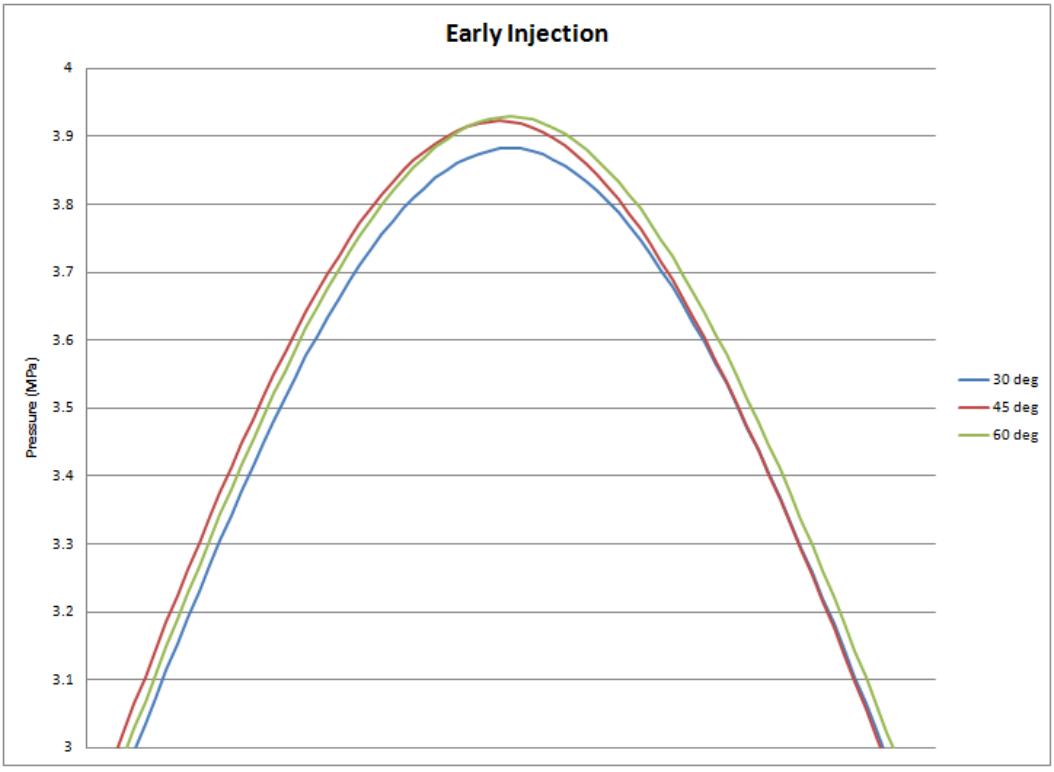

Figure 4.3.3 Early injection pressure peaks for different injection angles near peak

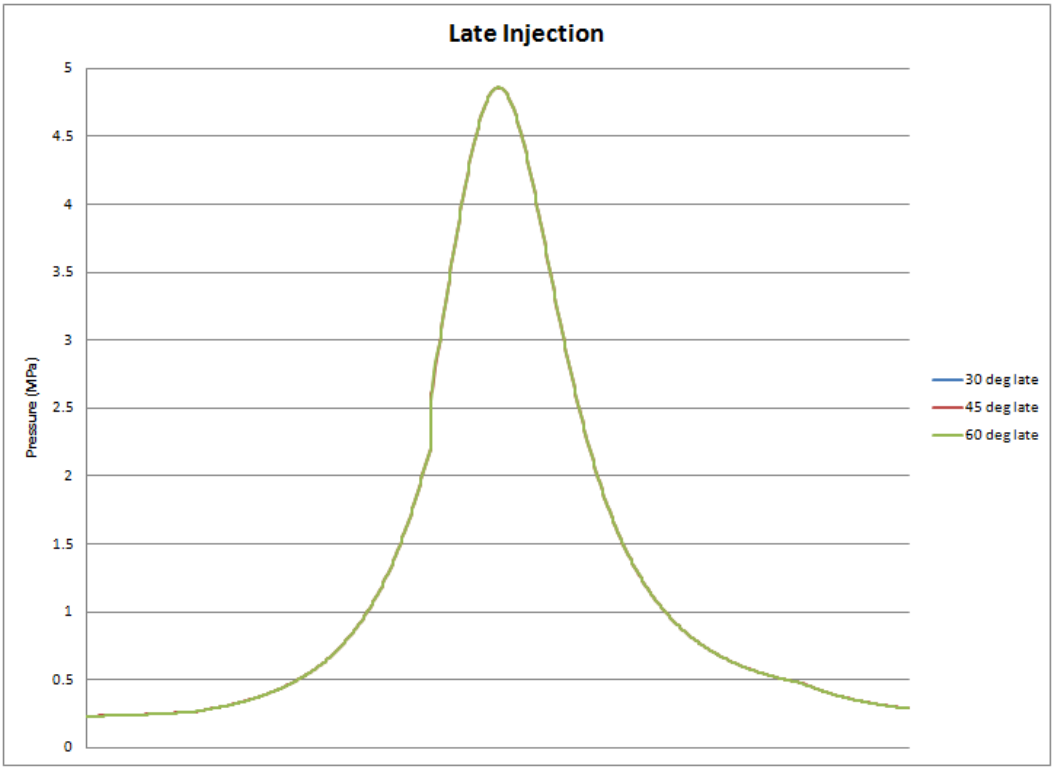

Figure 4.3.4 Late injection pressure peaks for different injection angles

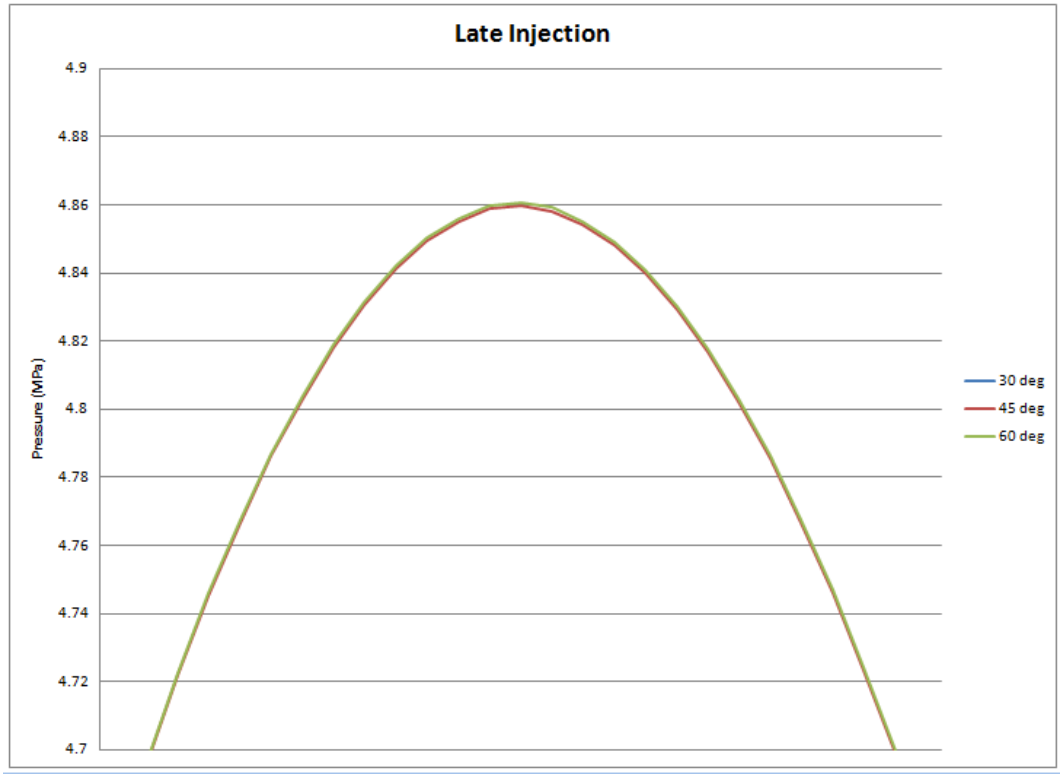

Figure 4.3.5 Late injection pressure peaks for different injection angles near peak

4.4 Injection Timing

It is well know that level of turbulence is essential in the fuel-air mixing process. For DISI operated in a homogeneous charge combustion mode (an early injection mode) where fuel is injected early in the intake stroke, the combination of high turbulence intensity and low mean velocity at the spark gap is desirable to produce a homogeneous air-fuel mixture. For DISI using stratified charge combustion mode (a late injection mode) where fuel-injection at the end of the compression stroke, a flow field with elevated mean velocity and reduced turbulence level is preferred [11]. Figure 4.4.1 below shows an increase of the pressure peak when the fuel is injected in the compression stroke as opposed to the injection stroke.

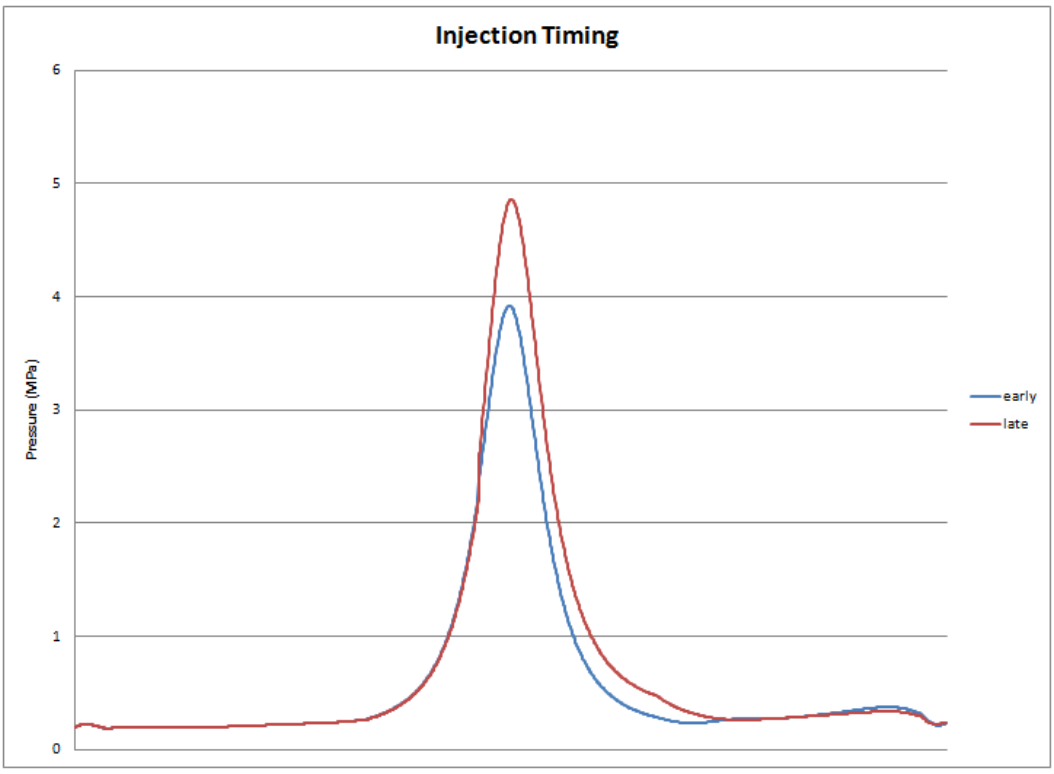

Figure 4.4.1 Pressure as a function of injection timing

4.5 Spark Energy Study

The final parameter explored was the energy that was released by the spark to begin the combustion process. Table 4.5.1 shows the three spark energies used for this study with the spark size the same for all three. Each energy released represents an order of magnitude different than the previous. Figure 4.5.1 shows the pressure plots for the three cases plotted together. It can be seen that the pressures are nearly identical; therefore a detailed view was needed to discern any difference in pressure peak. Figure 4.5.2 shows the area around peak pressure from the previous plot. It was noted that the difference in peak pressure for the highest and lowest cases was on the order of 0.04 MPa. From this it can be determined that the influence of spark intensity has little effect on pressure peak. So long as the energy released by the spark plug is sufficient to initiate combustion, it will have negligible impact on the peak pressure obtained through the combustion process.

Case	Spark Energy (J)
1	0.01
2	0.1
3	1

Table 4.5.1 Spark Energy

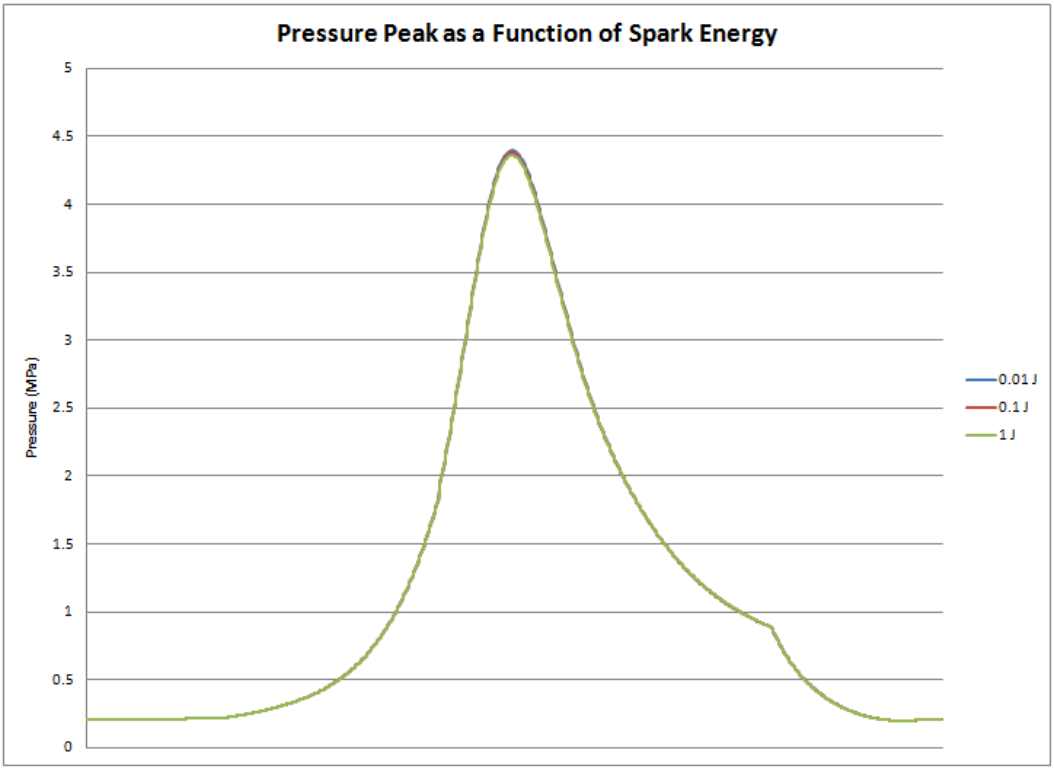

Figure 4.5.1 Pressure peak as a function of spark energy

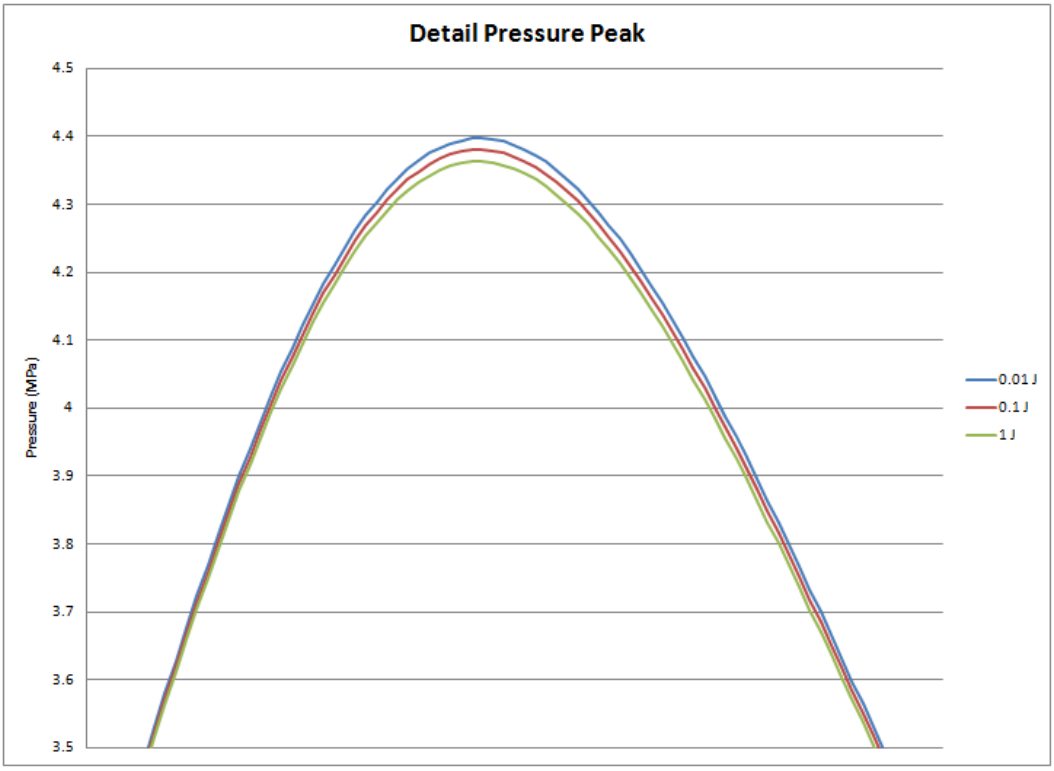

Figure 4.5.2 Detail view of pressure peak as a function of spark energy

4.6 Conclusions

In the first section it was shown that when the port fuel pressure trace is compared to that of the direct injection case an increase is seen with all other parameters held constant. Also, when looking at the actual fuel in the cylinder, the direct injection case is proven to be more effective at delivering all the fuel from the injection to the combustion chamber. This is by the very nature of the injection method. Furthermore, when spark timing is analyzed, it is seen that the port fuel injection spark timing is also best for direct injection. This is more related to the given engine and load conditions then the injection method. Maximum pressure peak was observed to be insensitive to injection angle for the flat piston discussed in this chapter. This was noted during both early and late injection conditions. However, late injection resulted in a higher pressure peak then early injection. Finally the effect spark intensity played on peak pressure in the cycle was discussed. It was determined that peak pressure was insensitive to the amount of energy used to begin the combustion process. For this analysis, stock spark timing and intensity coupled with late injection provided the best pressure peak.

Chapter 5: Bowl Piston Direction Injection Study

Advanced piston design applied to direct injection allows for more precise mixing and distribution of fuel within the combustion chamber over the varied operating modes. The designer has the ability to inject a stratified charge directly to the spark area using a reflecting bowl piston and a late injection strategy while still being able to provide additional tumble or swirl motion in the homogeneous operating mode with early injection timing. This chapter seeks to explore the effects that piston design has on engine operation by applying the piston from a production direct injection automobile to the Rotax 914 engine. The piston has been meshed and implemented exactly as the original piston discussed in chapter 2. The compression ratio has been kept the same as well to ensure that the results depict only the influence of the piston design on performance.

5.1 Cold Flow / Charge Motion Study

The fluid motion of the flat piston case was discussed in chapter 3; however, with a new piston design it is prudent to revisit some of the aspect discussed previously. Figure 5.1.1 shows the fuel vaporization of the bowl piston in early injection timing. It can easily be seen that the fuel is reflected off the piston with an increased tumble motion as compared to the flat piston. Additionally, the fuel vaporizes much faster with this piston then was possible with the flat piston. It can be seen that all of the fuel has been vaporized before 60° bTDC, whereas the flat piston case still had liquid fuel present even as late as 30° bTDC.

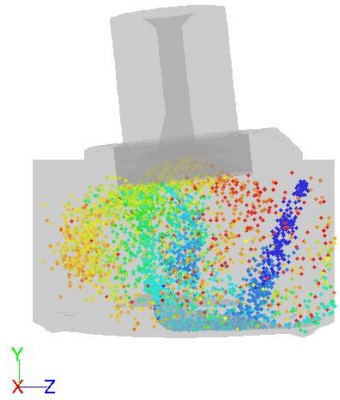

(a) 270° bTDC

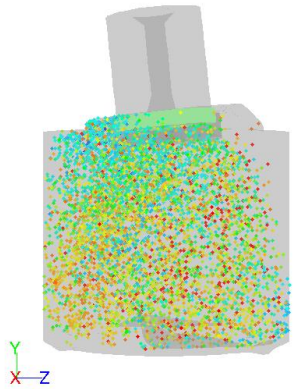

(b) 210° bTDC

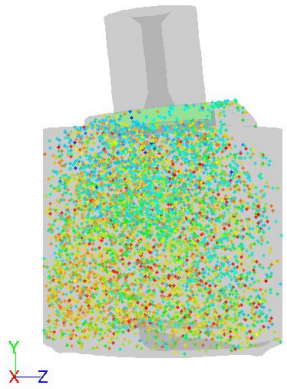

(c) BDC

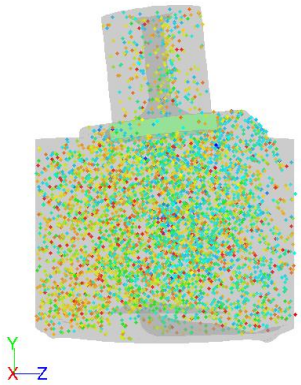

(d) 120° bTDC

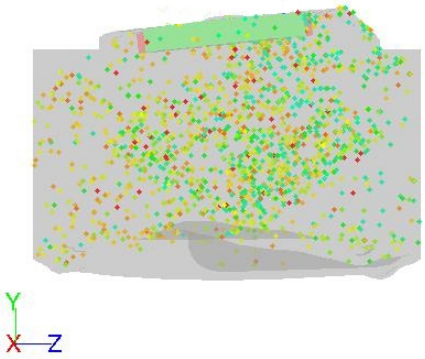

(e) 90° bTDC

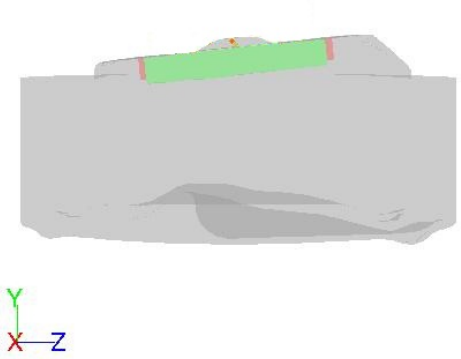

(f) 60° bTDC

Figure 5.1.1 Vaporization of fuel in the cylinder

Figure 5.1.2 shows the more pronounced tumble and swirl that are present in the bowl piston version of the Rotax engine. This additional fluid movement helps the fuel to better mix with the air and increases the rate of vaporization as seen in figure 5.1.1 [50, 51, 52]. Additionally, figure 5.1.3 shows better fuel distribution in the cylinder before combustion when compared to the flat piston case. Here fuel nearly homogeneous at BDC while with the flat piston, the charge was not completely homogeneous until more than 30° after BDC.

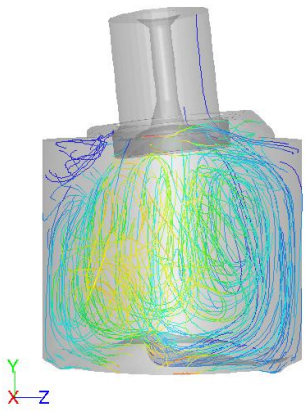

(a) Tumble

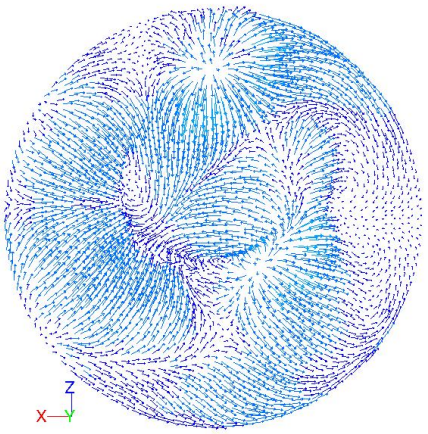

(b) Swirl

Figure 5.1.2 Tumble and swirl motion of air in cylinder

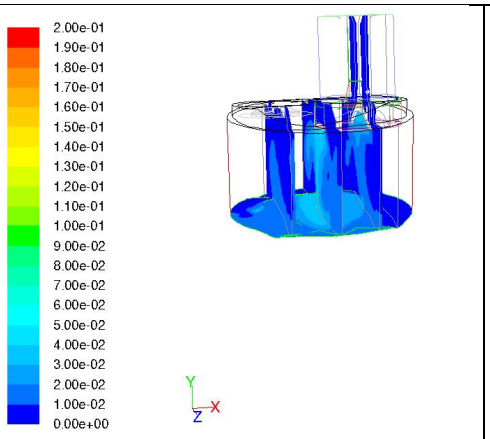

(a) 270° bTDC

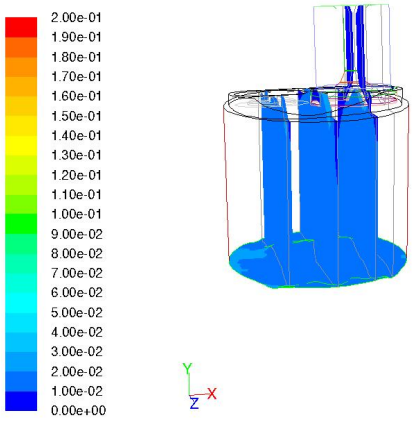

(b) BDC

Figure 5.1.3 Fuel distribution before combustion

As a result of the better prepared air-fuel mixture in the chamber, the combustion in the bowl piston engine is more complete as seen by the contours of fuel in figure5.1.4 and the contours of CO_2 produced in figure 5.1.5. This leads to smoother and more consistent operation with less likelihood of fuel left in the chamber between cycles and a more efficient use of the fuel injected into the chamber.

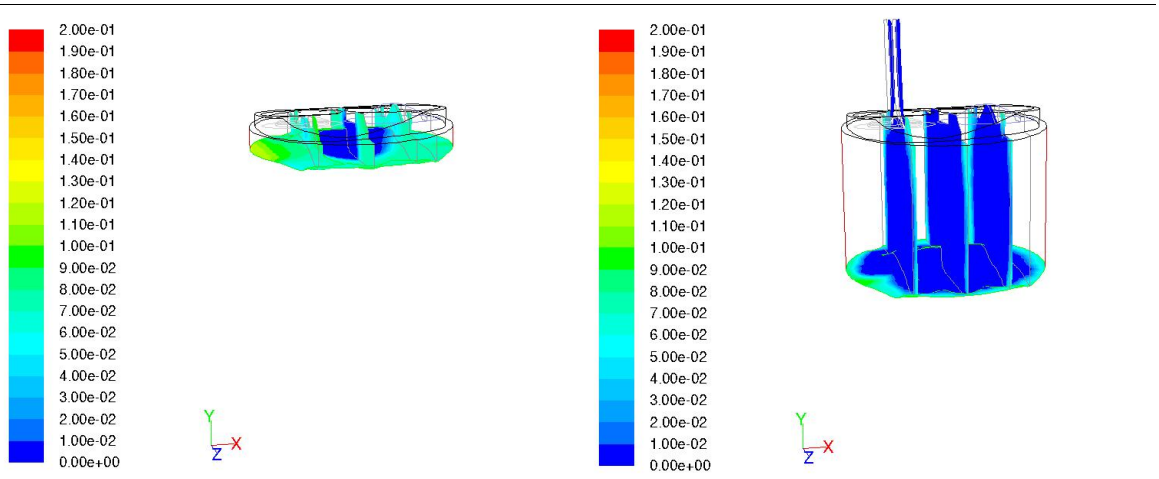

(a) TDC

(b) 120° aTDC

Figure 5.1.4 Fuel distribution during combustion and expansion

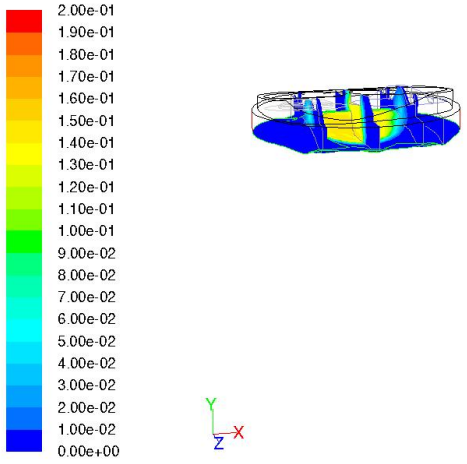

(a) TDC	(b) 120° aTDC
Figure 5.1.5 Production of CO_2 during combustion cycle	

5.2 Injection Angle

The injection angle study shown here follows the same method as the one for the flat piston direct injection case. All injections were performed from the approximate location of one of the spark plug holes in the actual engine. Injections were executed in the Y-Z plane in the direction of the piston. Table 5.2.1 shows the three different injection angles that were evaluated for both early and late injection timing. Figure 5.2.1 shows a visual representation of the injection within the combustion chamber for each injection angle.

Case	Angle
1	30°
2	45°
3	60°

Table 5.2.1 Fuel injection angle

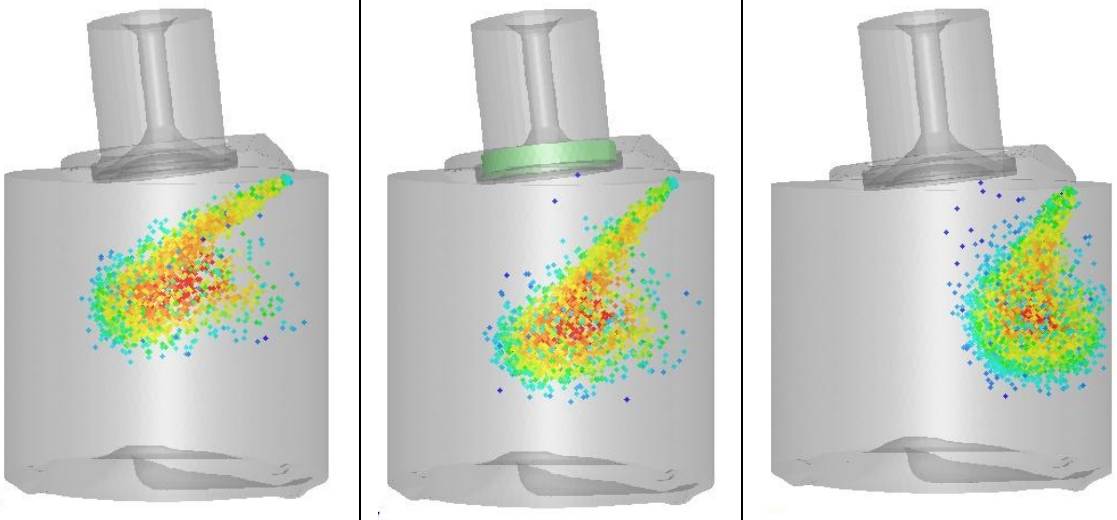

(a) 30°

(b) 45°

(c) 60°

Figure 5.2.1 Injection angle in the combustion chamber

Figure 5.2.2 shows a comparison of the pressure peaks for each of the injection angles under early injection timing. The difference between each case is even less noticeable with each case nearly identical to the previous. This would suggest that the pressure peak produced in the bowl piston as a result of combustion is independent of injection angle. In this case no matter the injection angle, the fuel is suitably mix and ready for combustion likely due to the increased swirl and tumble motion of the charge in the chamber compared to the flat piston case.

Figure 5.2.3 shows the same comparison of pressure peaks for each of the injection angles under early late timing. However, it can be seen that the pressure peaks vary widely with injection angle for the bowl piston. This indicates that there is a relationship between pressure peak and injection angle for the bowl piston operated under late injection. This is contrary to what was observed during the flat piston discussion and

confirms the importance of piston design. Additionally, it is noted that the pressure peak for the case of 45° injection angle is substantially lower than that of the either the 30° injection angle or the 60° injection angle. The reason for this is the interaction between the injected fuel and the piston movement which will be discussed further in the next section.

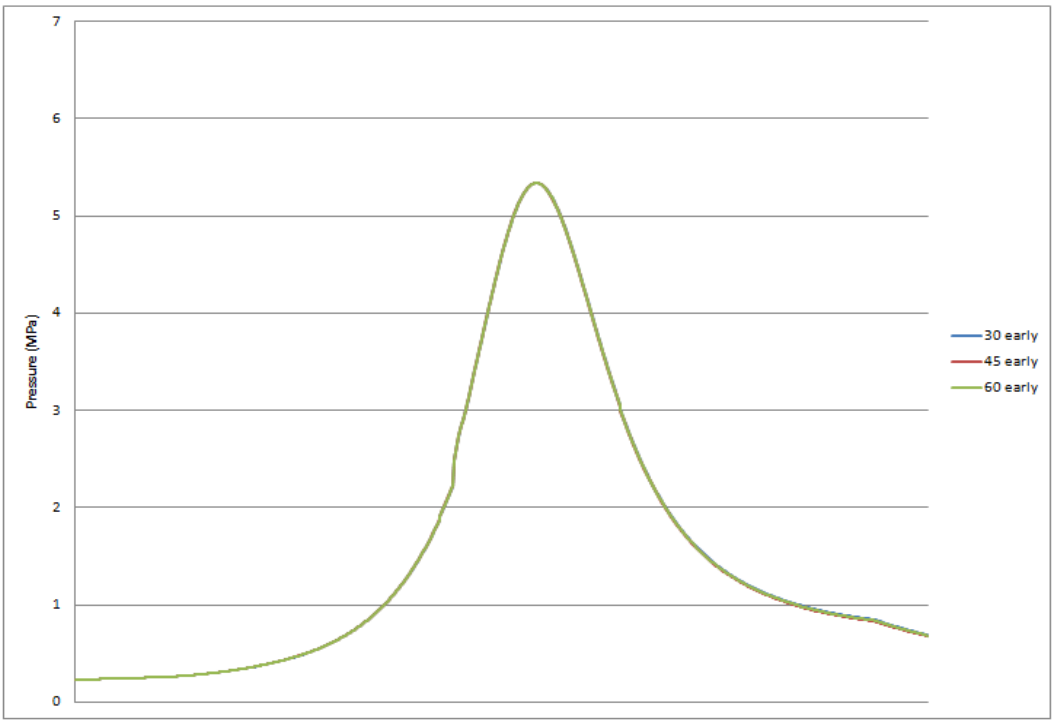

Figure 5.2.2 Early injection pressure peaks for different injection angles

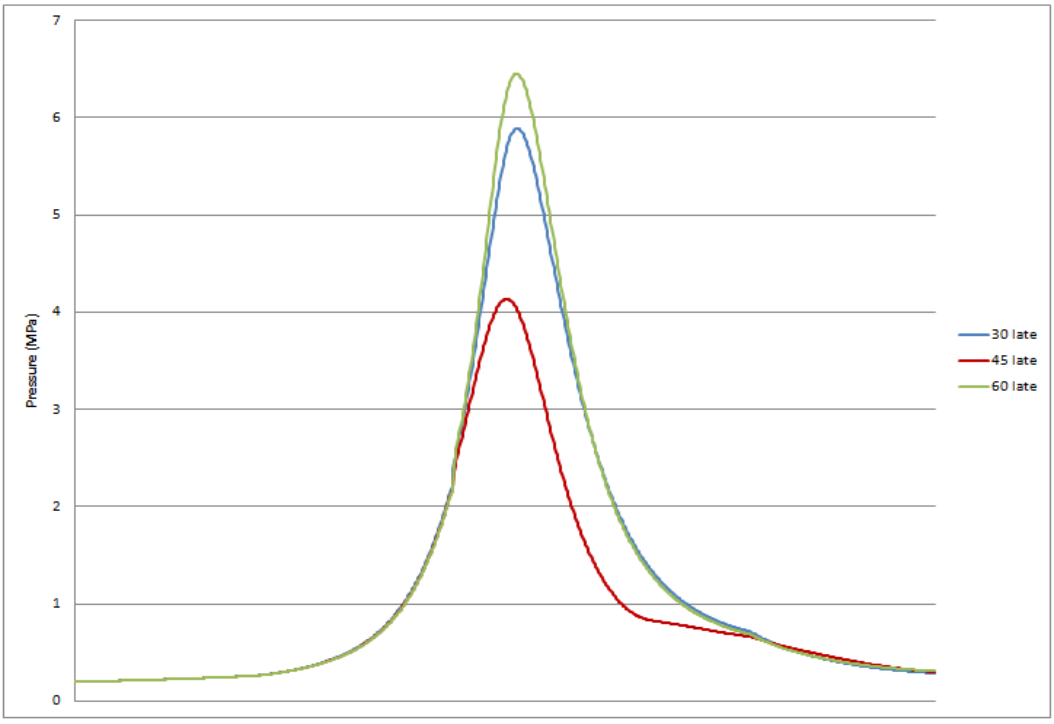

Figure 5.2.3 Late injection pressure peaks for different injection angles

5.3 Injection Timing

As discussed in the previous chapter, injection timing plays a key role in determining the mixture formed in the combustion chamber. Early injection times result in a homogeneous mixture formation, while late injection times generally produce a stratified mixture. This is one of the key benefits that the bowl piston seeks to exploit by utilizing wall guided spray. This allows the charge to better mix in the early injection case while also reflecting the spray up to the spark plug area during the late injection strategy.

Figures 5.3.1-3 show the comparison of pressure plots for early and late injection timing for each of the three injection angles. The results for 30° injection angle shown in

figure 5.3.1 as well as the results for 60° injection angle shown in figure 5.3.3 show the same trend observed with the flat piston, late injection timings produce higher pressure peaks than early injection timings. However, figure 5.3.2 appears to be contrary to this conclusion with the early injection timing resulting in a higher pressure peak than the late injection timing.

At first this appears to be an anomaly with the simulation; though, when the fuel distribution in the cell is analyzed it is discovered that this low pressure peak is the result of poor mixing of the fuel with the air in the chamber. Figure 5.3.4(a)-(d) shows the interaction of the fuel and the piston at several points during the compression stroke. The fuel is injected at BDC as seen in figure 5.3.4(a). As the piston begins the upstroke the fuel progresses through the combustion chamber as seen in figure 5.3.4(b). The fuel contacts the piston behind the reflection bowl as seen in figure 5.3.4(c) and disperses around the back side of the piston as shown in figure 5.3.4(d). As the fuel flows through the chamber much of it is vaporized and mixed with the air; however, figure 5.3.5 shows that some of the fuel remains on the piston behind the bowl. This fuel does not completely vaporize resulting in the lower pressure peak as compared to early injection. This fact supports the need for CFD as a tool to analyze and visualize complex and difficult to observe phenomenon such as the flow interaction within an internal combustion engine. It also serves to display the importance the design and analysis of fuel injection orientation and its interaction with the moving piston within an engine utilizing advanced piston designs.

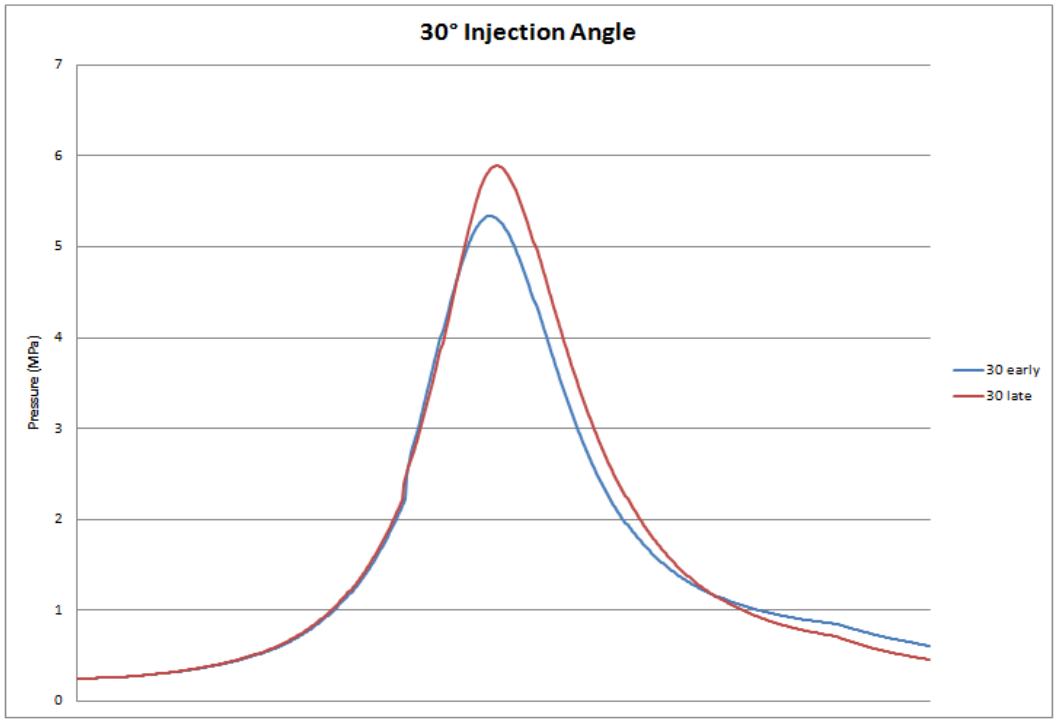

Figure 5.3.1 Comparison of early and late injection timing for 30° injection angle

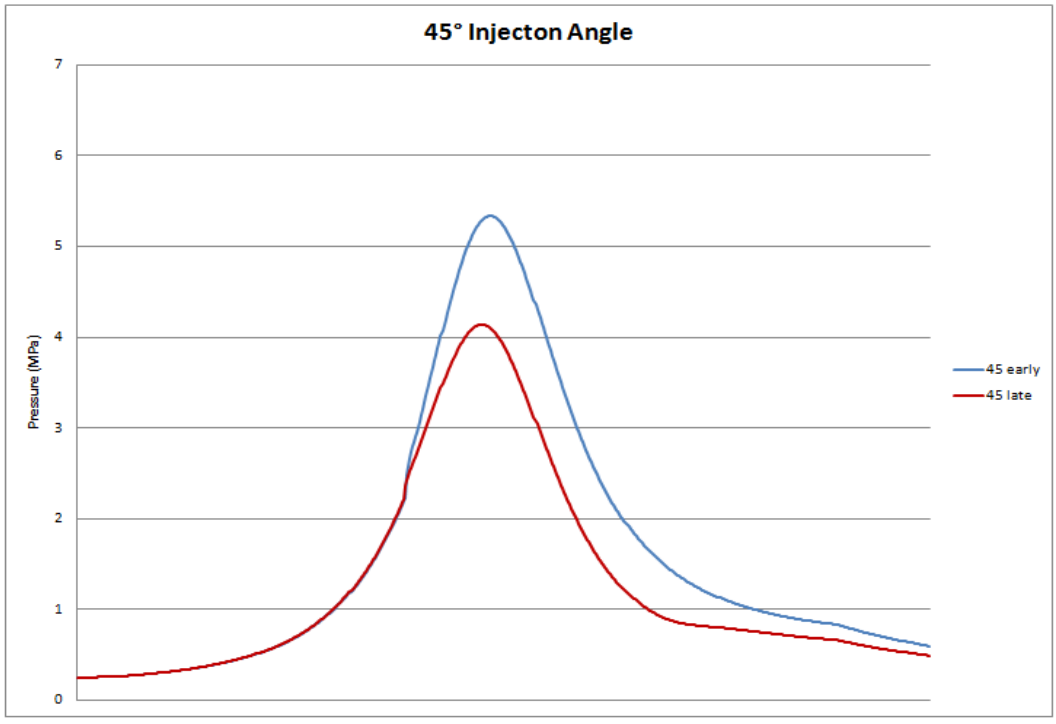

Figure 5.3.2 Comparison of early and late injection timing for 45° injection angle

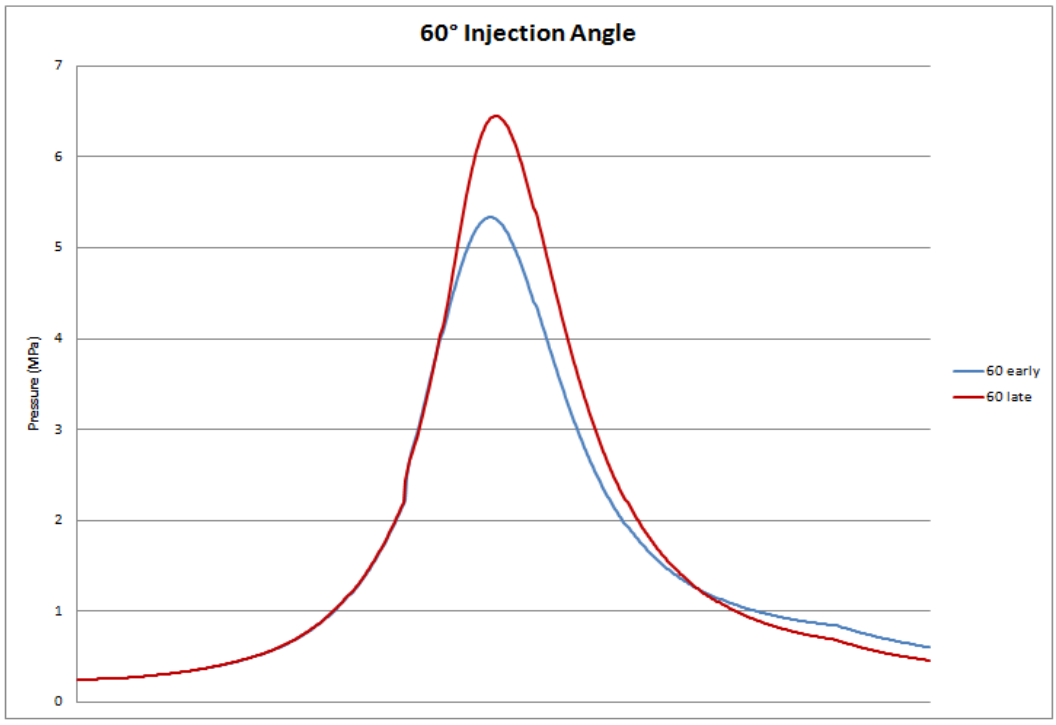

Figure 5.3.3 Comparison of early and late injection timing for 60° injection angle

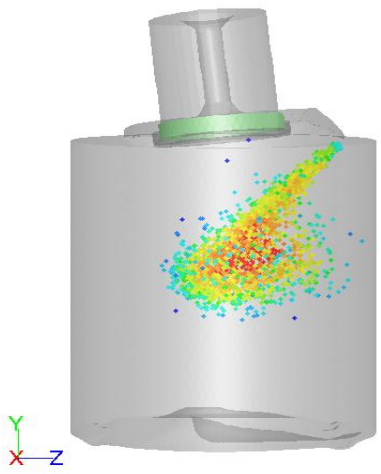

(a) 180° bTDC

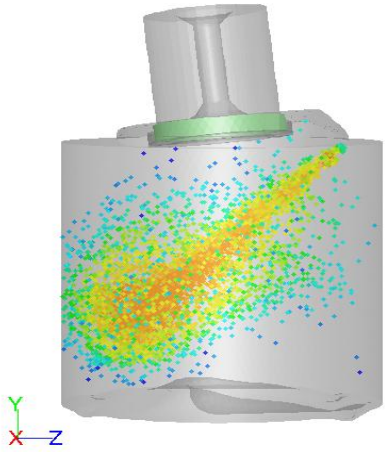

(b) 150° bTDC

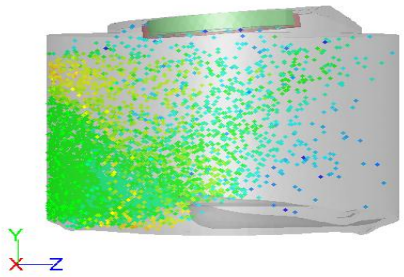

(c) 100° bTDC

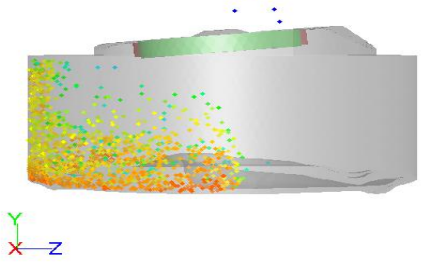

(d) 60° bTDC

Figure 5.3.4 Interaction of fuel injected with piston movement

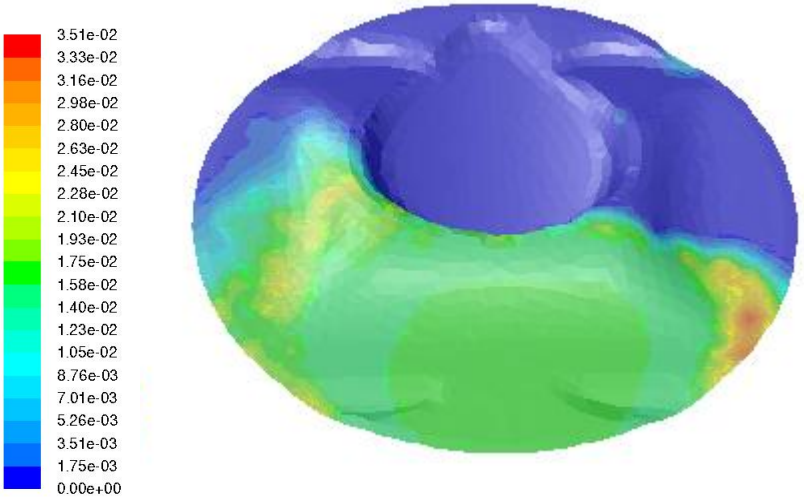

Figure 5.3.5 Fuel on the piston

5.4 Conclusions

With the application of a new advanced piston design to the engine analyzed in the last chapter, a charge motion study was performed to determine the motion of the air in the chamber before fuel is applied as well as the interaction between air and fuel after injection. It was observed that the swirl and tumble motion present in the flat piston case was more well defined with the application of the bowl piston. Additionally, fuel was observed to vaporize faster and more efficiently as a result of this increased motion teamed with the interaction between the injection and the reflective bowl piston.

However, it was noted that the interaction between the injection and the piston motion should be well coordinated in order to maximize mixing and vaporization as well as to avoid adverse interaction such as the one noted in the previous section. While the piston design presented here is not necessarily the optimal design for this application, it shows the benefits and pitfalls of advanced piston design when used with direct injection.

Chapter 6: Future Work and Recommendations

Although direct injection spark ignition is by no means a new technology, the application within the aviation field is definitely uncharted waters. While this study presents several models of the application of DISI to small aircraft engines, much work needs to be done to experimentally study and refine these techniques and explore other ways to advance the technology in this sector. With all the redundancies and failsafe required for an aeronautical application, a great deal of effort needs to be utilized to ensure the technology that goes into the engine is fully matured and consistently reliable in extreme operating conditions. Whereas the typical automotive engine operates in a fairly narrow range of altitude and pressure, an aviation DISI engine must be capable of performing within a much larger operational envelope.

This study has shown the importance of computational fluid dynamics in the design and analysis of complex problems such as the one presented here. By continuing to employ CFD, expensive and time consuming experimental analysis can be limited greatly. Being able to visualize complex flow phenomenon such as those presented in this paper, will aid in the understanding of complex outcomes such as those presented in Chapter 5. Furthermore, the accumulation of additional models, including knock and heat transfer due to engine cooling, will only serve to improve the prediction capabilities of this model for additional operation parameters.

In literature, multiple injections have been shown provide additional power by supplying extra fuel after the initial combustion event has occurred [4, 39]. Yang and

Anderson [4] discuss using two injections; one during the intake stroke and a second, smaller injection late in the compression stroke. By separating the injection into two independent events, an overall stoichiometric charge can be achieved with a lean homogeneous mixture throughout most of the combustion chamber and a local rich region near the spark plug. Consequently volumetric efficiency is increased by means of the fuel injected during the intake stroke while still providing charge cooling with the fuel injected during the compression stroke. Other advanced injection strategies can be investigated by means of computational fluid dynamics to provide an optimal solution for multiple injections per cylinder.

Air assisted direct injection [6, 7, 8, 41] could also be examined by means of CFD to determine the effects of its application to the Rotax 914 engine. It has been shown to enable very lean combustion without modification to the intake airflow characteristics. The use of air assisted injection also results in highly atomized fuel spray facilitating faster evaporation of fuels which is beneficial for heavy fuels that are harder attain the small particle size of octane. Additionally this would require less mixture preparation time, allowing for injection later in the cycle at all load conditions.

Injection is not the only area where CFD can be applied. Alternative ignition approaches could also be studied to increase the engine stability limit beyond that of a conventional spark plug [15, 42, 43, 44]. Plasma-jet and flame-jet ignition can help to move the energy release of the ignition from the spark plug on the cylinder head towards the center of the cylinder. This helps to ignite mixtures that may be difficult to start combusting with a traditional ignition system. In addition it transitions the flame from

the traditional laminarlike flame to a turbulent flame which results in greatly reduced flame development time. Furthermore this can help to extend the lean stability operating limit as well as prevent misfires from occurring. These and other methods of initiating combustion can be observed to determine their benefit to the different combustion modes within a direct injection engine.

Piston surface design plays an important role in charge preparation and direct injection operation, as seen in the previous chapter. Investigation into optimal piston design could allow more power to be obtained from a given engine or a better charge stratification obtained. While it has been shown that DISI will work in an engine with a nearly flat piston, most automotive applications employ advanced piston design to ensure optimal charge preparation prior to combustion. With additional research, an optimal piston design could be devised that would allow for better operational efficiency and maximum power.

In the automotive industry, direction injection is often accompanied by other advanced engine technologies [3] including variable valve timing and variable valve lift, advanced intake manifolding, exhaust gas recirculation, etc. The effects of these other advanced engine technologies should be further explored to determine their possible application and benefits to DISI aviation application. Many of these could be easily simulated in a computational environment in order to determine their effectiveness even before their physical application.

Beyond the components that make up the engine, additional research needs to be conducted with regards to the optimal application of the different direct injection

combustion modes: stratified charge mode, homogeneous mode, homogeneous lean-burn mode, homogeneous stratified charge mode, homogenous anti-knock and stratified charge engine-heating [34, 35]. Each of these approaches to in cylinder combustion has its advantages. Although they must be applied under the appropriate conditions in order to reap their maximum benefits. CFD parametric study could guide the application of the different combustion modes over the operational envelope of the engine before experimental work even had to be performed.

Another advantage of direct injection technology not evaluated in this thesis is the use of multiple fuel types in the same engine [13, 14]. Little work has been done applying lower octane fuels or even bio-fuels to internal combustion aviation power plants. The ability to operate on a wider variety of fuel would be extremely beneficial, especially for military applications. The majority of the air vehicle inventory operated by the US Air Force derives their propulsion from power plants designed and optimized to run on JP8 jet fuel. However, newer unmanned aerial systems (UAS) often operate on high octane gasoline which presents several operational and logistical problems. JP8 is prevalent on most every Air Force base and advanced location, while high octane gasoline may be more difficult to acquire especially in remote locations. Additionally, storing and transporting high octane gasoline can cause the octane levels to deteriorate over time. Being able to use a variety of fuels in these smaller UAS engines would help to solve these operational and logistical barriers.

This study merely scratches the surface of what can be applied to aviation internal combustion engines. Much work needs to be done to fully adapt direct injection

technology for aeronautical applications while maintaining the high levels of redundancies and failsafes necessary for supportable operation.

Chapter 7: Conclusions

A computational fluid dynamics model was developed from an actual Rotax 914 engine to investigate the effects of direct injection on the engine. Gambit was adopted for geometry generation and meshing, while Fluent was used for fluid motion and combustion simulation. A port fuel injected version of the computational model was validated against experimental results of the Rotax 914 engine in order to add fidelity to the model. Direct injection spark ignition was then applied to the model and a parametric study was performed to determine operation capabilities under different operating conditions.

It was shown that when the port fuel pressure trace is compared to that of the direct injection case an increase is seen with all other parameters held constant. Also, when looking at the actual fuel in the cylinder, the direct injection case is proven to be more effective at delivering all the fuel from the injection to the combustion chamber in a given cycle. This is by the very nature of the injection method and serves to increase the transient response of the engine to ever changing operating conditions. However, when spark timing is analyzed, it is seen that the port fuel injection spark timing is also adequate for direct injection. This is more related to the given engine and load conditions then the injection method. Maximum pressure peak was observed to be insensitive to injection angle for the flat piston discussed in this chapter. This was noted during both early and late injection conditions. However, late injection resulted in a higher pressure peak then early injection.

With the application of a new advanced piston design to the engine analyzed, a charge motion study was performed to determine the motion of the air in the chamber before fuel is applied as well as the interaction between air and fuel after injection. It was observed that the swirl and tumble motion present in the flat piston case was more well defined with the application of the bowl piston. Additionally, fuel was observed to vaporize faster and more efficiently as a result of this increased motion teamed with the interaction between the injection and the reflective bowl piston. However, it was noted that the interaction between the injection and the piston motion should be well coordinated in order to maximize mixing and vaporization as well as to avoid adverse interaction. While the piston design presented here is not necessarily the optimal design for this application, it shows the benefits and pitfalls of advanced piston design when used with direct injection.

REFERENCES

1. Colucci P J, Lee D, Lim C K, Goldin G. In-cylinder engine modeling developments at Fluent.Bents, D.J., Harp, J.L., Schmitz, P.C., "Propulsion system for very high altitude subsonic unmanned aircraft", NASA/TM -1998-206636.

2. Bedford F, Hu X, Schmidt U. In-cylinder combustion modeling and validation using Fluent.

3. Zhao, F., Lai, M.C., Harrington, D.L., "Automotive spark-ignited direct-injection gasoline engines", Progress in Energy and Combustion Science, Volume 25, 1999, p. 437-562

4. Yang J, Anderson W. Fuel injection strategies to increase full-load torque output of a direct-injection SI engine. SAE Technical Paper, No. 980495, 1998

5. Yunlong B, Zhi W, Jianxin W. Knocking suppression using stratified stoichiometric mixture in a DISI engine. SAE Technical Paper, 2010-01-0597, 2010

6. Houston R, Cathcart G. Combustion and emissions characteristics of Orbital's combustion process applied to multi-cylinder automotive direct injected 4-stroke engines. SAE Technical Paper, No. 980153, 1998

7. Cathcart G, Zavier C. Fundamental characteristics of an air-assisted direct injection combustion system as applied to 4-stroke automotive gasoline engines. SAE Technical Paper, 2000-01-0256, 2000.

8. Cathcart G, Tubb J. Application of air assisted direct fuel injection to pressure charged gasoline engines. SAE Technical Paper, 2002-01-0705, 2002.

9. Payri F, Benajes J, Margot X, Gil A. CFD modeling of the in-cylinder flow in direct-injection diesel engines. Computers & Fluids, Volume 33, 2004, p. 995-1021.

10. Cao L, Bhave A, Su H, Mosbach S, Kraft M, Dris A, McDavid R. Influence of injection timing and piston bowl geometry on diesel PCCI combustion and emissions. *SAE Int. J. Engines* October 2009 2:1019-1033

11. Papageorgakis G, Assanis D. Optimizing gaseous fuel-air mixing in direct injection engines using RNG based k-ε model. SAE Technical Paper. 980135, 1998.

12. Suh E, Rutland C. Numerical study of fuel/air mixture preparation in a GDI engine. SAE Technical Paper, 1999-01-3657, 1999.

13. Falkowski D, Abata D L, Cho P. The performance of a spark-ignited stratified-charge two stroke engine operating on kerosene based aviation fuel. SAE Technical Paper, No. 972737, 1997

14. Singh R, McChesney R. Development of multi-fuel spark ignition engine. SAE Technical Paper, 2004-32-0038, 2004.

15. Heywood, John B., "Internal Combustion Engine Fundamentals," McGraw Hill, 1988.

16. Launder B E, Spalding D B. Lectures in Mechanical Models of Turbulence. Academic Press. London, England. 1972.

17. Yakhot V, Orszag S A Renormalization Group Analysis of Turbulence: I. Basic Theory. Journal of Scientific Computing, 1(1):1-51, 1986.

18. Shih T-H, Liou W W, Shabbir A, Yang Z., Zhu J. A New k-ε Eddy-Vorticity Model for High Reynolds Number Turbulent Flows – Model Development and Validation. Computers Fluids, 24(3):227-238, 1995.

19. Lipatnikov A N, Chomiak J. Turbulent Flame Speed and Thickness: Phenomenology, Evaluation and Application in Multidimensional Simulations. Progress in Energy & Combustion Science, 28:1-74, January 2002.

20. Reitz RD. Modeling Atomization Processes in High-Pressure Vaporizing Sprays. Atomization and Spray Technology, Vol. 3, p. 309-337, 1987

21. Liu S C, Mather D, Reitz R D. Effects of Drop Drag and Breakup on fluid Sprays. SAE Technical Paper 930072, 1993.

22. Spalart P, Allmaras S. A one-equation turbulence model for aerodynamic flows. Technical Report AIAA-92-0439, American Institute of Aeronautics and Astronautics, 1992.

23. Douaud A M, Eyzat P. Four-Octane-Number Method for Predicting the Anti-Knock Behavior of Fuels in Engines. SAE Technical Paper, v87 780080, 1978.

24. Hardenburg H O, Hase F W. An Empirical Formula for Computing the Pressure Rise Delay of a Fuel from its Cetane Number and from the Relevant Parameters of Direct Injection Diesel Engines, SAE Technical Paper, 790493, 1979.

25. Vandoormaal J P, Raithby G D. Enhancements of the SIMPLE Method for Predicting Incompressible Fluid Flows. Numer. Heat Transfer, 7:147-163, 1984.

26. Issa R I. Solution of Implicitly Descretized Fluid Flow Equations by Operator Splitting. Journal of Computational Physics. 62:40-65, 1986.

27. Ferzieger J L, Peric M. Computational Methods for Fluid Dynamics. Springer-Verlag, Heidelberg, 1996.

28. Tannehill J C, Anderson D A, Pletcher R H. Computational Fluid Mechanics and Heat Transfer. Second Edition, Taylor & Francis, 1997.

29. Hirsch C. Numerical Computation of Internal and External Flows. Second Editin, John Wiley & Sons, 2007.

30. Holmes D G, Connel S D. Solution of the 2D Navier-Stokes Equations on Unstructured Adaptive Grids. AIAA 9th Computational Fluid Dynamics Conference, 1989.

31. Rauch R D, Batira J T, Yang N T Y. Spatial Adaption Procedures on Unstructured Meshes for Accurate Unsteady Aerodynamics Flow Computations. Technical Report AIAA-91-1106, 1991

32. Anderson W, Bonhus D L. An Implicit Upwind Algorithm for Computing Turbulent Flows on Unstructured Grids. Computers Fluids, 23(1):1-21, 1994.

33. http://www.cfd-online.com/Wiki/

34. http://autospeed.com/cms/A_107830/article.html

35. http://en.wikipedia.org/wiki/

36. Choi H, Kim M, Min K, Lee J. The Stratified Combustion Model of Direct-Injection Spark-Ignition Engines. Proceedings of the Combustion Institute, Vol 29:695-701, 2002.

37. Alkidas A C. Combustion Advancements in Gasoline Engines. Energy Conservation and Management 48:2751-2761, 2007.

38. Wallesten J, Lipatnikov A, Chomiak J. Modeling of Stratified Combustion in a Direct-Ignition Spark-Ignition Engine Accounting for Complex Chemistry. Proceedings of the Combustion Institute, Vol 29:703-709, 2002.

39. Husted H L, Piock W, Ramsay G. Fuel Efficiency Improvements from Lean, Stratified Combustion with a Solenoid Injector. SAE Technical Paper, 2009-01-1485, 2009.

40. Drake M C, Fansler T D, Lippert A M. Stratified-Charge Combustion: Modeling and Imaging of a Spray-Guided Direct-Injection Spark-Ignition Engine. Proceedings of the Combustion Institute, Vol 30:2683-2691, 2005.

41. Boretti A A, Jin S H, Zakis G, Brear M J, Attard W, Watson H, Carlisle H, Bryce W. Experimental and Numerical Study of an Air Assisted Fuel Injector for a DISI Engine. SAE Technical Paper, 2007-01-1415, 2007.

42. Dale J D, Checkel M D, Smy P R. Application of High Energy Ignition Systems to Engines. Prog. Energy Combust. Sci., Vol 23 p379-398, 1997.

43. Linkenheil K, Ruoβ H-O Grau T, Seidel J, Heinrich W. A Novel Spark-Plug for Improved Ingition in Engines with Gasoline Direct Injection. IEEE Transactions on Plasma Science, Vol 33 (5), 2005.

44. Piock W, Weyand P, Wolf E, Heise V. Ignition Systems for Spray-Guided Stratified Combustion. SAE Technical Paper, 2010-01-0598, 2010.

45. Bosch Annual Report 2008.

46. Dixon D, Hanks B, Harker N, Stock C, DenBraven K R. University of Idaho's Direct-Injected Two-Stroke Snowmobile Using E85 Fuel. SAE Technical Paper. 2008-32-0031, 2008.

47. HENTSCHEL, W. "OPTICAL DIAGNOSTICS FOR COMBUSTION PROCESS DEVELOPMENT OF DIRECT-INJECTION GASOLINE ENGINES," *Proceedings of the Combustion Institute* Vol. 28, 2000, pp. 1119–1135.

48. Wakisaka, T., Imamura, F., Nguyen, T. T., Takeuchi, S.-i., and Chung, J.-H. "Numerical Simulation of Hollow-Cone Sprays in Gasoline Direct-Injection Engines," *Seoul 2000 FISITA World Automotive Congress*, 2000.

49. CHOI, H., KIM, M., MIN, K., and LEE2, J. "THE STRATIFIED COMBUSTION MODEL OF DIRECT-INJECTION SPARK-IGNITION ENGINES," *Proceedings of the Combustion Institute* Vol. 29, 2002, pp. 695–701.

50. Kim, S., Nouri, J. M., Yan, Y., and Arcoumanis, C. "Effects of intake flow on the spray structure of a multi-hole injector in a DISI engine," *International Journal of Automotive Technology* Vol. 10, No. 3, 2009, pp. 277-284.

51. Ra, Y., and Reitz, R. D. "The application of a mul ticomponent droplet vaporization model to gasoline direct injection engines," *International Journal of Engine Research* Vol. 4, No. 3, 2003.

52. Christoph Garth, Robert S. Laramee, Xavier Tricoche, Jurgen Schneider, and Hans Hagen. "Extraction and Visualization of Swirl and Tumble Motion from Engine Simulation Data".